Turbulent Fluxes of CO_2, H_2O and Energy in the Atmospheric Boundary Layer above Tropical Vegetation investigated by Eddy-Covariance Measurements

Dissertation

zur Erlangung des Doktorgrades

der Mathematisch-Naturwissenschaftlichen Fakultäten

der Georg-August-Universität zu Göttingen

vorgelegt von

Ulrike Falk

aus Meerbusch

Göttingen, 2004

.

Contents

Chapter 1

Introduction

Global Climate Change is one of the major topics discussed in scientific literature as well as in international public since the end of the last century. It has become evident that human activity, especially since the industrial revolution, has a significant impact on the earth's biogeochemical cycles. Among the first recognized alterations has been the modification of the global carbon cycle, which is also the most prominent (Malhi et al., 2002). CO_2 as a greenhouse gas is trapping thermal energy within the earth's atmosphere and thus warming global climate. The rate of increase in CO_2-concentration in the last 100 years is at least an order of magnitude greater than in the last 20000 years (Prentice *et al.*, 2001). The worldwide rising CO_2-levels may have effects on terrestrial ecosystems as increasing plant growth rates or modification of ecosystem species composition, and thereby might lead to an alteration of the competitive balance between species. Fossile fuel combustion and loss of original forest result in an increase in atmospheric CO_2. The human induced carbon emissions through land-use change, in especially the conversion of forests and other natural landscapes, into agriculturally used land, still accounts for approx. 25% of total anthropogenic emissions (Malhi et al., 2002). Changes in biosphere and forest cover are most dramatic in the tropics. Net emmissions from changes in tropical land-use are contributing about 22% human induced carbon emissions (IPCC, Schimel et al. (1996)). Only few continuous observations of carbon budgets in tropical regions exist. This is mainly due to the politically and economically unstable situation, and unsufficient infrastructure in tropical countries. Hence, the uncertainty in the net tropical carbon emissions is rather high, $1.6 \pm 1.0 \, Gt - C \, yr^{-1}$ (Schimel et al., 1996). Good forest management, prevention of deforestation and forest regrowth are counter measures that could significantly lessen the carbon disruption. The political and socioeconomic implications concerning CO_2 emissions and impacts of global carbon cycle by the Kyoto Protocol of 1997 depend on accurate measures of global biospheric changes

(Running et al. (1999), Schimel (1998)). With this background it becomes apparent, that global terrestrial monitoring and modeling programs to investigate carbon metabolisms are important and necessary.

The influence of climate by the land surface is due to the direct contact of the atmosphere with the surface. The surface acts as a boundary for atmospheric flow and as a source or sink for atmospheric moisture, enthalpy, and matter, as well as a sink for atmospheric momentum. The exchange between atmosphere and surface is realized through turbulent transports of sensible and latent heat and radiative processes. The boundary conditions determined by the surface have regulatory character for important feedback cycles in the climate system (Viterbo and Beljaars, 2002). The evolution of soil wetness is determined by the partitioning of available energy at the surface into latent and sensible heat fluxes and among sea surface temperature and snow mass most important as 'memory' mechanism for time scales from weeks to seasons (Viterbo and Beljaars, 2002). Betts et al. (1998) show that the evaporative fraction of the turbulent heat flux, i. e. the ratio of latent to the sum of latent and sensible heat flux, is directly correlated to the soil water content for the data from the FIFE project in the Arkansas Red River basin. Surface weather variables are determined by the magnitudes of sensible and latent heat flux and directly influence the human living environment. The ratio of sensible to latent heat is called the Bowen ratio. Global averages range from values for the Bowen ratio over land to over sea (Gibson et al., 1997). The climate forcing through the surface energy balance terms is not only determined by the Bowen ratio but also by the albedo. Change in land-use cover or forest conversion into agriculturally used land always means a change of the primary regulator for net radiation energy available at the surface, the albedo. The ARME and ABRACOS projects in the Amazon, South America, determined the tropical forest albedo to be about 0.11 to 0.13 and describe a seasonal trend of the albedo with soil moisture (ARME: Shuttleworth et al. (1984), Shuttleworth (1988), Moore and Fisch (1986); ABRACOS: Gash and Nobre (1997), Grace et al. (1995)). For the pasture sites of the ABRACOS project, Culf et al. (1995) give an albedo of 0.18. Wright et al. (1995) state, that the albedo is increasing with the leaf area index (LAI) from 0.16 to 0.2 for the pasture sites. Investigations in South-East Asia within GAME have shown that land-use change results in decreasing precipitation in India (Kanae et al., 2001) and in Thailand (Suzuki et al. (2001), Toda et al. (2002)), but also that human induced landcover change have modified monsoon circulation in East China (Fu (1996), B.Fu and Wen (1999)).

The atmosphere as a physical system can be described by a small set of basic equations where the biosphere serves merely as a boundary condition. Generally, a boundary layer is defined as the fluid layer directly at a surface, that is confining the fluid, where the

gradients are different from those in the core flow, that is not influenced by the surface (Prandtl, 1904). Bioclimatology uses the physics of fluid mechanics to describe atmospheric flow and combines it with the ecology of the biosphere as an interdisciplinary science. The theoretical restrictions of Eddy-Covariance measurements and the assumptions made in order to apply this technique are rarely met perfectly. At lower latitudes, micrometeorological and biophysical investigations have to deal with diurnal courses of energy input to the surface and meteorological boundary conditions and seasonal patterns. These rather fast changes in the micrometeorological boundary parameters still pose a problem of how to interpret the experimental data.

In 2000, an EC-measurement campaign was accomplished at the Surumoni crane station (Anhuf and Winkler, 1999), within the project "Die atmosphärische und biologische Steuerung des Wasserhaushaltes eines neotropischen Tieflandregenwaldes in Amazonien/Venezuela", From 2001 until 2003, Eddy-Covariance measurements were carried out above a cocoa plantation within sub-project B1, part of the international collaborative research project "The Stability of Rainforest Margins" (STORMA), a joint project (Sonderforschungsbereich SFB 552) between the universities of Göttingen and Kassel in Germany and the universities in Bogor and Palu in Indonesia (Sonderforschungsbereich 552 (003b) and 552 (003b)). Another task of the sub-projects B1 and Z2 was to build a micrometeorological tower within the undisturbed montane rain forest in the Besoa valley, which was accomplished in February 2003. Both research projects were funded by the German Research Foundation (DFG).

Transmigration programs in the 1970's under the Sueharto regime included the resettlement of people from more populated areas from Java, to the outer islands, and also to the area around the TNLL on Sulawesi. Unkept promises of land for farming by the government to the transmigrants and the political vacuum that has been created since the resignation of the Sueharto government, created a rather tense situation. The demand for tropical wood by the industrial nations and the paper industry, but also the ongoing political agitation in Indonesia, i. e. the shifting of power from Jakarta to the regencies lead to a massive logging incident and claim of land in the research area in July 2001. In about 3 days forests of the National Park area in the vicinity of the research site was logged about 18 km and 300 m to the left and right along the road. The ongoing logging and the tension between local people, non-governmental organizations (NGO) and the government is a perfect medium for capitalistic interest groups like logging companies but also for ordinairy farmers in the pursuit of farming land. As mentioned before, changes in land-cover is likely to modify local climate. Thus it is likely, that the rapid changes as could be observed in the above mentioned event, do have an impact on local and regional climate in the research area.

Subject of this work is the design and installation of measurement sytems, and successful accomplishment of measurements to quantify the exchange processes between atmosphere and different tropical vegetation. The main focus is on measurements above agriculturally used land in Central-Sulawesi, Indonesia, where the plantations are managed by small-stake holders and the area of investigation shows a high heterogeneity. The surface boundary layer above heterogenous terrain is still poorly understood (Kaimal and Finnigan, 1994) and thus one one focal point of this work is to investigate the applicability of the applied method. By comparing the measurements above managed land to those above undisturbed rain forests, this work assesses the potential impact of land-use change on the carbon, water and energy cycle between atmosphere and vegetation, and thereby on local climate.

Chapter 2

Basics

The eddy-covariance (EC) method (see Chapter 2.2) is often applied in atmospheric sciences to measure the exchange of energy or a scalar quantity between the earth's surface and the atmosphere. Before getting to the theoretical background of this method, it is necessary to define the scaling laws that determine the exchange between atmosphere and surface (Chapter 2.1). The layer of atmospheric flow near the surface is also called the Prandtl or surface layer of the atmosphere. Within this layer, momentum or scalar quantities are transported mainly by turbulence. The scalar quantities of interest here are mean temperature, water vapour and CO_2. Chapter 2.1.2 gives a description of atmospheric turbulent spectra with respect to exchange processes that are subject of this work. The turbulent energy exchange of atmosphere and underlying surface is driven by the net radiative energy input to the surface. The underlying surface within this work are different vegetation forms as forest canopies. Hence, the heat flux into the vegetation is an important term of the energy balance at the canopies surface. Chaper 2.1.3 addresses the energy balance equation and the assessment of the heat flux into the vegetation. The energy balance is a useful means to verify the measured turbulent energy fluxes. From the equations governing the atmospheric boundary layer, the eddy-covariance equation used to compute the turbulent fluxes are derived, and the underlying theoretical assumptions and restrictions elucidated (Chapters 2.2, 2.3). More correct would be the term energy flux densities for the turbulent energy fluxes, since the unit is W/m^2. But for better reading when talking about fluxes always refers to the flux densities.

2.1   The atmospheric boundary layer

2.1.1   Scaling the surface layer

Basic statistical terms

The EC method is a direct measurement of atmospheric turbulence by recording the atmospheric variables at a frequency that is high enough to resolve the considered turbulent fluctuations. Through statistical analysis of the discrete time series of vertical wind and the considered variable the turbulent fluxes can directly be calculated. The concept and basic statistical terms will now shortly be described. Consider a variable a measured N times at time intervals (time steps) Δt. The time series of these measurements is then referred to as $a_k = a(t_k)$, $k = 1, ..., N$ and has the length $N\Delta t$. **Reynold's averaging** splits the actual value a_k into the arithmetic mean value,

$$\overline{a}^{N\Delta t} = \frac{1}{N} \sum_{k=1}^{N} a_k \,,$$

under the constraint that the mean value $\overline{a}^{N\Delta t}$ is stationary over the time intervall $N\Delta t$, and a fluctuation a'_k:

$$a_k = \overline{a}^{N\Delta t} + a'_k$$

The **variance** of a_k is given by

$$\sigma_a^2 := \overline{a'^2} = \frac{1}{N} \sum_{k=1}^{N} a'^2_k$$

and the **standard deviation** by

$$\sigma_a = \sqrt{\overline{a'^2}}.$$

The **covariance** of two time series a_k and b_k is calculated by

$$\sigma_{ab}^2 = \overline{a'b'} = \frac{1}{N} \sum_{k=1}^{N} a'_k b'_k$$

with the **correlation coefficient**

$$r_{ab} = \frac{\overline{a'b'}}{\sigma_a \sigma_b}.$$

The **autocorrelation function** is then given by

$$R_a(\xi_j) = \frac{\overline{a'(t_k)a'(t_k + \xi_j)}}{\sigma_a^2} = \frac{\frac{1}{N} \sum_{k=1}^{N} a'(t_k)a'(t_k + \xi_j)}{\frac{1}{N} \sum_{k=1}^{N} a'(t_k)^2},$$

where $\xi = j\Delta t$ for $j \in [1, ..., N-1]$, and describes the correlation of variable a with itself at time ξ_j for time series a_k.

With this statistical approach, the formulas for the vertical turbulent fluxes of sensible and latent heat can be derived from the averaged conservation equations and, disregarding air density fluctuations (i.e. $\rho = \overline{\rho}$), can be written as

$$H = c_p \overline{\rho} \overline{w'\theta'} \tag{2.1}$$

$$\lambda E = \lambda \overline{\rho} \overline{w'q'} \tag{2.2}$$

where c_p is the specific heat of air at constant pressure, λ the specific evaporation heat of water, ρ is the mean air density w', θ' and q' the synchronous fluctuations of the vertical wind component w, potential temperature θ and specific humidity q. The vertical flux of horizontal momentum, τ, is calculated by

$$\tau = \overline{\rho}\sqrt{\overline{u'w'}^2 + \overline{v'w'}^2} \tag{2.3}$$

where u and v are the horizontal wind components. This approach for calculating the vertical turbulent fluxes within the surface layer is discussed in more detail in chap. 2.2.

Monin-Obukhov theory

The hydrodynamic equations governing the atmospheric boundary layer are the conservation of mass (or continuity equation), conservation of momentum and energy, and the equation of state (or ideal gas law). In especially, the equations contain more variables than the number of equations is. Resolving (i.e. closing) these equations implicates the use additional information information (Stull, 1988). The Monin-Obukhov or Similarity theory is based on the organization of variables into dimensionless groups, and is an approach for the closure of the hydrodynamic eqations in the surface layer (Monin and Obukhov, 1954). The surface layer is defined as that part of the boundary layer where the vertical fluxes vary by less than 10% of their magnitude with height (Stull, 1988) and is called the **constant flux layer**. A detailed discussion can be found in Stull (1988) and Garrat (1992). A series of approximations are made for the mean flow in the surface layer (In the following the index "0" stands for the mean value in the surface layer of the regarded flow), (Businger, 1982):

- The considered flow is incompressible, that is the gradients of mean density and pressure are assumed negligible within the regarded flow.

- Phase transition of H_2O is negligible.

- Divergence of net radiation is neglected.

- Turbulent fluctations of air density and pressure is not considered, $\overline{\rho} = \rho_0$ and $\overline{p} = p_0$. Density changes resulting from pressure changes are negligible.

- For the near suface layer $T_0 = \overline{T}$ is assumed.

- Dynamic viscosity and molecular heat conduction are negligible, i.e. small temperature- and pressure-dependencies are neglected.

- Coriolis force affects only the horizontal wind $\vec{v}_h$.

For turbulence closure, the turbulent covariances are described by the vertical gradients of the average values (Schmidt, 1925).

$$\overline{w'X'} = -K_X \frac{\partial \overline{X}}{\partial z} \tag{2.4}$$

with $X = u, v, \theta, q$, where q is the specific humidity and θ the potential temperature. u and v denote the horizontal components of the three-dimensional wind vector, $\vec{v} = (u, v, w)$. K_X is the respective turbulent diffusion coefficient. When rotating the coordinate system, so that $v = \overline{u'v'} = 0$, the set of basic equations is reduced to:

$$u_\star^2 = -\tau/\rho = -\overline{u'w'}_0 \quad = \quad const. \tag{2.5}$$

$$\frac{g}{T_0} \quad = \quad const. \tag{2.6}$$

$$\frac{H}{\overline{\rho}c_p} = \overline{w'\theta'}_0 \quad = \quad const. \tag{2.7}$$

$$\frac{\lambda E}{\overline{\rho}\lambda} = \overline{w'q'}_0 \quad = \quad const. \tag{2.8}$$

$u_\star$ is called the friction velocity and is related to the magnitude of the surface stress τ. The **Monin-Obukhov length** is defined by

$$L = \frac{u_\star^3/\kappa}{(g/\overline{\theta})\overline{w'\theta'}_0} \,.$$

Its absolute value can be interpreted as the height where the absolute values of dynamically induced generation of turbulent kinetic energy equals to thermally induced generation ($L > 0$) or destruction ($L < 0$) of turbulent kinetic energy. Neutral stratification of the atmospheric surface layer means $L \to \infty$. The stability parameter ζ is defined by

$$\zeta = \frac{z}{L} \tag{2.9}$$

where z is the observation height. ζ is negative for unstable stratification as in the convection-driven daytime boundary layer, and positive for stable stratification. As L approaches infinity (neutral stratification), $\zeta \to 0$. The mean atmospheric variables are normalized by their respective scales:

$$z,\ z_0,\ L,\ \frac{u_\star}{\kappa},\ \frac{\theta_\star}{\kappa} := \frac{H}{\kappa u_\star \overline{\rho} c_p},\ \frac{q_\star}{\kappa} := \frac{\lambda E}{\kappa u_\star \overline{\rho} \lambda}$$

in order to gain a set of dimensionless variables that can be written as a function of the parameters:

$$\frac{z}{L},\ \frac{z_0}{L}$$

where z_0 is the aerodynamic roughness length, i.e. the effective height of the roughness elements. The state of the atmospheric surface layer regime is therefore determined by these two parameters. The vertical gradients of horizontal wind, temperature and specific humidity can then be described by a set of profile functions of the stability parameter z/L:

$$
\begin{aligned}
\phi_m\left(\frac{z}{L}\right) &= \frac{\partial \overline{u}}{\partial z}\frac{\kappa z}{u_\star} \\
\phi_h\left(\frac{z}{L}\right) &= \frac{\partial \overline{\theta}}{\partial z}\frac{\kappa z}{\theta_\star} \\
\phi_q\left(\frac{z}{L}\right) &= \frac{\partial \overline{q}}{\partial z}\frac{\kappa z}{q_\star}
\end{aligned}
$$

These empirical functions are also called similarity or profile functions and a compilation of the profile functions from different meteorological experiments can be found in Kaimal and Finnigan (1994), where $\phi_h = \phi_q \equiv \phi_{hq}$ is assumed (Panofsky and Dutton, 1984). The roughness length can then be derived from vertical wind profile measurements by

$$u(z) = \frac{u_\star}{\kappa}\left(ln\left(\frac{z-d}{z_0}\right) - \phi_m\left(\frac{z}{L}\right)\right).$$

The potential temperature, θ, is defined in Stull (1988) as

$$\theta = T\left(\frac{p_0}{p}\right)^{0.286} \approx T + (g/c_p)\cdot z\,.$$

Taylor's hypothesis

Instead of creating a 3-dimensional snapshot of the boundary layer above a specific surface and its turbulence regime, i.e. looking at the spatial distribution of size of eddies and scales of motion, investigations at one point in space over a long time period are more applicable. Taylor's hypothesis (Taylor, 1938) suggests to consider turbulence as *frozen*, as it advects with the mean wind past the measurement system, i.e. the state of an eddy can be regarded

stationary over a certain time period. Looking at the 1-dimensional conservation equation (i.e. with the wind vector $\vec{v} = (\overline{u}, 0, 0)$) of a scalar quantity C, this means that the time scale of change of state dt is much greater than the local time scale ∂t and time scale of advection $\partial x / \overline{u}$:

$$\frac{dC}{dt} > \frac{\partial C}{\partial t} + \overline{u} \frac{\partial C}{\partial x} \approx 0 \,.$$

An eddy with the wavelength Λ is advected in the time t at mean wind speed $\overline{u}$ past the sensors

$$\frac{\partial C}{\partial t} \approx \overline{u} \frac{\partial C}{\partial x} \to \Lambda \approx \overline{u} t \Leftrightarrow f \approx \overline{u}/k$$

where $k = 2\pi \Lambda$ is the wave number and f the frequency of the eddy. Taylor's hypothesis is fundamental for turbulence measurements in the surface boundary layer

2.1.2   Energy spectra of the atmosphere

The atmospheric turbulent flow consists of different scale size eddies, transporting impulse or scalar properties vertically. Investigations by Van der Hoven (1957) found a spectral gap at frequencies between $0.001\,Hz$ and $0.0001\,Hz$ corresponding to time scales of approx. $0.5\,h$ and $3\,h$ in these spectra between the convection-driven boundary layer scales and synoptic scales. Stull (1988) defines the surface boundary layer as that part of the troposphere that is directly influenced by the presence of the earth's surface, and responds to surface forcings with a timescale of about one hour or less. The spectral gap is implicit for the development of spectral forms in surface boundary layer studies as carried out in this work, since it is separating the surface forcings from synoptic forcings. Figure 2.1 shows a schematic distribution of spectral energy density of a scalar or momentum to the wave number, originating from Kolmogorov (1941). Eddies with wavelengths of about $10\,m$ to several kilometers transport vertically the highest amount of kinetic energy. Section A in Figure 2.1 denotes the spectral area where turbulent kinetic energy (TKE) is produced thermally and dynamically. The maximum depends on the integral length scale of the turbulent flow and is at a wavelength of about $100\,m$ (Kaimal and Finnigan (1994), Stull (1988)). The *inertial subrange* is the region, where energy is transported from bigger eddies to smaller eddies (section B in Figure 2.1). In the double-logarithmic presentation the energy is declining linearly with smaller wave numbers with a gradient of $-5/3$. The dissipation describes the region, where TKE is transformed into heat through molecular dynamic viscosity and heat conduction (section C in Figure 2.1).
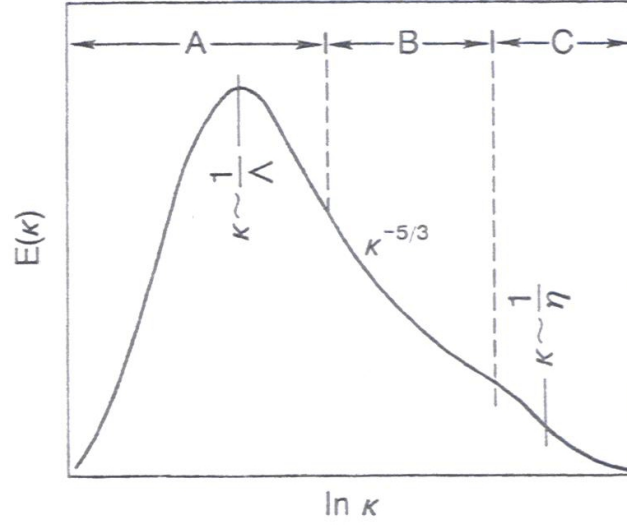
Figure 2.1: Schematic diagram of turbulent spectra for the surface boundary layer of the atmosphere. Displayed is the energy density of a scalar such as temperature and humidity, or of momentum, $E(\kappa)$, versus the natural logarithm of wavenumber κ, $ln\,\kappa$, out of (Stull, 1988) but originally from Kolmogorov (1941).

2.1.3   Energy balance equation and resistance analogue

Since a surface can not store energy, the sum of all energy fluxes directed towards and away from the surface has to be equal to zero. The energy balance of a surface confining the atmospheric boundary layer can thus be written as:

$$R_n - G - H - \lambda E = 0\,,\tag{2.10}$$

where H and λE are the turbulent fluxes of sensible and latent heat respectively as defined in chap. 2.1.1, and G the heat flux into the soil or vegetation cover, as will be discussed later in this chapter. R_n denotes the net radiation flux at the surface and can be split into its longwave (wavelength $\lambda > 4\,\mu m$) components L and its shortwave (wavelength $\lambda < 4\,\mu m$) components K, the arrows indicating the direction of the radiation energy fluxes

$$R_n = (L\downarrow + K\downarrow) - (L\uparrow + K\uparrow)\,.\tag{2.11}$$

This partitioning is reasonable since the sun and earth emittance spectra only have a small overlap between $\lambda = 3\ldots 4\,\mu m$. Since only 0.4% of the total extraterrestric solar radiation energy is transmitted via wavelengths $\lambda > 5\,\mu m$, and the earth's thermal spectrum lies above $\lambda = 4\,\mu m$ (Campbell and Norman, 1998), $K\downarrow$ denotes the direct and diffuse solar radiation.

The term diffuse refers to all scattered radiation. $L\downarrow$ is the atmospheric (thermal) longwave radiation and $K\uparrow$ is the shortwave radiation reflected at the earth's surface. $L\uparrow$ denotes the longwave radiation of the earth's surface. The albedo α is defined by the ratio of solar irradiance received at the earth's surface to reflected shortwave radiation, and is a parameter specific for each surface type.

$$\alpha = \frac{K\downarrow}{K\uparrow} \tag{2.12}$$

The heat flux into the soil or vegetation can be derived from the change in temperature profile T_G within the layer below the surface

$$G(z=0) \equiv G_0 = \int_{z_\star}^{0} \rho_G c_G \frac{\partial T_G}{\partial t} dz + G(z_\star)$$

where $G(z_\star)$ denotes the heat flux through level $z_\star$, and can be described by Fourier's law of heat conduction

$$G(z_\star) = \lambda_G \left.\frac{\partial T_G}{\partial z}\right|_{z_\star}$$

where z is the vertical distance in m to the surface, ρ_G is the density, c_G the specific heat and λ_G the thermal conductivity of the soil. For ecological studies though, the interaction between
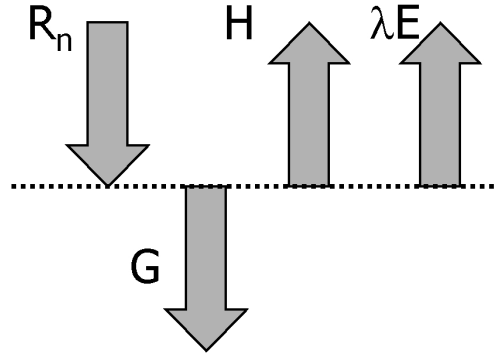

Figure 2.2: Schematic of the energy balance terms for a surface, the fluxes are positive defined in direction of the arrows

the surface, in especially canopies, and the atmosphere is not sufficiently described by the above equation. When investigating the interactions between atmosphere and canopies, the vegetation stand cannot be regarded as a homogeneous layer (single leaf approach) where heat conduction within are described by the above equations. The stand represents a complex system with different mechanisms driving the exchange processes of energy within and above the forest. The **resistance analogue** approach addresses the canopy as an electrical circuit

described by Ohm's law analogues, and associates resistances to different exchange processes (Figure 2.3). Analog to Ohm's law $U = R \cdot I$, the transport process between vegetation and atmosphere can be described by a potential difference in density of a scalar X that is proportional to the flux, i.e. $\rho_X(z_2) - \rho_X(z_1) = F_X \cdot r$, where the resistance r is the proportionality factor. The same refers to the transport of momentum. The plane, where the logarithmic wind profile becomes zero does not coincide with the canopy's surface. The vertical displacement of the zero plane to the canopy's surface is called displacement height d. The resistance r_a in Figure 2.3 is allocated to the transport within the atmospheric surface layer, i.e. above the height $z_0 + d$, whereas r_b is the resistance for the transition between canopy crown space and bottom of the atmospheric boundary layer. The leaf surface and stomatal resistance are r_s and r_{st}, respectively. The **resistance analogue** approach is discussed in
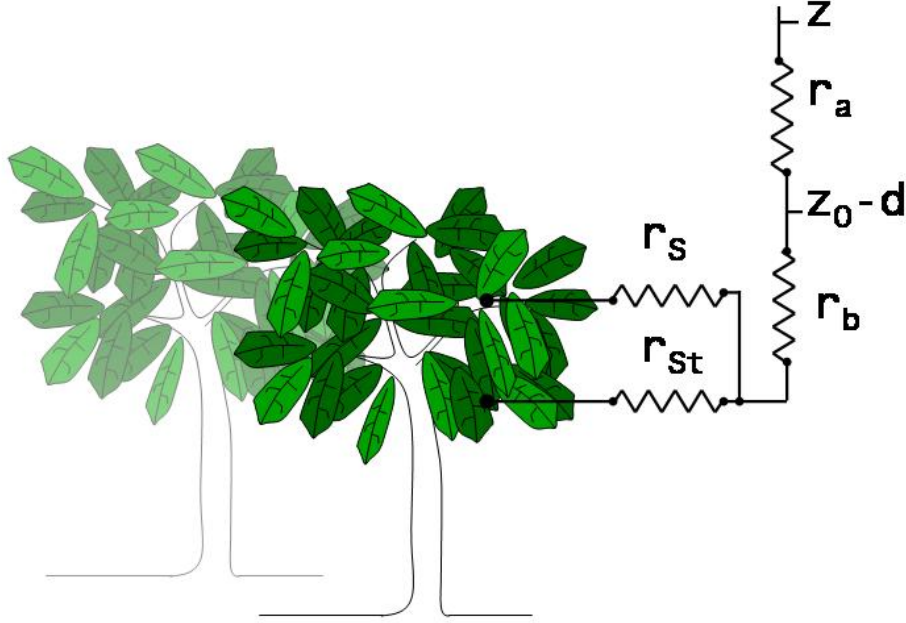

Figure 2.3: Resistance model for a plant in a stand of vegetation, r_s is the leaf surface and r_{st} the stomatal resistance, r_a is the aerodynamic resistance, r_b is allocated to the transition between canopy crown space and bottom of the atmospheric surface layer at $(z_0 - d)$.

detail by Monteith and Unsworth (1990). In the following, a short summary is given. Using Equation 2.4 for sensible heat, the sensible heat flux can be rewritten as $(r_a \equiv r_{aH})$

$$H = -\rho c_p \frac{1}{r_{aH}} \frac{\partial \theta}{\partial t} \tag{2.13}$$

$$\approx -\rho c_p \frac{1}{r_{aH}} [T(z) - T(z_0 + d)] \tag{2.14}$$

where $r_{aH} = u(z)/u_\star^2$ denotes the aerodynamic resistance between a fictitious surface at height $(d + z_0)$ and z. For the turbulent transport of latent heat all resistances have to be connected in line $(r_a \equiv r_{aV})$,

$$r_{tot} = r_{aV} + r_b + \frac{r_S \cdot r_{St}}{r_S + r_{St}} \equiv r_{aV} + r_c \,.$$

and by defining the general surfaces resistance r_c that sums up the resistances of surface, stomata and crown boundary layer, the appropriate expression for the latent heat flux can be written as:

$$\lambda E = -\frac{\rho c_p}{\gamma} \frac{e(z) - e^\star(T_s)}{r_{tot}} \tag{2.15}$$

$$= \frac{\rho c_p}{\gamma} \frac{e^\star(T_s) - e(z)}{r_{aV} + r_c} \,. \tag{2.16}$$

where $e(z)$ is the vapour pressure, $e^\star(T)$ is the saturation vapour pressure, T_s the surface temperature, $\gamma = c_p p/\lambda \varepsilon$ the psychrometric constant, λ is the latent heat of vaporization, $\varepsilon = 0.622$ the ratio of molecular weight of water to molecular weight of dry air and $r_{aV} = r_{aH} = u(z)/u_\star^2 \equiv r_a$.

Assuming a linearised form for the saturation vapour pressure at temperature T_s eliminates the surface temperature from Equation 2.16,

$$e^\star(T_s) \approx \Delta(T - T_s) + e^\star(T) \,.$$

Introducing these equations into the energy balance equation gives

$$\lambda E = \frac{\Delta(R_n - G) + \rho c_p \left\{ e^\star(T(z)) - e(z) \right\} / r_a}{\Delta + \gamma^\star} \tag{2.17}$$

where $e_s(T)$ denotes the saturation vapour pressure, Δ is the slope of the saturation vapour pressure curve and $\gamma^\star = \gamma(1 + r_c/r_a)$. Eq. 2.17 is called the **Penman-Monteith** equation (Monteith, 1965). For a more detailed derivation see Monteith and Unsworth (1990). This equation can be resolved to the canopy surface resistance r_c, if the latent heat flux is measured separatly:

$$r_c = r_a \left(\left(\frac{\Delta}{\gamma} \left(\frac{R_n - G}{\lambda E} \right) - 1 \right) - 1 \right) + \frac{\rho c_p \gamma \left\{ e^\star(T(z)) - e(z) \right\}}{\lambda E} \tag{2.18}$$

Using again the energy balance equation and substituting $R_n - G = H + \lambda E$, eliminates the available energy $R_n - G$ from the equation. The Bowen ratio is defined as the ratio of sensible to latent heat flux, $\beta = H/\lambda E$. Introducing this ratio into Equation 2.18 leads to the expression:

$$r_c = r_a \left(\frac{\Delta \beta}{\gamma} - 1 \right) + \frac{\rho c_p \gamma \left\{ e^\star(T(z)) - e(z) \right\}}{\lambda E} \tag{2.19}$$

The canopy conductance is the reciprocal canopy resistance

$$g_c = 1/r_c$$

and is normally used in the formulation of atmospheric transport. In this chapter the basic theoretical background of atmospheric boundary layer theory have been discussed, and in the following chapter, the introduced equations will be used to introduce the background of the Eddy-Covariance method, that is subject to this work.

2.2 Eddy-Covariance equation and post-processing

Eddy-Covariance measurements are based on statistical analysis of the measured time series of wind vector and a scalar quantity C. In the following an the necessary assumptions and restrictions are also discussed and their implication for the measured fluxes (see also Aubinet et al. (1999)).

The conservation equation for a scalar quantity C is given by

$$\frac{dC}{dt} = \frac{\partial C}{\partial t} + \frac{\partial(u_i\,C)}{\partial x_i} = D_C\,\frac{\partial^2}{\partial x_i{}^2}\,C + S_C = 0 \qquad (2.20)$$

using Einstein's summation convention, i.e. whenever two identical indices appear in a term, the sum over $1,..,3$ is implied. The wind vector components are denoted by u_i, $i = 1, 2, 3$. Here D_C is the molecular diffusion coefficient, and S_C is the net source strength fo the scalar quantity C. Applying Reynold's averaging (see chap. 2.1.1) and averaging the equation with respect to time, so that terms of single fluctuations disappear leads to

$$
\begin{array}{cccccc}
\frac{\partial}{\partial t}\overline{C} & +\overline{u_i}\frac{\partial}{\partial x_i}\overline{C} & +\frac{\partial}{\partial x_i}\overline{u_i'\,C'} & = & D_C\,\frac{\partial^2}{\partial x_i{}^2}\overline{C} & +\overline{S_C} \\
(1) & (2) & (3) & & (4) & (5)
\end{array}
$$

where term (1) denotes the storage of the scalar C, term (2) describes the advection with the mean wind and term (3) is the term of flux divergence. Here incompressible flow is assumed, i.e. $(\partial u_i/\partial x_i) = 0$. Term (4) stands for the mean diffusion and term (5) for the mean source or sink strength .

The first important simplification of horizontal homogeneity, i.e. the first derivatives of all variables in horizontal directions are set to zero, leads to

$$\frac{\partial}{\partial t}\overline{C} + \overline{u_3}\frac{\partial}{\partial x_3}\overline{C} + \frac{\partial}{\partial x_3}\overline{u_3'\,C'} = D_C\,\frac{\partial^2}{\partial x_3{}^2}\overline{C} + \overline{S_C(x_3)}\,. \qquad (2.21)$$

Assuming, that there is no extreme thermal convection, i.e. no measurable mean vertical wind $\overline{u_3} = 0$ and the only source or sink of the scalar C is at the surface, leads to

$$\frac{\partial}{\partial t}\overline{C} + \frac{\partial}{\partial x_3}\overline{u_3' C'} = 0 \,. \tag{2.22}$$

The scalar properties considered in this work, are temperature, ρ_{CO_2} and ρ_{H_2O}. The last assumption can be made, since CO_2 is inert when transported through the atmospheric surface layer, that means no sources or sinks of CO_2 exist other than at the surface. Morgenstern (2000) shows on the basis of an example calculation that the release of sensible heat through condensation of water vapour in the atmospheric boundary layer is negligible. Thus, the assumption of the only sources/sinks for latent heat are at the surface is a justifiable approximation. The production of sensible heat through absorption of radiation is of great importance at the surface, but it is generally disregarded for the column of air between the surface and point of measurement. Assuming all statistics of all variables are stationary, i. e. $\partial \overline{C}/\partial t = 0$, reduces equation 2.22 to the **Eddy-Covariance (EC)** equation ($u_3 \equiv w$)

$$F_C = \overline{u_3' C'} = \overline{w'C'} = \overline{S_{C,ground}} \tag{2.23}$$

The last assumption is the application of **Taylor's hypothesis**. There are some corrections applied to the derived flux F_C. The most prominent is the correction described by Webb et al. (1980). It corrects for air density variations that show an effect in the measured vertical fluxes of water vapour and heat transfer . The post-processing developed in the Institute of Bioclimatology (Morgenstern (2000), Ibrom (2000)) includes:

- Despiking routines

- Cross wind corrections of the ultrasonic temperature (Gros, 1998)

- Sensorhead correction of the measured wind field (see Chapter 4.1)

- Coordinate rotation for alignment of the x-axis with the mean horizontal wind component and to achieve $\overline{w} = 0$

- Removing a linear trend from the data sets before computing the statistics.

- Maximization of the covariances, i. e. the time series of vertical wind is shifted against the time series of a scalar quantity so that the covariance is maximal.

The last step of the post-processing applies in first instance to EC measurement system that include a closed-path sensor, since the air sample is sucked through a tube of several meters

length into the sample cell. Hence, there is a time difference in the measurements of the wind components and scalar quantities as CO_2 and H_2O. The open-path sensor measures the scalar components *in situ*, and the maximation of the covariances seems not applicable at first sight. The EC system as deployed in the cocoa plantation in Nopu does include such an open-path sensor. As will be discussed in Chapter 4.3.2 the internal delay of signal processing within the sensors electronics results in a time delay of several *ms*. The CO_2- and H_2O-signal synchronised with the time series of vertical wind by the maximization of covariances in the last step of the post-processing.

2.3   Stationarity of turbulence

Stationarity of turbulence means that the statistical are independent of time, i.e. it turbulence is statistical invariant with respect to translation of the time axis. Turbulence is homogeneous if statistically invariant to translation of the spatial axis, and isotropic if statistically independent of translation, rotation and reflection of spatial axes. Only on sufficiently small scales is the ABL isotropic (Garrat, 1992). Taylor's hypothesis of stationarity of turbulence (see Chapter 2.1.1) is fundamental for the application of EC technique. Foken and Wichura (1996) describe a means to verify the stationarity of the data by segmenting the data set after removing an existing trend into $N = 4..8$ part intervals. The turbulent flux of a scalar C is then being calculated by computing the covariances of w and the scalar $C = \theta$, q, u (see Chapter 2.2), for every of the N part intervals. The N values of the covariances have to be averaged over the dataset

$$Cov_N(w, C) := \overline{w'C'}_N = \frac{1}{N} \sum_{k=1}^{N} \left(\overline{w'C'} \right)_k .$$
(2.24)

The result is compared to the covariances computed for the whole dataset $\overline{w'C'}$. If $\overline{w'C'}_N$ is not differing by more than 30% from the total flux $\overline{w'C'}$, the data can be regarded as stationary (Foken and Wichura, 1996).

Chapter 3

Instrumentation

3.1 Eddy-Covariance system design and sensor description

Eddy-Covariance (EC) systems measure the components of the 3-dimensional wind vector and scalar quantities, such as temperature, CO_2 and H_2O for instance, in order to derive the flux densities of the scalar quantities by means of the equations derived in Chapter 2.2. The central device of an EC system is in most cases an ultrasonic anemometer (USA) and the signals of all other sensors are collected and synchronized with the measurements of wind components and temperature within the USA. Throughout this work, ultrasonic anemometers (USA-1/3 and USA-1 by METEK, Elmshorn) have been used. Theory and measurement principle of ultrasonic anemometers have been described in various works (such as Kaimal and Finnigan (1994), Aubinet et al. (1999), Morgenstern (2000) etc.) and is described in Chapter 3.1.1. The ultrasonic anemometers used in this work measures in three directions, tilted by 120° against each other to obtain the three-dimensional wind vector. Since the ultrasonic anemometer itself constitutes an obstacle in the wind field it shall measure, the data of three-dimensional wind velocity have to be corrected with regard to the sensorhead symmetry (see Chapter 4.1). Ibrom (2000) points out that the incoming flow shows steeper angles when directed from the surface upward compared to the incoming flow directed from the atmosphere to the surface. In order to minimize the effects of flow distortion of the wind field by the ultrasonic anemometer's sensorhead, in especially the sensor mount, the EC systems employed in this work were designed with the sensor head pointing downwards. In that way a more unhindered incoming flow was assured. Apart from that, a sensorhead correction has to be applied to the wind data. This will be discussed with

other corrections applied to the EC measurements in Chapter 4.1. Two different kinds of infrared gas analyser (IRGA) for measurements of CO_2 and H_2O were used for this work. For the measurements above the neotropical rain forest at the Surumoni, a tributary of the upper Orinoco in Southern Venezuela (Anhuf and Winkler, 1999), a closed-path system was used (Chapter 3.1.2). For the measurements at above the cocoa plantation in Nopu, an open-path system was deployed (Chapter 3.1.3)

3.1.1   Measurement principle of ultrasonic anemometers

The principle of these sensors is based on the run-time measurement of ultrasonic pulses in ambient air. Two emitter/receiver-sensors opposing each other, are simultaneously emitting an ultrasonic pulse and the time it needs to travel the distance d from emitter to receiver is being measured. When the pulse is travelling with the wind, it is being accelerated and otherwise slowed down. From the run-time difference of the two pulses the wind speed and from the sum the air temperature can be calculated. The speed of sound in air is given by

$$c = \sqrt{\frac{p\kappa}{\rho}} \tag{3.1}$$

where p is the pressure, $\kappa = c_p/c_v$ the adiabatic compressibility and ρ the air density with κ and ρ depending on temperature and humidity of ambient air. The temperature T_s at which speed of sound in dry air is the same as in moist air is defined by Kaimal and Businger (1963) as

$$T_s = T\left(1 + \left(1 - \frac{m_w}{m_a}\right)\frac{e}{p}\right) = T\left(1 + 0.32\frac{e}{p}\right) \tag{3.2}$$

with e the partial pressure of water vapour. m_w and m_a are the molecular weights of water vapour and dry air, respectively. Kaimal and Gaynor (1991) defines the virtual temperature T_v as the temperature at which dry air has the same density as a given sample of moist air, by

$$T_v = T\left(1 + \left(\frac{\gamma_w}{\gamma_a} - \frac{m_w}{m_a}\right)\frac{e}{p}\right) = T\left(1 + 0.38\frac{e}{p}\right) \tag{3.3}$$

where γ_w and γ_a are the specific heat for water vapour and air respectively. Eq. 3.1 can be rewritten as

$$c = \sqrt{\frac{c_p}{c_v}RT_s} \tag{3.4}$$

using the gas law with temperature T_s. In order to obtain the wind speed v along the sonic pathway between two receiver/emitter transducers opposing each other, each of the transducers is emitting an ultrasonic pulse, one travelling with the wind and the other against it. In most cases, wind direction is not aligned with the sonics pathways and the wind speed

is split into a component v_d parallel to the pathway and a component v_n orthogonal to it. Geometric analysis as described in Morgenstern (2000), shows that v_d can be written as

$$v_d = \frac{d}{2}\left(\frac{1}{t_1} - \frac{1}{t_2}\right) T_s = \frac{c_v}{Rc_p}\left(\frac{d^2}{4}\left(\frac{1}{t_1} - \frac{1}{t_2}\right)^2 + v_n^2\right) \tag{3.5}$$

where d is the path-length between emitter and receiver. t_1 and t_2 are the run-time measurements of the two ultrasonic pulses. The last term in equation 3.5 is the cross-wind correction. Since most ultrasonic anemometers are using three paths, also the somic temperature T_s can be calculated by

$$T_s = \frac{c_v}{Rc_p}\left(c^2 - \frac{1}{3}(v_{n,1}^2 + v_{n,2}^2 v_{n,3}^2)\right) \tag{3.6}$$

where j in $v_{n,j}$ is the index of the three paths.

3.1.2 EC closed-path system

The air sample is sucked by a pump through the intake near the center of the ultrasonic anemometer, through a tube into the IRGA's chamber at a flow rate of $0.8\,l/min$. Since the air sample travels a finite time span through the tube before arriving in the gas chamber, the signals of CO_2 and H_2O will lag behind the sonic signal. Two methods for adjusting the time
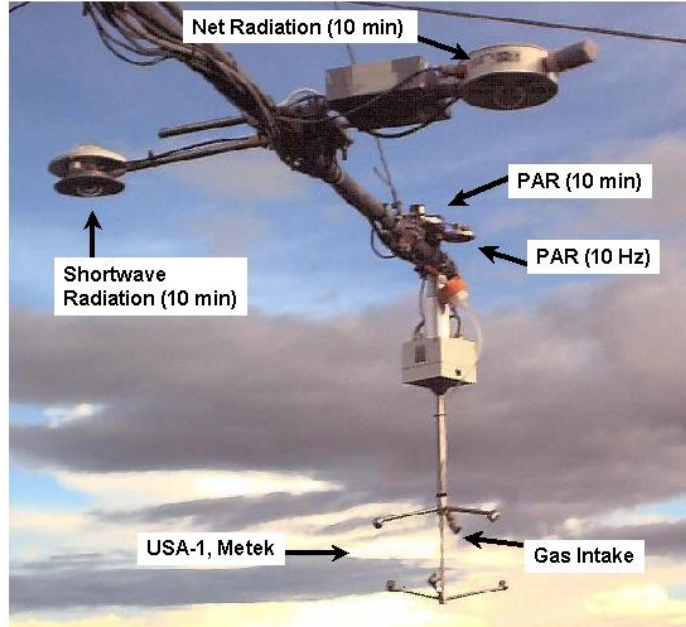
Figure 3.1: EC system at the Surumoni Crane station
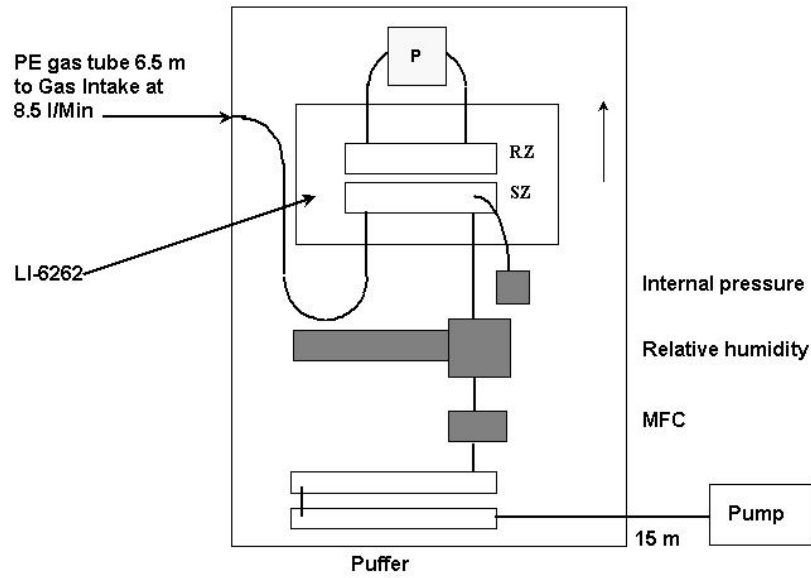
Figure 3.2: Schematic air sample circuit of the closed-path IRGA within EC system deployed at the Surumoni Crane station. SZ is the sample cell and RZ the reference cell of the IRGA. MFC stands for mass flow controller, and P for the pump in the reference circuit.

series are available. One involves the calculation of the air sample's travel time through the tube from the mass flow through the system and pressure drops across the intake tube, filters and valves have to be taken into account (Schütz, 1996). Along with the other method, time lags between the time series of the vertical wind velocity, $w(t)$, and gas density measurements of CO_2 and H_2O are corrected by maximizing the calculated covariances by adjourning the time series of w against the time series of CO_2 or H_2O respectively. The CO_2- and H_2O- signal also have to be corrected for the internal air pressure and air temperature of the sensor chamber (Aubinet et al., 1999). A comparison of the two methods is described in Schütz (1996) and Blank (2000), showing good accordance. Included in the EC system was also a PAR sensor (Li-190, LI-COR, Lincoln, Nebrasca) that measures photon flux density in the spectrum of photosynthetic active radiation (=PAR), i.e. within $400...700\,nm$ wavelength. The Li-190 has a response time of $2\,\mu s$ to changes in light conditions and can therefore be very well used for measurements at $10\,Hz$ most EC systems are run with.

3.1.3   EC open-path system

Due to the relative high power demand of an EC system including a closed-path infrared gas analyzer (IRGA), mainly contributed to by pumps, it is recommendable to use open-path sensors when measuring in remote areas with not reliable power supply and bad transportation routes. Open-path sensors are measuring directly in the wind field simultaneously to the sonic anemometer (see Chapter 4.3.2), when deployed next to the anemometer. This is in contrary to the closed-path sensor where the air sample is sucked through a tube of several meters length from the point of measurement into the sample cell. The Li-7500 sensor's infrared source is situated underneath a window in the sensor's body and has a color temperature of $1300\,K$ to produce a broadband IR beam. Absorption by CO_2 and H_2O are measured at a wavelength of $4.26\,\mu m$ with a bandpass of $0.15\,\mu m$ and $2.59\,\mu m$ with a bandpass of $0.05\,\mu m$ respectivly. The cross sensitivity between the CO_2- and the H_2O-signal is handled internally in the Li-7500's signal processing (see LI-COR LI-7500 manual).

If the window is wet due to rain fall or dew, more of the intensity of the IR radiation beam reaching the window is absorbed by the water thus pretending the air sample has a higher H_2O-density than it actually has. The Li-7500's sensorhead was tilted to facilitate rain water runoff. Therefore, the data needs to be filtered, using data from the Automatic Weather Stations (AWS) (see Chapter 3.3) recording rain events. Table 3.1 shows that data loss in the H_2O-flux amounts to $9 \pm 2\%$ during rain events, and to $34.5 \pm 1.5\%$ of half-hours with precipitation. Higher ratios of data loss are observed in the CO_2-flux with $13 \pm 1\%$ during rain events, and $91 \pm 9\%$ of half-hours with precipitation. The higher sensitivity of the CO_2-flux to precipitation events might be attributed to the cross sensitivity of the CO_2-signal to the H_2O-signal. The high sensitivity of the CO_2-signal to rain fall can be seen in the high half-hour standard deviation of CO_2-density, $std(CO_2)$, at half-hours of rain fall. An alternative filter to the above described use of precipitation data observed by AWS, is a limit value of $std(CO_2)$. Here $std(CO_2)_{limit} = 0.8$ is chosen. Rain events as were observed in the cocoa plantation, lasted normally from $0.5\,h$ to $2.5\,h$. The loss of data poses a disadvantage to the closed-path system, but also the ultrasonic anemometer is not functioning properly during rain fall due to scattering of the ultrasonic pulse by rain drops in the pulses pathways. The number of lost half-hourly data is acceptable, since the loss of half-hour data does not exceed the half-hours of rain events. It can be concluded that the sensor window's surface dries off relatively fast. The ratio of lost half-hourly data to total amount of measured half-hourly data is approx. 6%. Thus, the open-path IRGA proved to be very suitable for the conditions met in the tropical regions.

Table 3.1: Loss of half-hours of data from the open-path sensor LI-7500 due to rain events at the second site in the cocoa plantation, Nopu, measurement period March 17, 2003 to April 18, 2003. Total precipitation during this period amounted to $357.6\,mm$.

Number of half-hours	All data	Daytime data, 7:00-18:00 LT	Ratio to N_{prec} All data	Ratio to N_{prec} Daytime
with precipitation ($\equiv N_{prec}$)	237	134		
of lost data during rain events for the H_2O-flux	27	10	0.11	0.07
of lost data in total for the H_2O-flux	86	44	0.36	0.33
of lost data during rain events for the CO_2-flux	32	16	0.14	0.12
of lost data in total for the CO_2-flux	195	134	0.82	1.0

The EC system used for the measurements in Indonesia includes an open-path IRGA (Li-7500, LI-COR, Lincoln, Nebrasca). Assembled into this system were also two passive infrared temperature sensors (Raytek, Berlin) to measure the surface temperature of the canopy with a beam widening fraction of 1 : 2. The sensors are not only receiving the thermal radiation of the canopy surface but also of the air column between the sensorhead and the surface. For relative humidities below 90%, the thermal radiation of the air column can be disregarded (Witte, 1993). Daytime relative humidity was observed to range from 40% to 80% in the cocoa plantation in Nopu, Indonesia. The sensors were mounted at $6\,m$ above mean canopy height. The thermal radiation of the air column between point of measurement and surface can thus be disregarded. IR temperatures of the canopy surface were measured in South and North direction of the EC system to account for the heterogenity of the canopy's composition (see Chapter 5.2). Total configuration of the system can be seen in Figure 3.3 The loss of covariance due to the sensor separation of the ultrasonic anemometer and the CO_2- and H_2O-measurements are described in more detail in Chapter 4.3.3.
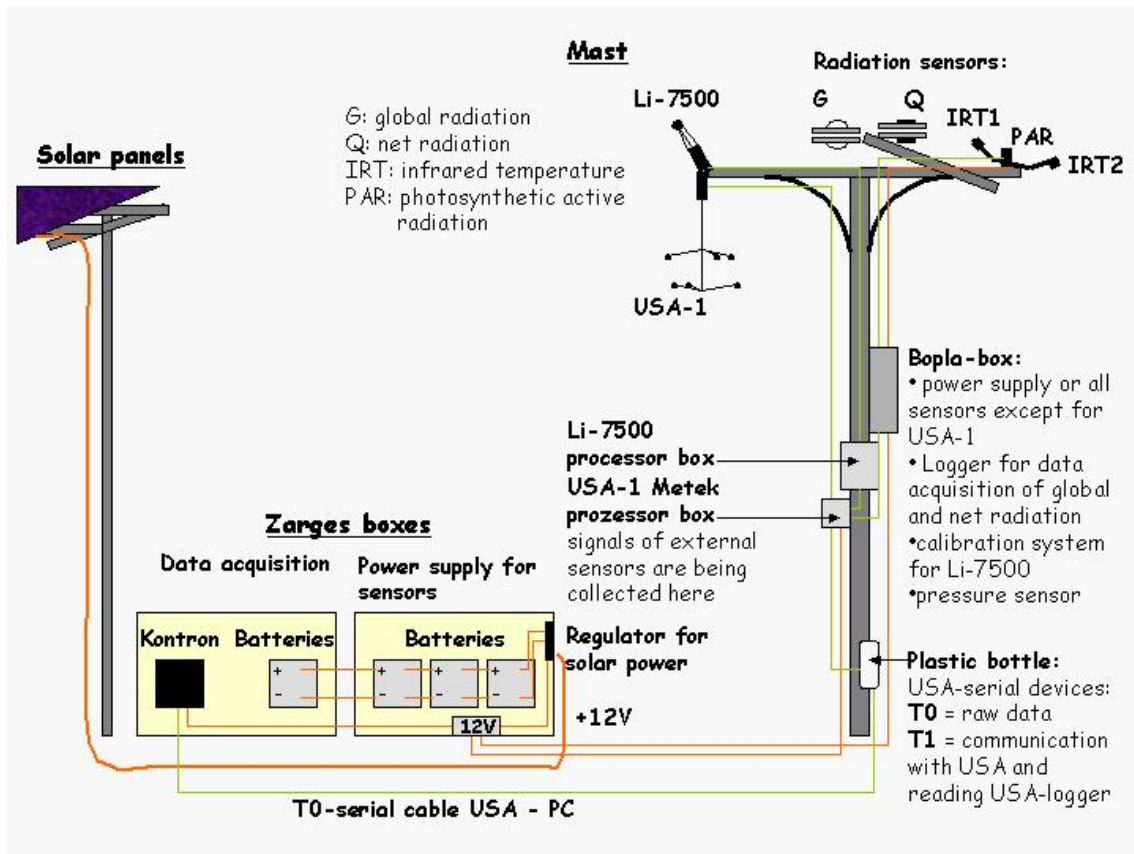
Figure 3.3: EC system design for EC measurements in the cocoa plantation, Nopu, the same system configuration is installed at the micrometeorological tower site, Besoa, Inonesia

3.2 Energy balance components and carbon fluxes

Additional information and data are needed for the correction and the verification of the EC measurements. The energy balance equation (Chapter 2.1.3) is used as a plausibility check to verify the measurements of the turbulent heat fluxes. The net radiation is derived from measurements of the up- and downward directed long- and shortwave components $L\uparrow$, $L\downarrow$, $K\uparrow$ and $K\downarrow$ (see Chapter 2.1.3).

3.2.1 Measurement of long- and shortwave components of net radiation

The components of the net radiation are measured by two net pyrgeometers CG1 (Kipp and Zonen, Delft, Netherlands) for the up- and downward longwave components, $L\uparrow$ and $L\downarrow$, and two pyranometers CM6B (Kipp and Zonen, Delft, Netherlands) for the up- and

downward shortwave components $K \uparrow$ and $K \downarrow$. The pyrgeometer CG1 is a sensor designed for measuring the infrared radiant flux on a plane surface and the pyranometer CM6B for neasuring the irradiance on a plane surface, which results from the direct solar radiation and the diffuse radiation incident from the hemisphere above. The sensor signal's are then computed to radiation flux densities in W/m^2. Data acquisition was realized by a datalogger Combilog (Friedrichs, Hamburg). The sensors were sampled every second and data were stored as $5\,min$ averaged mean values. For the analysis of the EC measurements the barometric pressure is also needed (see Chapter 2.1). A barometric pressure sensor Barotransmitter Typ 5002 (Friedrichs, Hamburg) was included into the radiation measurement system. The sensitivity of the pressure sensor at temperature $T = 20\,^{\circ}C$ is at $\pm 0.3\,hPa$ (Technisches Datenblatt, Friedrichs, Hamburg).

3.2.2   Transfer processes within a vegetation stand, and between vegetation and atmosphere

The components of the water balance equation and CO_2-budget were estimated using the Soil-Vegetation Atmosphere-Transport model MixFor-SVAT (Oltchev et al. (1996), Oltchev et al. (2002)). MixFor-SVAT is a multi-layer model that describes the vertical distribution of radiation, momentum, energy and matter fluxes within- and above mono- or multi-specific tree stands at 30-min resolution. Water fluxes in the plants are computed using a non-steady-state approach (Hunt et al., 1991). MixFor-SVAT is a modular model that integrates other sub-routines describing radiative transfer, turbulent transfer, soil water dynamics, plant water use, and net- and gross ecosystem production. All parameters determining the physical boundary conditions as well as biological stand parameters were either measured at the experimental site (Merklein, 2003) or taken from the literature (e.g. Deng et al. (1990), Miyaji et al. (1997)). A list of the principal input parameters of the model was provided by A. Oltchev and is diplayed in the Appendix B.1. The heat transfer between atmosphere and vegetation is needed for completion of the energy balance equation. The core of a SVAT model is the computation of the **Penman-Monteith** equation 2.17 and the stomatal and aerodynamic resistances of a canopy (see Chapter 2.1.3) The meteorological boundary conditions in the surface layer and within the canopy set up the framework for the interactions between vegetation and atmosphere.

In this work, measurements of the turbulent heat fluxes are compared to the output of the MixFor-SVAT model by Oltchev et al. (1996), Oltchev et al. (2002). In February until April 2002, a field campaign was carried out by Merklein (2003) to determine photosynthesis

parameters, from the light response curves of the plants, as maximal photosynthesis rate and leaf respiration. Merklein (2003) also gives structural parameters, such as distribution and species of trees in the regarded plantation, and leaf area index (LAI). As input for the atmospheric boundary conditions, the respective atmospheric variables derived from EC and automatic weather stations (see Chapter 3.3) measurements are used. Results from the SVAT model are also used for completion of the energy balance equation in Chapter 5.3.

3.3   Automatic Weather Stations (AWS)

During rainfall, EC systems are not working properly as discussed in Chapter 3.1. Rain drops within the optical pathway of the ultrasonic anemometer causes scattering of the ultrasonic pulses and spikes in the data set. The reason for the malfunction of the open-path infrared gas analyzer is the wetting of the window under that the infrared source of the Li-7500 is situated, leading to higher absorption of the IR beam and to an overestimation of water vapourthe content in ambient air. Rainfall data from two AWS described in the following is used to extract data at rain events from the data set. Automatic weather stations are designed to measure atmospheric variables on a long-term basis with minimal maintenance, including measurements of relative humidity, air temperature and wind speed at one or more heights, wind direction, rain fall, soil temperatures, soil heat flux, and radiative components. Within the project STORMA (see introduction), a net of AWS was set up and maintained by Heinrich Kreilein and Thomas Grelle (IBK, Univ. Göttingen), around the Lore Lindu National Park (=TNLL). One of the AWS was situated in a corn field near the village Rahmad in the vicinity of the EC site, coordinates 01°10.768' S and 120°05.021' E until March 2003, and on a meadow, coordinates 01°03'30.4" S and 120°03'34.2" E from April 2003 on. An additional AWS with slightly different configuration was set up by Kleinhans (2004), $STORMA$ subproject B2, on a hill slope above the cocoa plantations, in about $2\,km$ distance, and included into the AWS network. From both stations, rainfall data as $5\,min$-averaged means are used to identify flawed raw data. These data are excluded in the further analysis of the EC measurements.

3.4   Mapping of the Nopu catchment area

The research site in the Palolo valley (see map Chapter 5.1) near the village Nopu-Rahmat lies within an area that is covered with small cocoa plantations that form one big area

of cocoa, and matches the requirements of the applied EC technique (see Chapter 2.2). Around 1989, the area of investigation was cleared of rain forest, according to the farmers, and planted with Cacao trees, *Theobroma Cacao* L.. Since cocoa trees need to be shaded especially when younger, shadow trees, *Gliricidiae sepium (Jacq)*, had been planted in a certain pattern (Merklein, 2003) and trees of the former forest had been left standing to serve as wind breaks and sun shades. The plantations in Nopu consist not only of fields of cultivated cocoa, but also serve as environment and home to the farmers and their families. The whole area of cocoa plantations is interspersed with wooden farm houses, which also represent sources of carbon dioxide due to e.g. cooking or small power plants. A detailed mapping of the Nopu catchment area was carried out in march 2002 by a team of UNTAD students working for subproject B1. The investigation included mapping of the area within $500\,m$ circumference around the EC mast with tape measure, GPS device and barometric pressure sensor. In order to achieve information about the amount and time of use of fuel for small power plants and wood or gas for cooking and other human activities connected with possible release of carbon into the atmosphere, a survey of the households within the catchment area of the EC measurements was carried out. The results of this survey are used in Chapter 5.2 for the footprint analysis of the measured turbulent fluxes.

Chapter 4

Data analysis

4.1 USA1 sensorhead correction

The ultrasonic anemometer itself is constituting an obstacle in the wind field it measures and is therefore causing disturbances in the wind field. These effects have to be corrected for. The usual way to calibrate wind sensors is in a windtunnel, where the sensor is exposed to a horizontal laminar wind flow with a known velocity. Bleyl (2001) carried out a calibration for the USA-1 sensorhead. In the following, the azimuthal angle denotes the horizontal and the tilt angle Θ_{wk} the vertical tipping of the sensorhead towards the vertical axis of the wind flow. The sensor was mounted upside down from the ceiling in the wind tunnel, i.e. $\Theta_{wk} = 0°$. If the sensor was pointed into the incoming flow, the tilt was counted positive and negative in the other direction. Due to the mounting of the sensor in the wind tunnel (upside down from the ceiling of the wind tunnel), tilt angles in the range $[-25°, 25°]$ could only be measured. His results show a clear symmetry of $120°$ in the azimuth that is induced by the sensorhead's design (see Figure 3.1). The tilt angles used in the sensorhead calibration denote the tipping of the incoming flow versus the vertical axis of the USA-1 sensorhead.

Looking at the distribution of tilt angles occuring in atmospheric flow (Ibrom, 2000), the need for a sensor head correction for a tilt range within $[0°, 90°]$ for incoming flow becomes obvious. In 2002 a bachelor thesis was conducted at the IBK to build an enhanced correction for the sensorhead of the USA-1 (METEK, Elmshorn). Within his master thesis Krüger (2002) carried out a field campaign with two USA-1 sensorheads at the Göttinger Forest site (Institute of Bioclimatology, Germany). He used one ultrasonic anemometer USA-1 as reference with vertical tilt of $\Theta = 0°$ of the sensorhead, and the other one measuring at tilts from $90°$ (upside) to $0°$ and in horizontal plane at azimuths in the range of $[0°, 120°]$

and $[180°, 300°]$. Both, azimuth and tilt, were rotated in steps of $15°$. Comparison of the correction matrix for a measured wind field derived from the wind tunnel calibration in the tilt range of $[-25°, 25°]$ show accordance by 93.46% (Krüger, 2002). From the measurements A. Ibrom calculated a correction matrix and developed a software routine. This routine was used here and included in the post-processing software that originated from Morgenstern (2000) and adapted to the new measurement systems.

The application of both sensorhead corrections to the data of the EC measurements in Nopu show an average increase in fluxes of approx. 12% for the wind tunnel correction and 24% for the insitu correction. (Bleyl, 2001) finds an increase in the horizontal wind velocity u of 15% and in the turbulent sensible heat flux H of 25% compared to the uncorrected values of u and H respectively. This is about in good accordance with the factor of 1.15 METEK applies to the wind data for sensorhead correction. Analysis of the data from the Nopu site show an increase in w of 17% and in H of 12% when applying the wind tunnel correction. For the application of the insitu correction, an increase in w of 20% and in H of 24% is found. Ibrom (2000) points out, that the vertical fluxes from the canopy to the atmosphere can often be associated with high tilt angles of the incoming flow to the ultrasonic anemometer, in especally $|\Theta_{wk}| > 25°$. Thus it can be concluded, that the insitu sensorhead correction is better suited for the measurements in the field.
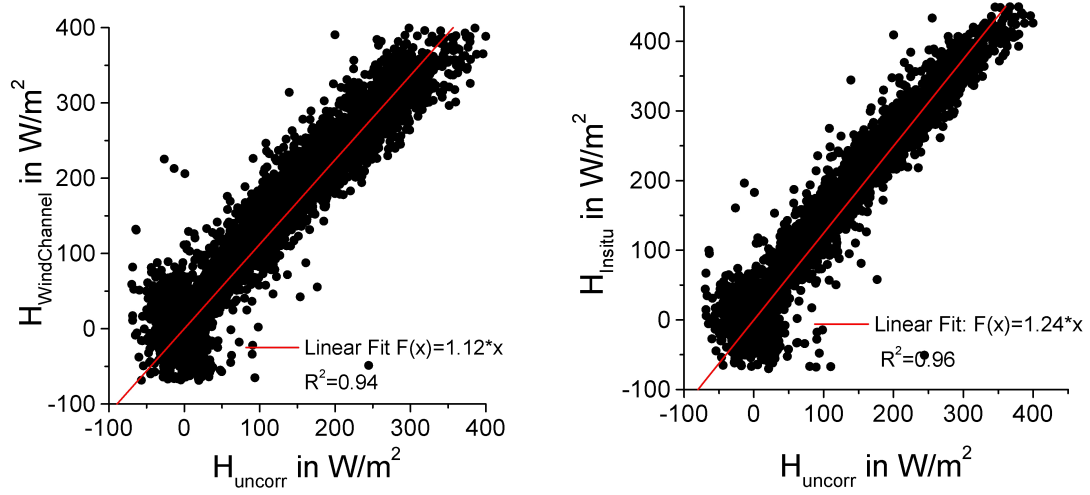
Figure 4.1: The sensible heat flux corrected by the Windtunnel-Correction (left) and corrected by the Insitu-Correction (right) against the uncorrected sensible heat flux, plotted are half-hourly averaged mean values
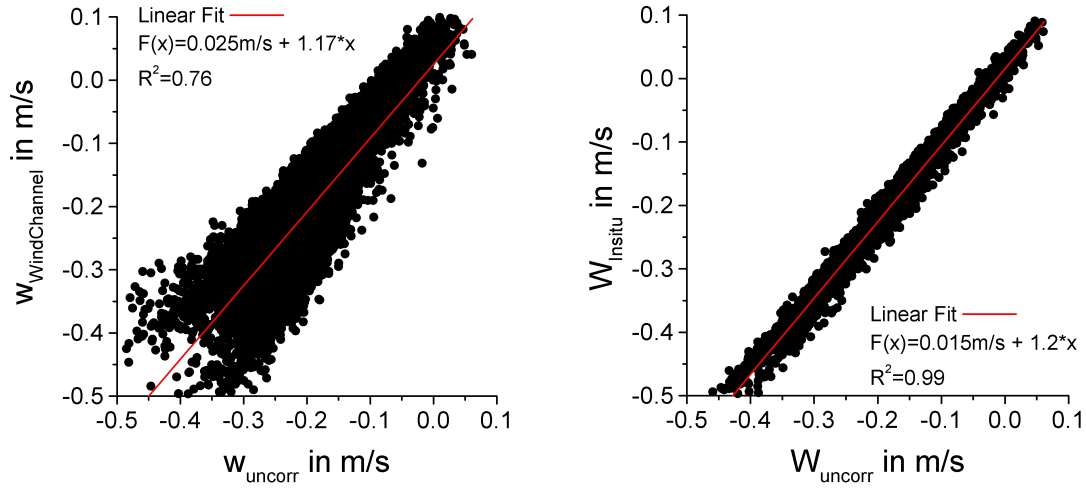
Figure 4.2: The vertical wind velocity corrected by the Windtunnel-Correction (left) and corrected by the Insitu-Correction (right) against the uncorrected sensible heat flux, plotted are half-hourly averaged mean values

4.2 Licor calibrations

4.2.1 Closed-path IRGA, LI-6262

LI-COR uses a third order polynomial, F_{CO_2/H_2O}, determined by factory calibrations for calculating the mixing ratio C of CO_2 or H_2O from the Li-6262 output V in $Volt$ (LI-COR, 1991b). The mixing ratio of CO_2 and H_2O in ambient air is then given by

$$C = F_{CO_2/H_2O}\left(s(V - off)\frac{P_0}{P}\right)\frac{T}{T_0}, \tag{4.1}$$

relating signal output to gas mixing ratio's. Here, T and P are temperature in K and pressure in hPa in the Li-6262's sample cell and T_0 and P_0 the respective atmospheric variables at measurment height. s and off are the span and the offset, that have to be determined by calibration measurements. For offset calibration, a zero gas, i.e. a gas with zero mixing ratio C_0, has to flow through the sample cell of the Li-6262. The offset is then given by

$$0 = F_{CO_2/H_2O}\left(s(V_0 - off)\frac{P_0}{P}\right)\frac{T}{T_0}. \tag{4.2}$$

Due to the structure of the polynomial F_{CO_2/H_2O} the only solution is $V_0 = off$. Span calibration is done with a gas of known mixing ratio C_s:

$$C_s = F_{CO_2/H_2O}\left(s(V_s - off)\frac{P_0}{P}\right)\frac{T}{T_0} \Rightarrow \frac{F_{CO_2/H_2O}^{-1}\left(s(V_s - off)\frac{P_0}{P}\right)}{\frac{P_0}{P}(V_s - V_0)} = s. \tag{4.3}$$

For the CO_2 and H_2O measurements at the Surumoni site (see chap. 6.2), a closed-path sensor, Li-6262 (LI-COR, Lincoln, Nebraska) was used. The calibration of offsets for CO_2- and H_2O-channel of the Li-6262 was realized by zero gas measurements in a closed cycle, where residual CO_2 and H_2O was removed by cycling the flow through desicant reservoirs filled with soda lime (for CO_2) and magesium perchlorate (for H_2O) following the instructions by LI-COR (1991b). Span measurements of the Li-6262's H_2O-channel were achieved by assembling a calibrated measurement device A1H (Rotronic, Ettlingen) into the measurement cycle, giving the relative humidity and temperature of the incoming flow as reference. Span measurements of the Li-6262's CO_2-channel require a calibration standard with gas of known CO_2 mixing ratio. Transportation of a pressurized gas bottle by airplane is not an easy issue. It was thus decided to acquire the gas standard for the CO_2-span measurements in Caracas, capital city of Venezuela, and have it transported to the Surumoni crane site. Despite the combined efforts and help of the German embassy and local alumni, it turned out to be impossible to have the calibration gas transported to the Surumoni crane site in

Table 4.1: List of Calibrations of the Li-6262's CO_2- and H_2O-signals at the Surumoni crane site

Date	CO_2 offset	CO_2 span	H_2O offset	H_2O span
11.04.2000	378	0.7498	106	0.8952
01.06.2000	478	0.8226	780	-
04.06.2000	470	-	805	1.4955
10.06.2000	947	1.0014	1726	-

time. For the onsite-span calibration, a gas bottle was filled by a compressor with ambient air. Samples of that gas were brought in three steel containers to Germany for analysis of the CO_2-content of the span gas used at the Surumoni site. Span measurements of CO_2 on April 11th (see Table 4.1) were done with a photosynthesis measurement device, Li-6400 (LI-COR, Lincoln, Nebraska). The Li-6400 can produce an air outflow with calibrated CO_2-mixing ratio by mixing CO_2 into the air flow that was directed into the Li-6262's sample cell. Measurements at the Solling site (Morgenstern, 2000) show a slow drift of span and offset with regard to time, whereas Figure 4.3 show a rapid change in both. This is due to water entering the the Li-6262's sample cell on June 06th, 2000. A net was assembled over the gas intake to provide protection from the numerous bees and wasps entering the intake tube. During a heavy rainfall event the net was wetted and the water sucked with ambient air into the sensor's sample cell. This led to a discrete jump in the offset and span of both CO_2- and H_2O-channel. In order to avoid a further water inleakage, the intake was covered by a plastic shelter. For analysis, the calibrations of CO_2 and H_2O from date 01.06.2000 and 04.06.2000 are used for the measurement period before the water break-in and calibrations from date 10.06.2000 for the period after.

Figure 4.4 shows the derived water vapour and carbon and sensible fluxes for the measurement period above neotropical rain forest at the Surumoni crane site, Venezuela. Throughout the three weeks of measurements the latent heat flux is exceeding the sensible heat flux during daytime. During nighttime, the heat fluxes are slightly negative or close to zero. The net ecosystem exchange NEE_{CO2} shows an uptake of CO_2 by the vegetation of about $-10\,\mu mol\,m^{-2}s^{-1}$ in the overage over the measurement period. Interestingly, peaks in the transfer of CO_2 from the vegetation to the atmosphere can be observed in the morning hours. The build-up of the convective boundary layer and the rising wind velocities seem to "flush out" the CO_2 from the canopy respired by the plants at nighttime. Further analysis will be carried out in Chapter 6.2.
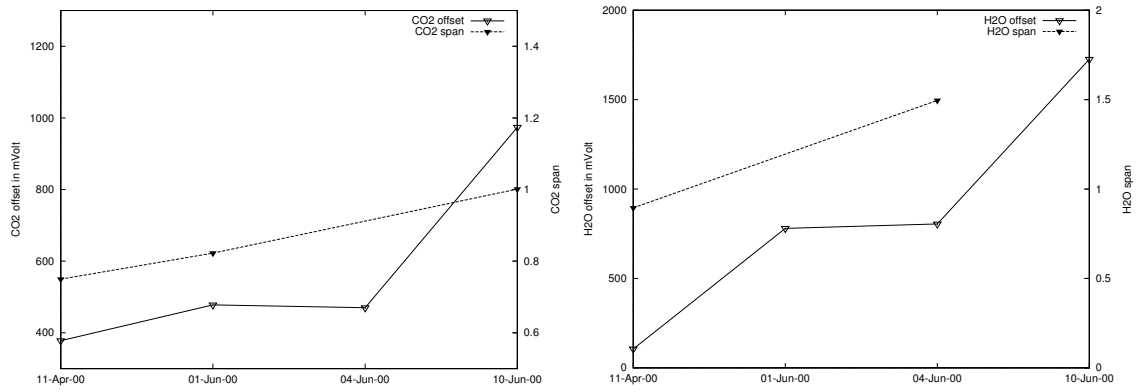
Figure 4.3: Calibrations of the Li-6262's CO_2- and H_2O-channel at the Surumoni crane site
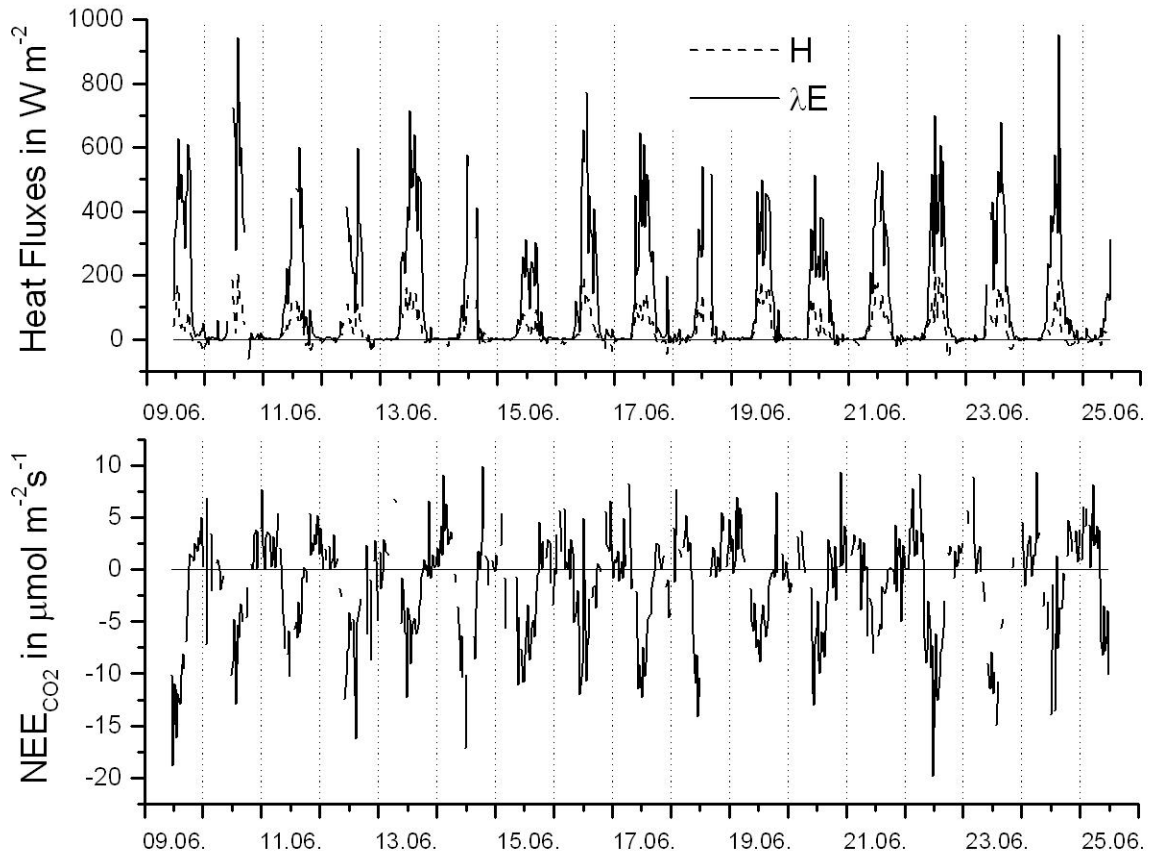
Figure 4.4: Measurements of turbulent fluxes of latent (blue) and sensible (red) heat (above) and CO_2 (below) at the Surumoni crane site in the period from June 9th to June 25th 2000. The direction of the fluxes from the canopy into the atmosphere are defined as positive

4.2.2 Open-path IRGA, LI-7500

The electrical signals of the CO_2 and H_2O channel outputs underlie shifts with regard to time, due to aging of the sensor's components and commotions as for instance appear when transporting the sensor. Calibration of the signals therefore have to be carried out in sufficient small time periods. For calibration, a cuvette has to be brought into the beam aisle and gas of a known CO_2 and H_2O -concentration sucked through a tube and the cuvette by a $12\,V\,DC$ pump. For the CO_2 channel, a one-point calibration was used with zero-gas, gas with zero concentrations of CO_2 and H_2O respectively, and a gas standard as span-gas. The zero-gas was provided from ambient air sucked through a CO_2-desiccant (i.e. lime soda) reservoir and a H_2O-desiccant (i.e. magnesium perchlorate) reservoir. The order of the desiccants is important, since the CO_2-desiccant needs a small amount of water vapour to extract the CO_2 out of the air sample and the purgation of the zero-gas from H_2O to avoid possible cross spectral effects of water vapour in the CO_2 absorption spectrum. By purging the chamber with desiccated ambient air, residuals of CO_2 and H_2O in dead volumes of the tube and cuvette are slowly removed from the calibration circuit. Visualization of the CO_2- andH_2O-signal show an exponentially decline and an oscillatory behaviour thereafter. The set of the zero calibration can be conducted if the signal is stably set on one value and the above behaviour cannot be seen any more. It can then be safely assumed that the gas in the sample beam aisle is indeed of zero-gas concentration. For span-gas a standardized gas of $369.4\,ppm$ was used. Calibration of the H_2O channel was realised with a dew point generator, the Li-610 (LI-COR, Lincoln, Nebrasca), for measurements at different dew points and ambient air sucked through two H_2O-desiccant reservoirs to provide a zero-gas. The Li-610 Portable Dew Point Generator is a completely self-contained instrument used to generate a moist air stream with a known dew point (LI-COR, 1991a).

The dew point τ is the temperature at which moist air will be saturated with water vapor if it is cooled at constant pressure and mole fraction. The saturation vapor pressure of moist air at a given temperature θ measured in $\deg C$ is given by the Magnus formula

$$e_W^\star(\theta) = 6.1078 \cdot e^{\frac{17.1 \cdot \theta}{235 + \theta}} \,,\ [e^\star(\theta)] = hPa \tag{4.4}$$

The calibration system for the EC system was designed for the use on a tower, in especially the tube lengths were designed to be short and not exceeding a length of $2\,m$. The tubes used for the calibration cycle are out of polyethylene (PE), a component that releases a small amount of CO_2 when exposed to high amounts of solar radiation. Since the EC system was mounted on a $11\,m$-mast in the cocoa plantation with no platform to bring up the calibration

system, the tube length extended over $12.5\,m$. Additionally, insolation near the equator is rather high. Calibrations in July 2002 showed, that no stable CO_2- or H_2O-signal could be achieved, while the EC system was mounted on the mast. After dismantling the system and before moving the measurements to the second site in the cocoa plantation, a whole calibration of the Li-7500 was carried out on the 15th and 17th of march 2003 in a small wood house, allocated by a farmer for use as a field station. Analysis of the calibration data from March 2003, show a zero-shift in the CO_2-signal of $39.9\,ppm$ and a span-factor of 1.05313. For the H_2O-signal, a zero-shift of $0.28\,mmol/mol$ and a span-factor of $1.0546\,mmol/mol$ was measured (see Table 4.2 In June 2003, the Li-7500 was brought back to Germany for alteration of the reference filters (see chap. 4.3.1), where repeated calibrations showed a zero-shift in the H_2O-signal of $0.38\,mmol/mol$ and in the CO_2-signal of $42.25\,ppm$. That can be ascribed to the impact of transportation, but also to the systems configuration, in which the sensor is included. In Nopu, the sensor was calibrated running within the EC system, whereas in Germany, the sensor was calibrated as a stand-alone system. Besides that, the two calibrations are in very good accordance and prove the long-term stability of the open-path sensor. The transportation of the measurement equipment to the cocoa plantation was realised by ox cart, and although safely packed, the sensors were probably subject to some bounces. Thus, the calibration in Nopu is used for the entire measurement period there. The fluxes of CO_2 and H_2O need further corrections as will be discussed in the following subchapters, the corrected fluxes of CO_2 and H_2O will be discussed in Chapter 5.

Table 4.2: List of Calibrations of the Li-7500's CO_2- and H_2O-channel at the Nopu site

Date	Place	CO_2 offset	CO_2 span	H_2O offset	H_2O span
15.03.2003 + 17.03.2003	Nopu, Indonesia	$39.9\,ppm$	1.05313	$0.28\,mmol/mol$	1.0546
30.07.2003	Effeltrich Germany	$42.25\,ppm$		$0.38\,mmol/mol$	1.0263

4.3   Corrections of the Li-7500 signal

4.3.1   Influence of solar radiation and low frequency corrections

The Li-7500 open-path infrared gas analyzer uses an infrared source with a color temperature of $1300\,K$. CO_2 absorption is measured at $4.26\,\mu m$ with a bandpass of $0.15\,\mu m$, whereas H_2O absorption is measured at $2.59\,\mu m$ with a bandpass of $0.05\,\mu m$. The Li-7500 measures the ratio of CO_2- and H_2O-absorption beam to a reference beam at $1.8\mu m$ for CO_2 and $2.35\mu m$ for H_2O. Unfortunately, the first release of the Li-7500 sensors turned out to be sensitive to direct solar radiation being reflected in the attenuation portion of the CO_2 filter at $1.8\mu m$ and H_2O filter at $2.35\mu m$. Since there is still a fair amount of solar energy beyond $1.8\mu m$, this was causing shifts in the CO_2 and H_2O output (4.7). A decrease in CO_2-density is
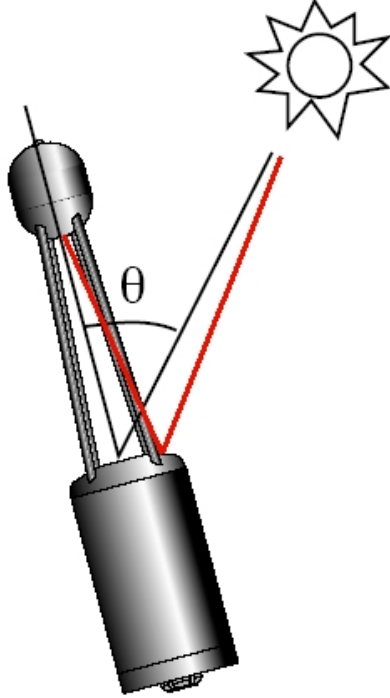
Figure 4.5: Schematic drawing of LI-7500 open-path IRGA sensorhead.

negatively correlated to quantum flux density (Figure 4.6). The infrared part of the solar spectrum received by the Li-7500 receiver causes the reference beam of CO_2 and H_2O to be of higher intensity and thus leads to an underestimation of CO_2- and H_2O-densities measured by the Li-7500.

To investigate the potential effects caused by incident near-infrared, the sensors were shadowed in time steps of 5 to 10 s on a day with cloudless sky. Figure 4.7 shows an example
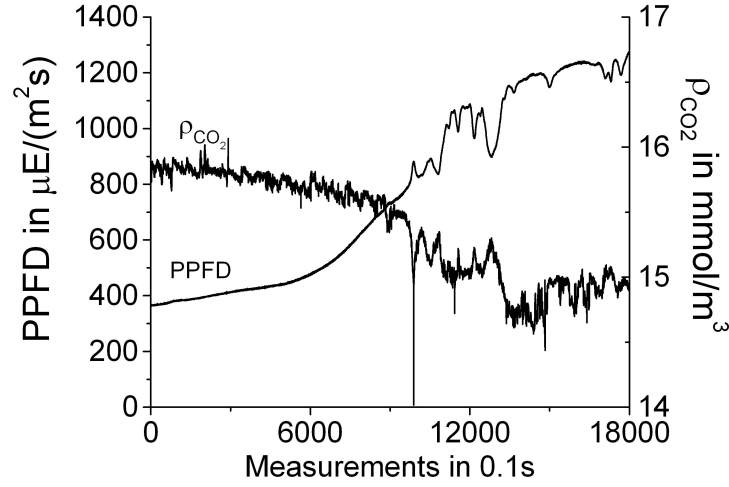
Figure 4.6: a) Uncorrected raw CO_2-density (right axis) photosynthetic photon flux density PPFD (left axis) measured by Li-7500 at the Nopu site, 21-Oct-02 9:15 LT.

of such a timeseries. Shadowed time periods are apparent in the discrete decrease to higher densities of CO_2 and H_2O . The offset caused by insolation on the H_2O-density is approximately the same magnitude then the H_2O-fluctuations in the surface layer of the atmosphere. Thus an effect on the derived covariance can not be seen for most times. The effect on the CO_2-densities on the other hand is an order of magnitude higher than the atmospheric CO_2-fluctuations. This introduces additional covariance of $Cov(w, CO_2)$ that is not a component to the "true" flux.

In order to investigate this further, a calibration was carried out on the 7th of August together with the company Walz (Effeltrich, Germany), distributing the Licor systems in Germany. The Li-7500 sensorhead was mounted on a tripod above grassland, where tilt angle Θ_{lic}, and azimuth angle ϕ, could be varied in the range of $[0° : 90°]$ and $[0° : 360°]$ respectively. Here, $\Theta_{lic} = 0°$ denotes the parallel alignment of the Li-7500 sensorhead with the incoming solar radiation. The tilt angle was changed in steps of 5° from 85° to 5°. The red line in Figure 4.8 denotes the sequence of measurements for tilt angles from 85° to 5° in steps of 5°. There are two tilt areas with a marked response in the measured CO_2-density to solar radiation, $\Theta_{lic} = 10°$ and $\Theta_{lic} = 35°$. This can be explained with the sensors symmetry. The incident shoulder around the source window is bevelled for rain water run-off. When the angle between the sensor's vertical axis and the incoming solar radiation is 35°, incident radiation is reflected into the Li-7500's receiver window. The next peak at $\Theta_{lic} = 10°$ can
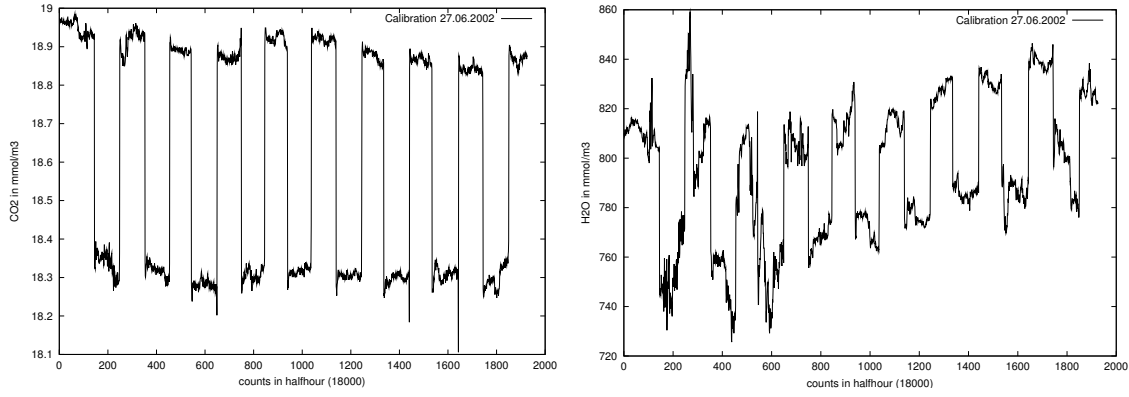
Figure 4.7: Effect of direct solar radiation on the CO_2-channel (left) and H_2O-channel (right) of the Li-7500 gas analyser measured by shadowing the sensor in time intervalls of 5 to $10\,s$ on 27.06.2003

be explained by reflections at the source window itself. The minimum at $\Theta_{lic} = 5°$ is caused by the Li-7500 receiver shadowing the window. Additionally, the sensor was rotated for tilts with high response of the CO_2-signal to solar radiation, i.e. for tilts $\Theta_{lic} = 25°, 30°, 35°, 40°$, so that the shadows of the struts supporting the receiver were fully (black dots), partly (blue dots) or not at all (black dots) over the source window. The shadowing caused by the struts shows large variances is the measured densities. Thus, creating a correction function as indicated by the blue line in Figure 4.8, was abandoned and instead a filtering technique applied to the measurements of CO_2 and H_2O for the Nopu site as will be described in the following. The effects of incident radiation on CO_2- and H_2O-densities follow the diurnal cycle of the sun, and are caused by changes in cloudiness. The first leads to a trend in first order in the Li-7500 signal output, as can be seen in Figure 4.6, and can be removed by detrending the $30 - min$ data sets of the EC measurements in Nopu.

The changes in cloudiness can appear on different scales from long term changes up to changes on the scale of more than one hour or less than one minute. Transforming the data sets of CO_2 and H_2O using Fast Fourier Transformation (FFT, Press et al. (1992)), the frequencies can be removed after a cut-off frequency f_c and applying the reverse FFT, the frequency-cleaned data sets of CO_2 and H_2O respectively are achieved. The computed covariance $Cov(w, CO_2)$ is plotted against the cut-off frequency f_c in Figure 4.9 (right). Cospectral similarity between the vertical wind velocities and scalar quantities can be assumed (see Chapter 2.1). Thus, the cleaned CO_2- and H_2O-frequencies can be replaced by the respective frequencies of the temperature spectrum with respect to the ratio of cleaned spectral density to the spectral
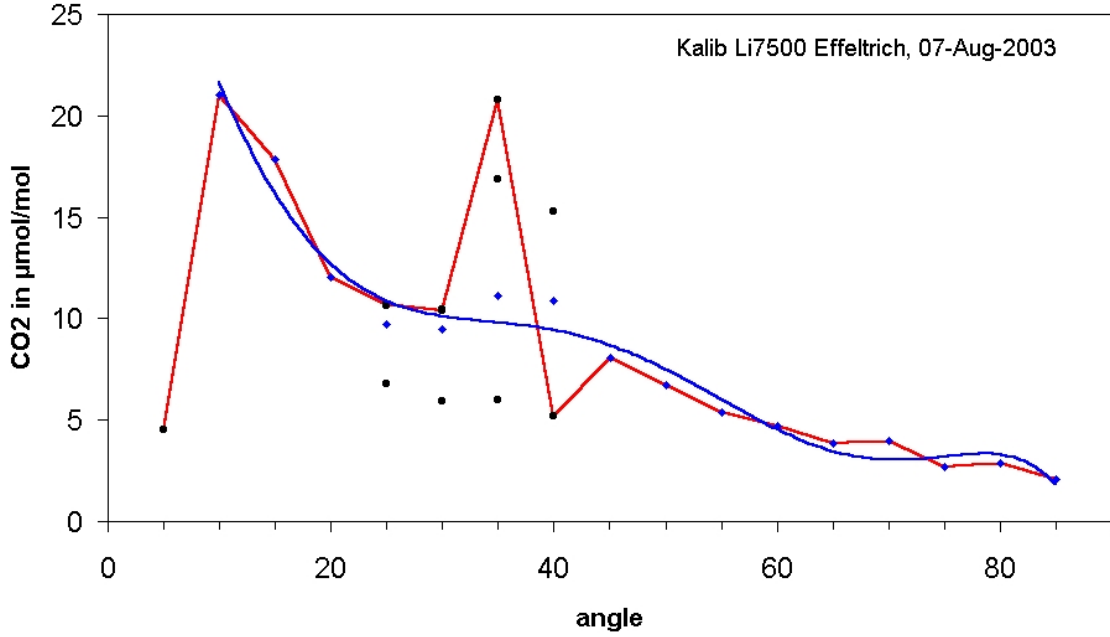
Figure 4.8: Measurement of the Li-7500 gas analyser's response to direct solar radiation versus the angular of the sensor's vertical axis to inclination measured by shadowing the sensor in time intervalls of 5 to $10\,s$ on 08.07.2003 on a grassland in Effeltrich, Germany. The red line indicates the sequence of measurements from angle $\Theta_{lic} = 85°$ to 5° in steps of 5°. Additional measurements within the range $[25° : 40°]$ were made subsequently. The blue line shows a fit by a 3rd order polynomial.

density of the unaltered part of the spectrum.

$$\sum_{n=f_0}^{f_c} S_C(n) = \sum_{n=f_0}^{f_c} S_T(n) \cdot \frac{\sum_{n>f_c} S_C(n)}{\sum_{n>f_c} S_T(n)} \tag{4.5}$$

It is not recommendable to choose a cut-off frequency higher than the maximum of the spectrum, to limitate the uncertainty in the derived CO_2- and H_2O-spectra. The maximum lies above $f_{max} = 0.01\,Hz$ (Figure 4.9 (left)). Hence correcting the CO_2- and H_2O-data sets a cut-off frequency below the maximum, $f_c = 0.0089\,Hz$, is chosen here.
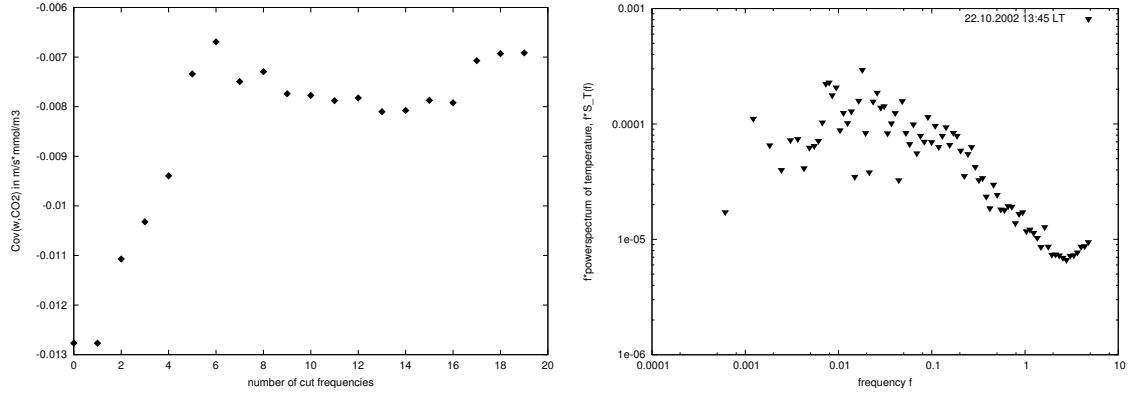
Figure 4.9: Example of the derived covariance Cov(w,CO_2) versus the number of cut-off frequency (left), and normalized air temperature spectrum $f * S_T(f)$ plotted against the frequency f (right), Nopu site on the 22.10.2002 13:45 LT.

4.3.2 Corrections of CO_2- and H_2O-fluxes handling internal lag time of Li-7500

The Li-7500 optical bench returns an analogue output signal to the Li-7500 processor box, where it is converted to a digital signal as input to the Digital Signal Processor (DSP) for computing the gas densities. This process has a fixed delay, which LI-COR specifies to vary between $138\,ms$ and $197\,ms$ for the actual DAC, version 2.0.4 (LI-COR communication, 2003). The signal is then converted back for analogue output to the ultrasonic anemometer, which takes about $50\,ms$. There is an additional user programmable delay to make the Li-7500 give an output on the sampling interval used within the EC measurement system, that is $6.579\,ms$ as delay step for the measurements at the Nopu site. With a number of 11 increment steps, this leads to a user programmable delay of $72.369\,ms$ and a total delay of about $250\,ms$ to $319\,ms$ (see table 4.3). To cope with this effect, in this work a covariance maximization is carried out. That means, the time series of H_2O and CO_2 are shifted against the time series of vertical wind speed by 0 to 5 sample steps and the covariances are calculated and the maximum covariance is taken as the true covariance of vertical wind with H_2O and CO_2 respectively.

Table 4.3: Delay times of the Li-7500 DAC output

Software Release	Delay Time (ms)	Delay Step (ms)	Delay Step Increment	Total Delay (ms)
Actual DAC (2.4.0)	138...197 mean (167 ± 30)	6.579	11	210...269 mean (250 ± 30)

4.3.3 Underestimation of CO_2- and H_2O-fluxes due to sensor separation of the infrared gas analyzer and the ultrasonic anemometer

The eddy-covariance method relies on the assumption that the scalar signal and the velocity signal are considered to refer to the same point in space. When measuring with two sensors, one for the scalar and one for velocity, this assumption is not valid. The two sensors have to be mounted with horizontal or vertical displacement, or both. Kristensen et al. (1997) classify the problem as an increasing function of the ratio of sensor displacement and the scale of turbulence. Lee and Black (1994) adress the case of horizontal sensor displacement and achieved a functional interrelation between the measured and the true flux for horizontally displaced sensors based on the similarity cospectrum obtained by Wyngaard and Coté (1972). Kristensen et al. (1997) point out that since the scales, and corresponding wavelengths and spectral maxima, of vertical wind and a scalar are approximately proportional to the height, the upper spectra are displaced with regard to the lower spectra. When calculating the cross spectrum, this leads to a density loss in the domain of higher frequencies. In the well-mixed surface layer, as occur during daytime (see fig. 5.7), the problem of vertical sensor displacement is ecpected to have a lower impact on the derived cospectra of vertical wind and CO_2- and H_2O-densities, since gradients of atmospheric variables are less steep (Stull, 1988). During nighttime though, the more stable stratified boundary layer suppresses turbulence and the vertical sensor separation will have a greater impact on the cospectra. This will be discussed in the following chapter for the measurements at the Nopu site with the means of the residuum of the energy balance equation. For the measurements in Indonesia at the Nopu site and the Besoa site (see chapters 5 and 6.1), the sensor measuring the scalars, CO_2 and H_2O, is mounted above the ultrasonic anemometer, thus with a vertical displacement of $d_v = 80\,cm$. Following the analysis by Kristensen et al. (1997), valid under the assumption of atmospheric neutral stability, this leads to an underestimation of the calculated fluxes of up to 10%. The displacement of the upper spectra with regard to the lower spectra can

be handled by covariance maximization in the post-processing. The scalar quantities and vertical wind scale with height (logarithmic wind profile). When measuring at two heights, this introduces an error into the calculated covariances of the vertical wind and the scalar quantity, which cannot be corrected for the measurements in Nopu.

4.4   Stationarity of the measured fluxes

One of the restrictions of EC measurements is the assumption of the stationarity of all measured fluxes over the averaging time (see Chapter 2.2). The investigation area in the cocoa plantations in Nopu, Indonesia, is characterized by heterogenous vegetation cover, as described in Chapter 5.1. The measurement height of $10.3\,m$ was chosen, since Cacao trees in that area reach a height of about $5\,m$ on the average. Cacao trees originate from rain forests in Southern America and need to be shadowed. The shadow trees within the Cacao tree stands reach a height of $7-8\,m$. Apart from the Cacao trees, there are also fruit trees and few relics of the former rain forest within the plantations. The EC technique implies that the mean values are constant over the averaging time. Regarding the heterogeneity of the plantation, it is likely that some of the flux observations are not entirely originated from Cacao trees, and this can affect the mean properties of the turbulent flow. As can be seen in Figure 4.10, the scatter of the part interval covariances is rather high and part of the observation points lie outside of the stationarity criterium suggested by Foken and Wichura (1996). The scattering is less pronounced for the covariance of vertical wind with temperature, $Cov(w, T)$, and non-stationarity occurs mostly for small values of of the covariance. About 30% of the temperature covariances have to be considered non-stationary. The covariances of vertical wind with the scalars water vapor content, $Cov(w, \rho_{H_2O})$, and carbon dioxide content, $Cov(w, \rho_{CO_2})$, a higher scattering can be seen. In total, about 40% of the observations are non-stationary. The higher scattering for the scalars measured by the open-path sensor, the LI-7500, can be explained by wetting of the sensor, as discussed in the previous chapters. After removal of flawed data by the method described in Chapter 3.1.3, no difference in stationarity between the turbulent fluxes can be observed. The non-stationary data are subseyuently disregarded in the further analysis and interpretation of the measurements.

In the following, the non-stationarity of the measurements will be discussed with the covariance of vertical wind and temperature, i. e. the "relative stationarity"

$$RelCov(w,T) = \left| \frac{Cov(w,T) - CovN(w,T)}{Cov(w,T)} \right| \tag{4.6}$$

Table 4.4: Fit parameters from linear fit of the average covariance of the N part intervals, $Cov_N(w, C)$, to the covariance over the whole interval, $Cov(w, C)$, for scalars $C = T$, ρ_{H_2O}, ρ_{CO_2}

Covariance	Offset of Linear Fit	Slope of Linear Fit	Correlation Coefficient R^2
$Cov(w, T)$	$0.0\,K \cdot m/s$	0.931	0.988
$Cov(w, \rho_{H_2O})$	$0.042\,m \cdot mmol/(m^3 s)$	0.96	0.951
$Cov(w, \rho_{CO_2})$	$0.0\,m \cdot mmol/(m^3 s)$	0.911	0.878

Figures 4.11 and 4.12 show, that non-stationarity of the observed temperature covariance is associated with low values of $u_\star$ and Xmax. Also can be seen, that the scalar flux fulfills the stationarity criterium at daytime. At nighttime though, the stationarity is a problem, especially at conditions of low friction velocities and small maximum source area distance of the measured turbulence signal.
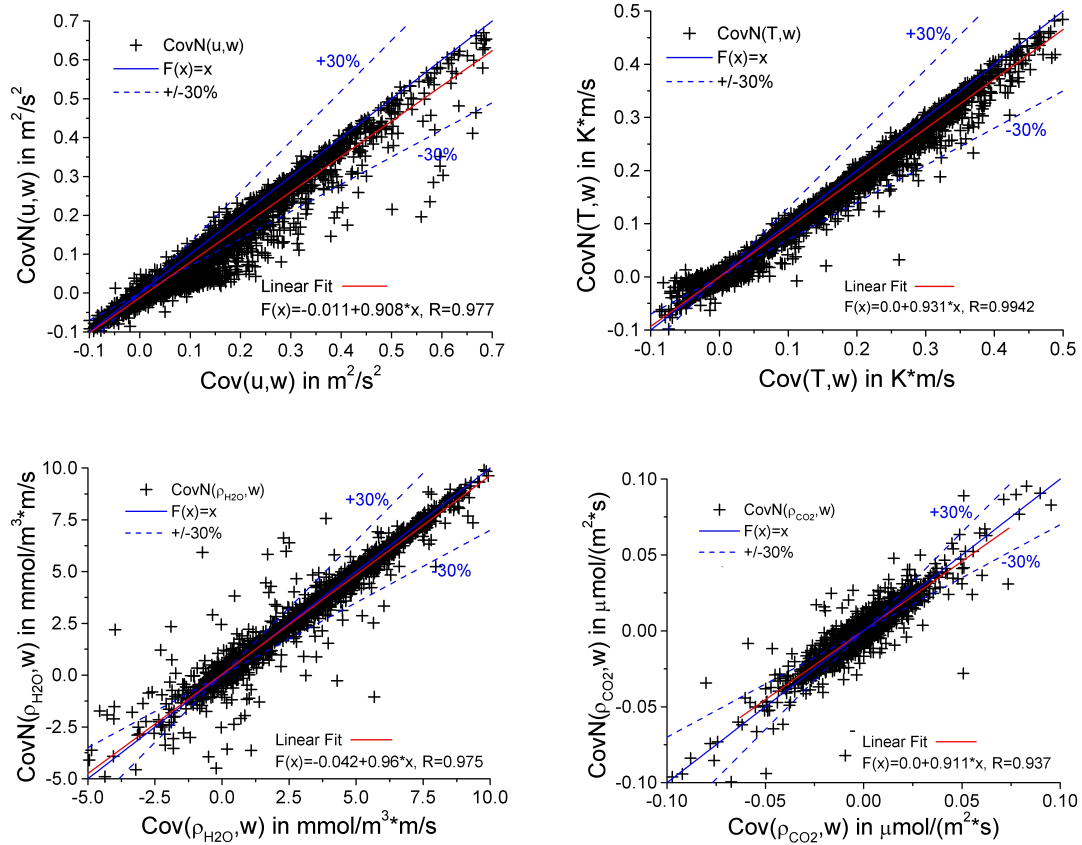
Figure 4.10: The average covariance of the N part intervals, $Cov_N(w, C)$, between the vertical wind component w and a scalar C is plotted against the covariance calculated over the whole interval, $Cov(w, C)$. The covariances displayed here, are the covariance of w with the horizontal wind component $C = u$ (left above), the virtual sound temperature $C = T$ (right above), the water vapour density $C = \rho_{H_2O}$ (left below) and the CO_2-content $C = \rho_{CO_2}$ (right below). The dashed blue lines denote the stationarity criterium, the blue solid line is the ascending slope $F(x) = x$ and the red solid line the linear fit.
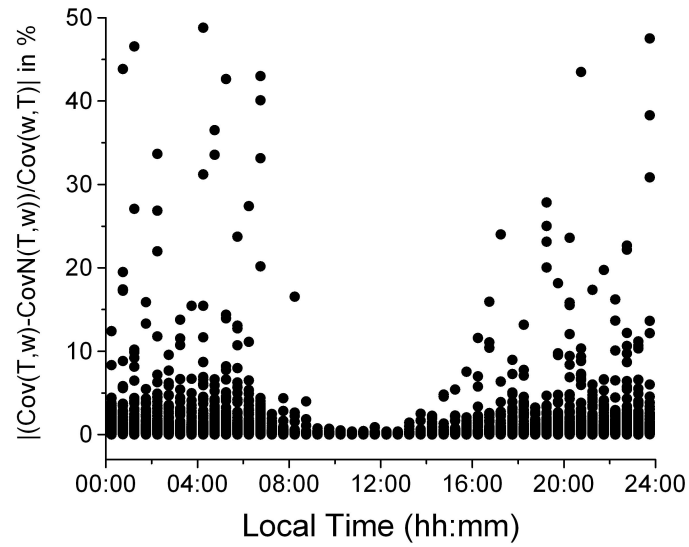
Figure 4.11: Shown is diurnal distribution of the relative stationarity, $RelCov(w,T)$ in %, plotted against the local time.
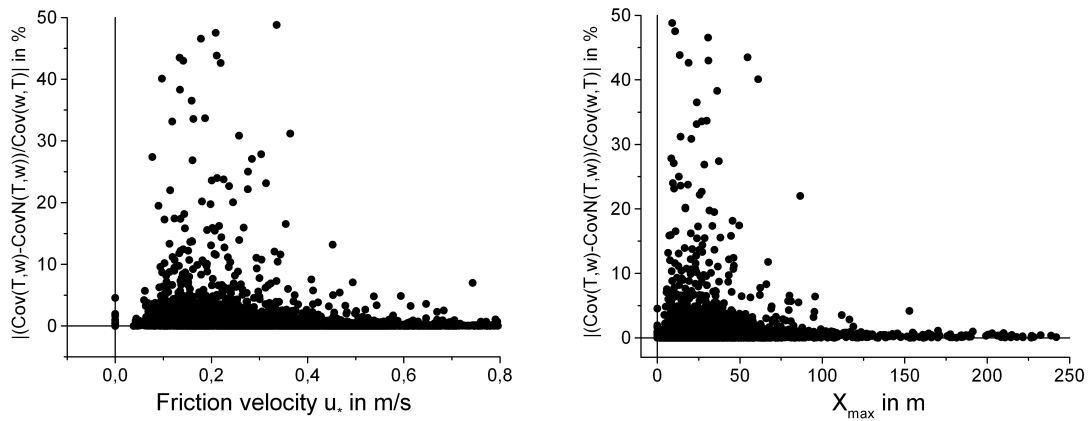
Figure 4.12: The relative stationarity, $RelCov(w,T)$ (in %) is plotted against the friction velocity $u_\star$ (left), and the maximal source area X_{max} (Wilson and Swaters, 1991) (right)

Chapter 5

Eddy-Covariance measurements above a cocoa plantation in the Palolo valley, Sulawesi, Indonesia

5.1 Experimental site

5.1.1 Setup of the EC system and journal of measurements

Due to the delay in the build-up of the micrometeorological tower, this work was shifted to agriculturally used land. Since one of the major land-use types is cocoa plantations, the task was now to find a suitable plantation for EC measurements, that matches the restrictions required by theory (see Chapter 2.2). Since no maps of land-use existed, every plantation to be considered had to be checked with regard to its extension and the homogeneity of the vegetation. Most farmers in or around the Lore Lindu National Park (TNLL) hold plantations of 1 to 3 hectares and in most places cocoa plantations are in direct vicinity of corn or rice fields or even fields of mixed vegetation.

The only suitable site found is situated in the Palolo valley at the eastern border of the TNLL. This plantation had been planted about 13 years ago (around 1994) transforming the former rain forest into agriculturally used land. After constituting the site, negotiations with the farmers owning the fields were accomplished. Also socialization with the villagers nearby the site to ensure the safety of the sensors and undisturbed measurements was achieved. The measurement mast on which the sensors were to be mounted, was manufactured in Palu, capital city of Central Sulawesi in cooperation with the Meteorological Department (BMG).

Its height of $11\,m$ seemed sufficient, since cacao trees, *Theobroma cacao* L., in the plantations reach a height of $5\,m$ on the average. Plantations of Cacao trees are named after the production good cocoa, i.e. cocoa plantations. In October 2001 the setup procedure started, first building the concrete basements for the mast, mounting it and installing the sensors. Since the next road ended about $1\,km$ away from the site, every material and equipment were transported either by man power, with barrow or with a cart hauled by oxes.

A first view of the vegetation from above could not be gathered until climbing the mast. It turned out that the surrounding plantations were interspersed with bigger trees, fruit trees or coconut palms for example, and relicts of the former rain forest. The plantations are interspersed with wooden farm houses, constituting sources of CO_2 due to cooking or small power plants, used during evening hours, i.e. from 6 to 10 pm. It was inevitable, that a detailed mapping of vegetation type, tree species and height and also possible sources of CO_2, like stoves or generators, had to be carried out, to be able to conduct a detailed analysis of the sources and the pathway of the turbulent fluxes measured by the EC system. This was done in February 2002 by a group of students from the Tadulako University of Palu, working for the project. The employed method and results are described in chap. 3.4 and 5.1 respectively.

Setup and beginning of operation in the Nopu cocoa plantation was in November 2001. In April 2002, the measurement stopped due to the failure in the power circuit of the ultrasonic anemometer. The sensor had to be brought back to Germany for repairs and reinstalled afterward resulting in the gap of two months data. In the beginning of 2002 the farmers started planting a fast growing tree, Kayu Jatih Putih, among the cacao trees, for sale to the paper industry. In December 2002, two of those trees caused another failure of the EC system by shadowing the solar panels. This lead to a breakdown of the power supply. In February 2003 the EC system was working again. In March 2003, the mast was moved to a second site that was more suitable for the radiation measurements to validate the fluxes measured at the first site by closing the energy balance equation. In April 2003 the data acquisition system, a field computer, failed due to constant exposure to the very unsuitable climatic conditions, i. e. high temperatures and relative humidity. A new hard disk drive and new CMOS battery had to be assembled into the computer.

In February 2003 the build-up of micrometeorological tower had been completed and in May 2003 the EC system was moved to rain forest tower site in the Besoa valley (see Chapter 6.1), and the main system, i.e. the anemometer, power supply and data acquisition, were successfully installed. The measurements of the CO_2- and H_2O-fluxes started in October 2003.
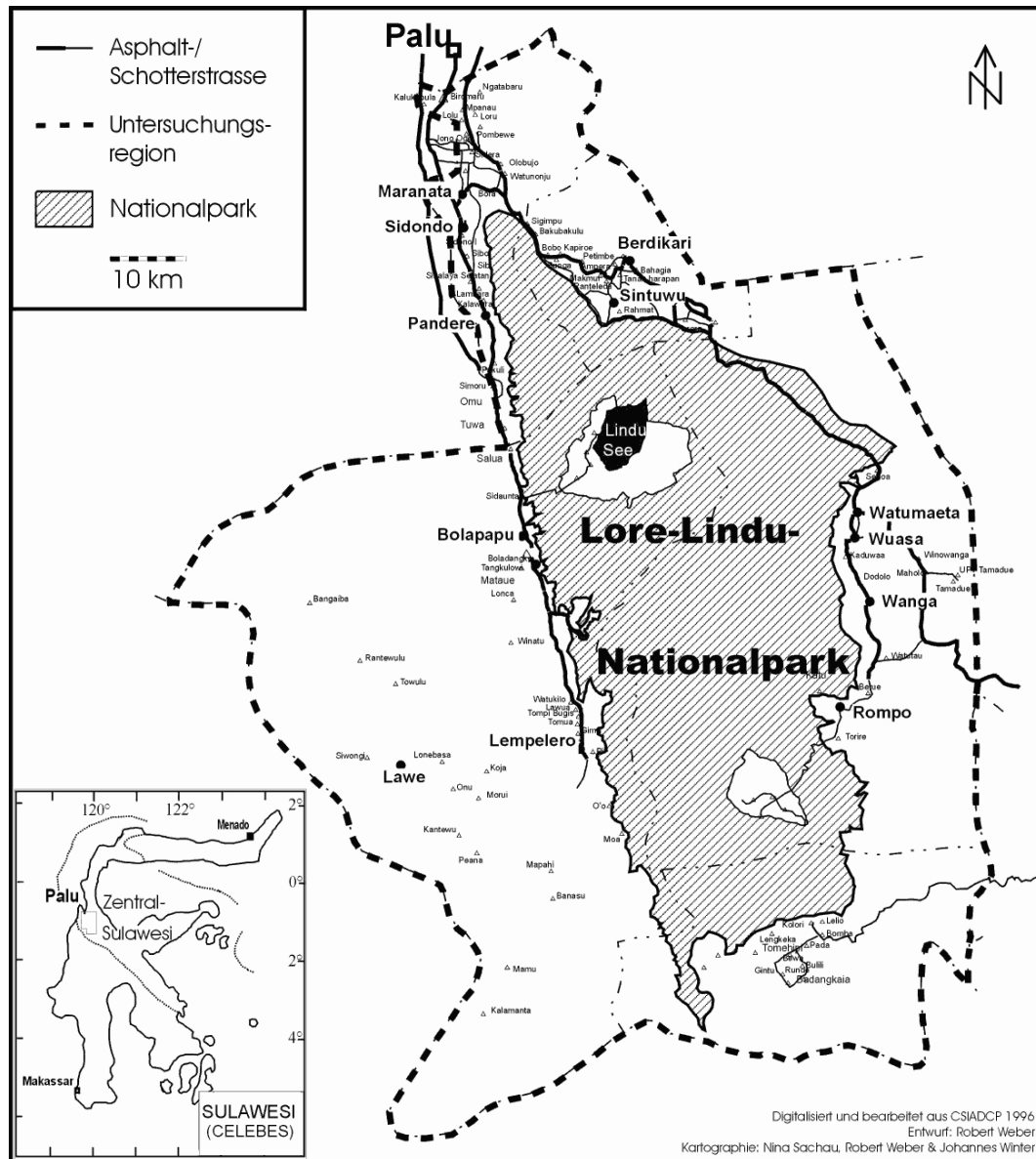
Figure 5.1: Map of the research area of the project STORMA (SFB 552) on Sulawesi, Indonesia, (552, 003b). The experimental site of B1 (EC Measurements) is situated S to SE of Sintuwu, near the village Rahmat (Nopu). The map was provided by Robert Weber, Dept. of Cultural and Social Geography, Institute of Geography, Univ. Göttingen.

5.1.2 Experimental site characteristics and meteorological settings

Nopu-Rahmat is a small village directly at the border of the Lore Lindu National Park (TNLL) at about $700\,m.a.s.l.$. The cocoa plantation itself lies ca. $2\,km$ north of the village Rahmat at $640\,m.a.s.l.$ at the coordinates 01°08′26.3″S and 120°03′33.1″E. The annual precipitation amounts to $2500..3000\,mm$ and mean annual temperature is $29\,°C$. Merklein (2003) investigated two model areas of $0.22\,ha$ and $0.28\,ha$ with respect to the physiological properties of the cocoa plantation under investigation. The cacao trees in the plantation are planted in a regular pattern with a mean tree distance of $3.1\,m$ and $3.3\,m$ between rows. Table 5.1 gives a summary of his results. The listed parameters are needed as input into a Soil-Vegetation-Atmosphere-Transfer model used in Chapter 5.3 for the energy balance closure of the investigated cocoa plantations. The seasonal pattern of dry season and rainy

Table 5.1: List of physiological parameters of the investigated cocoa plantation in Nopu-Rahmat, Merklein (2003)

Structural parameter	measured quantity for the cocoa plantation in Nopu
Trees per hectare	1053.74
Max. treetop radius	$2.6\,m$
Mean wood volume per tree	$0.037\,m^3$
Mean leaf dry biomass per tree	$5.08\,kg$
Mean leaf carbon-content per tree	$2.0\,kg$
Mean leaf carbon-content of trees per ha	$2122\,kg$
Leaf area index (LAI)	7.17

season is classified by Aldrian (2003) for the larger region of Central Sulawesi by means of the regionalized precipitation pattern, which show two periods of increased rainfall. Months with maximal rainfall are October to December. There is a second period with higher rainfall, but slightly lower maximums in the monthly sums of rainfall in the months March to May. The dry season falls within the months June to September due to the location of the Innertropical convergence zone (ITCZ, Hastenrath (1985). The monthly averaged diurnal course of global radiation, G, (Figure 5.2) from measurements at the Nopu site shows a slightly different pattern. Lower values of G during daytime indicate higher cloudiness as can be observed during the rainy season. This would mark the onset of the rainy season in November, which lasts until June. This is in accordance to the observations made by the farmers achieved in
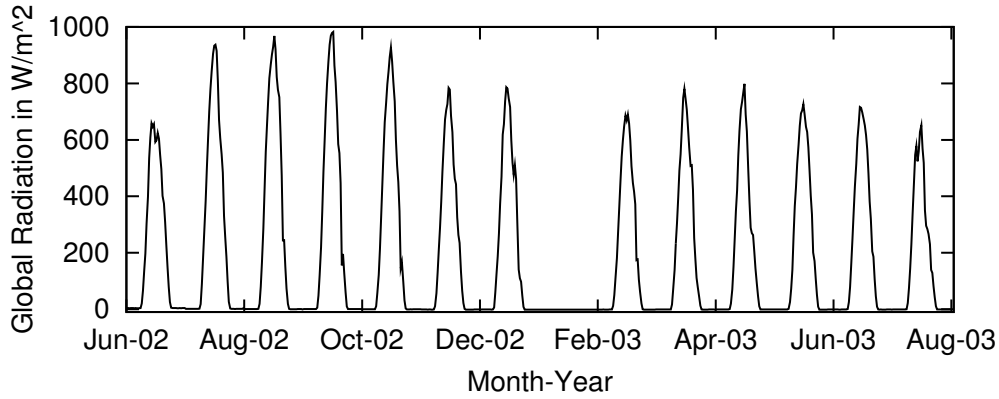
Figure 5.2: Monthly averaged diurnal course of global radiation G at the Nopu site, Palolo valley in Central Sulawesi, Indonesia. The analysis is based on the half-hourly mean values derived from the EC measurements. The tics on the time axis are at 00:00 LT

personal communication. There is no data available for the month January due to sensor malfunction. The dry season according to the analysis of the mean monthly diurnal course of global radiation starts in July and lasts until October.

This pattern is not quiet supported by the monthly sums of rainfall in Figure 5.3 from data of two AWS in the vicinity of Rahmat. Especially in the time period September 2001 until February 2002 the AWS seems to have not been working properly or the rain gauge might have been blocked by litter (Figure 5.3). Especially November 2001 was a month with maximal sum of precipitation, nearly $400\,mm$ at the AWS station in the slash&burn area. The rainy season lasted until July in 2002. Discussion of seasonal pattern has to be carried out on the basis of long-term meteorological data, though. The seasonal pattern described by Aldrian (2003) is probably also superimposed by the pattern of local valley-mountain circulation.

The monthly mean diurnal course of relative humidity is displayed in Figure 5.4. Nighttime rh amounts to nearly 100%, which means evolution of fog during nighttime. During daytime, rh drops down to nearly 40%, showing the heating of the atmosphere and transport of moist air from the surface layer into the upper atmosphere by turbulent transport. The seasonal pattern is also indicated in the monthly averaged diurnal course of the relative humidity (see Figure 5.4).

Figure 5.6 shows the pronounced wind system dominating the valley-mountain circulation pattern at the Nopu site. During nighttime, the wind flow is directed down the mountain range situated in the South-West of the EC site into the valley, wind direction is about 50°.
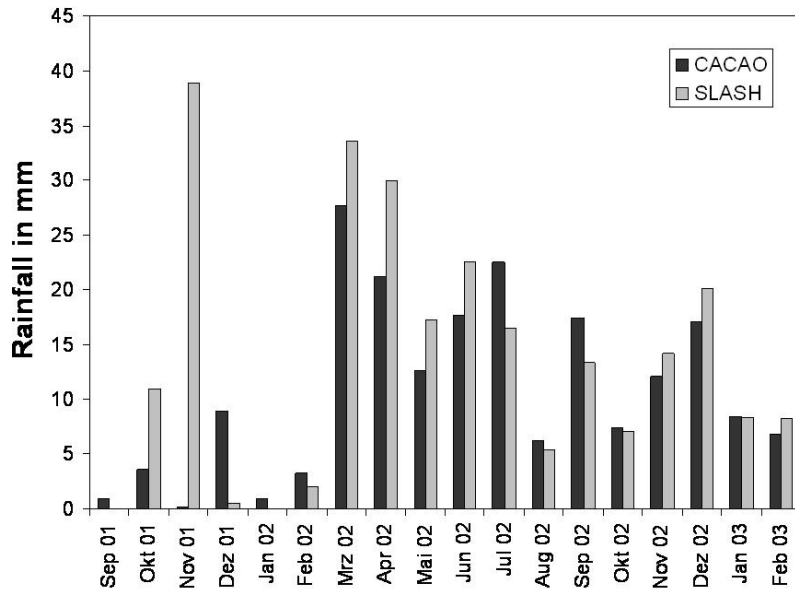
Figure 5.3: Monthly sums of precipitation from AWS data in a cocoa plantation and Slash& Burn area on the hill slope near Rahmat, Palolo valley in Central Sulawesi, Indonesia. Distance between the two stations is about 2 km.

In the early morning hours, the wind direction is gradually changing to about 220° at noon directed from the valley up hill slope. Please note that meteorological wind direction is the direction in which the wind flow is pointing. The wind data show the pronounced local wind regime with little or no effect of a superimposed larger scale windfield.

The monthly averaged diurnal course of the friction velocity also shows a seasonal variability with lower daily maxima, $0.4\,m/s$, during the rainy season, and higher daily maxima, $0.5\,m\,s^{-1}$ during the dry season. During nighttime, values for $u_\star$ are in the range of 0.1 to $0.15\,m\,s^{-1}$.

The stability parameter ζ (Equation 2.9) describes the stratification of the atmosphere's surface layer, where negative values, $\zeta < 0$, denote an unstabile stratified surface layer and positive values, $\zeta > 0$, denote a stably stratified surface layer. $\zeta = 0$ means neutral stratification. Figure 5.7 shows that during nighttimes, the surface layer at the Nopu site is slightly stable stratified with non-evanescent horizontal wind velocity (see Figure 5.6), $0.0 < \zeta_{night} < 0.15$, and unstable stratification of the surface layer during daytime, with daily minima of ζ in the range of $-0.6 < \zeta_{min} < -0.2$.

The annual variability of the barometric pressure during the measurements period from December 2001 until August 2003, $\Delta p_{annual} = 2\,hPa$, is small compared to the daily variability.
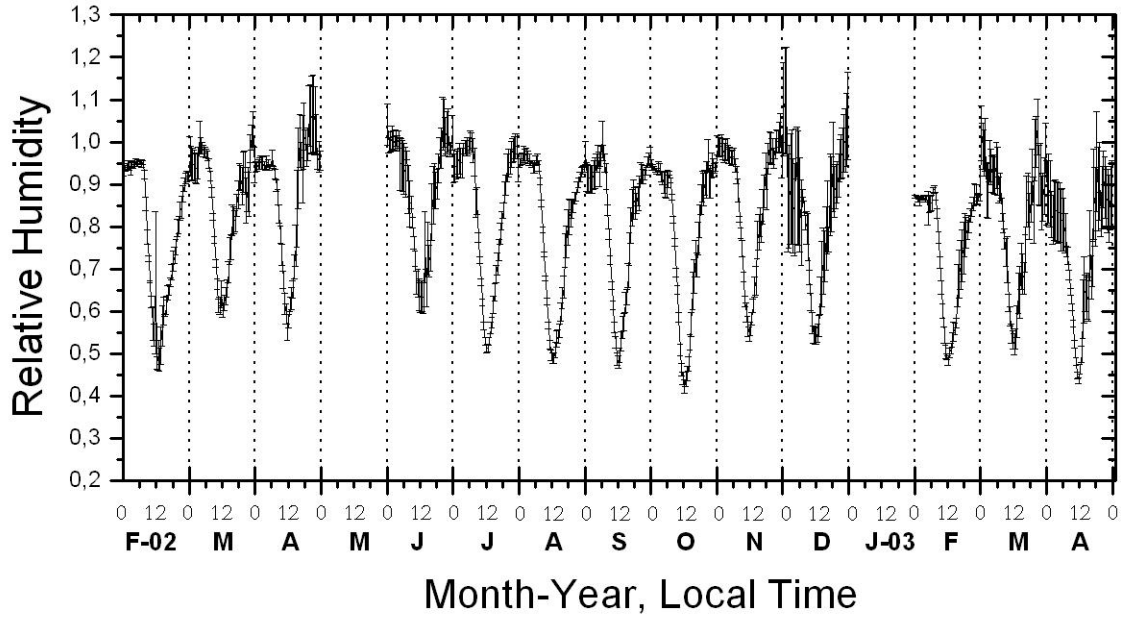
Figure 5.4: Monthly averaged diurnal course of relative humidity at the Nopu site. The analysis is based on the half-hourly mean values derived from the EC measurements. Measurement period from February 2001 until April 2003. Error bars denote the standard error.

Figure 5.8 shows the pronounced daily course of barometric pressure at the Nopu site. This pattern is typical for the tropics with a maximum at 9:30 LT and the a secondary maximum at 21:30 LT, showing the daily cycle in convergence and divergence of the wind pattern. The diurnal pattern of the barometric pressure is caused by waves of atmospheric tides (Hastenrath, 1985), which can be divided into 3 main types, the solar diurnal ($24\,h$), the semidiurnal ($12\,h$) and the ter-diurnal ($8\,h$) tide. A review of various tides and their thermal and gravitational nature can be found in Chapman and Lindzen (1996). Hastenrath (1985) states that for the tropics the 12-hourly wave dominates, whereas the superposition of the 24-hourly and the 8-hourly waves result in a generally larger morning than evening maximum. The largest divergence of the wind pattern can be found in the time period between the morning maximum and the daily minimum, whereas the largest convergence is found in the time period between the daily minimum and the secondary maximum of the barometric pressure (Hastenrath, 1985).

Figure 5.9 shows the monthly averaged diurnal fluxes of latent and sensible heat, λE and H. It can be seen, that during periods with less rainfall, the turbulent flux of sensible heat is exceeding the turbulent flux of latent heat. The higher energy input to the canopy surface by
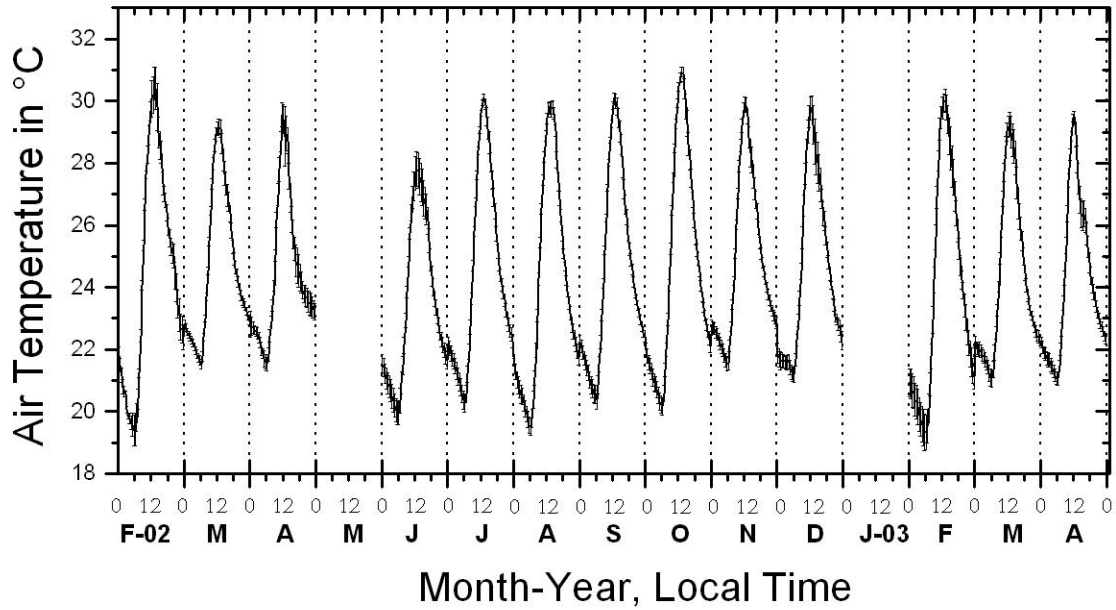
Figure 5.5: Monthly averaged diurnal course of temperature at the Nopu site. The analysis is based on the half-hourly mean values derived from the EC measurements. Measurement period from February 2001 until April 2003. Error bars denote the standard error.

solar radiation is compensated for by the turbulent flux of sensible heat. Thus, the monthly averaged daily maxima of the ratio of sensible to latent heat flux, the Bowen ratio, can be taken as an indicator for the seasonal pattern of rain and dry season. The Bowen ratio will be discussed further in Chapter 6. The monthly average of daily net ecosystem exchange of carbon, NEE_C, and daily evapotranspiration ET in Nopu, is displayed in Table 5.2 for the measurement period from February 2002 to April 2003. Gaps in the time series were filled using the respective monthly mean diurnal course. During the dry season, a release of carbon $NEE_C > 0$ by the Cacao trees into the vegetation was observed, and during rainy season an uptake $NEE_C < 0$. In the months June and end of October 2002, and in March 2003, the cacao pods were harvested. This might have had an impact on the carbon uptake of the cacao trees. On the average over the months of observations, the cocoa plantation released carbon into the atmosphere, that amounted to $0.12 \pm 0.06 \, g\text{-C} \, m^{-2} d^{-1}$. The daily evapotranspiration shows higher values during the rainy season and lower values during dry season, with a minimum in June 2002 and a maximum in March and April 2002. On the average over the months of observations, daily evapotranspiration amounts to $ET = 2.55 \pm 0.38 \, mm \, d^{-1}$.

Table 5.2: Monthly average of daily net ecosystem exchange of carbon NEE_C, and monthly average of daily evapotranspiration ET, with standard errors $sterr$, in the cocoa plantation in Nopu, Indonesia. Measurement period from February 2001 until April 2003.

Year-Month	NEE_C $g\text{-C}\,m^{-2}d^{-1}$	$sterr(NEE_C)$ $g\text{-C}\,m^{-2}d^{-1}$	ET $mm\,d^{-1}$	$sterr(ET)$ $mm\,d^{-1}$	Management applied
2002-Feb	-0.485	0.14	2.101	0.383	
2002-Mar	0.131	0.06	2.902	0.265	
2002-Apr	1.156	0.75	3.074	0.613	
2002-Jun	1.187	0.62	2.134	0.414	Harvest
2002-Jul	0.352	0.05	2.476	0.234	
2002-Aug	-0.096	0.06	2.605	0.207	
2002-Sep	0.178	0.33	2.753	0.280	
2002-Oct	0.026	0.06	2.483	0.310	Harvest
2002-Nov	0.096	0.06	2.746	0.373	
2002-Dec	-0.420	0.50	2.529	0.775	
2003-Feb	-0.406	0.50	2.238	0.289	
2003-Mar	0.070	0.49	2.638	0.447	Harvest
2003-Apr	-0.210	0.44	2.518	0.313	
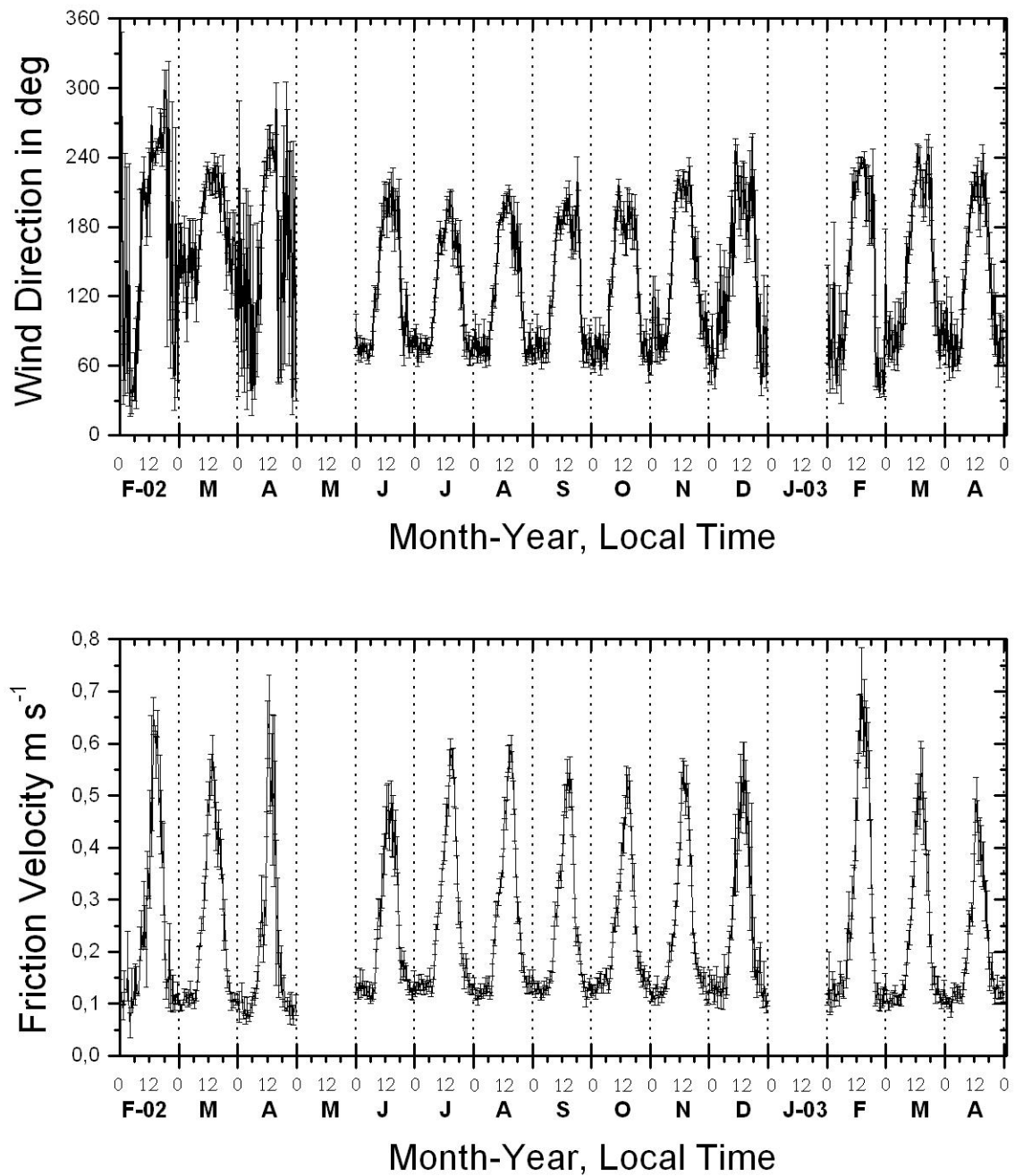
Figure 5.6: Monthly averaged diurnal course of wind direction (above) and friction velocity (below) at the Nopu site. Error bars are the standard error. The analysis is based on the half-hourly mean values derived from the EC measurements. Measurement period from February 2001 until April 2003.
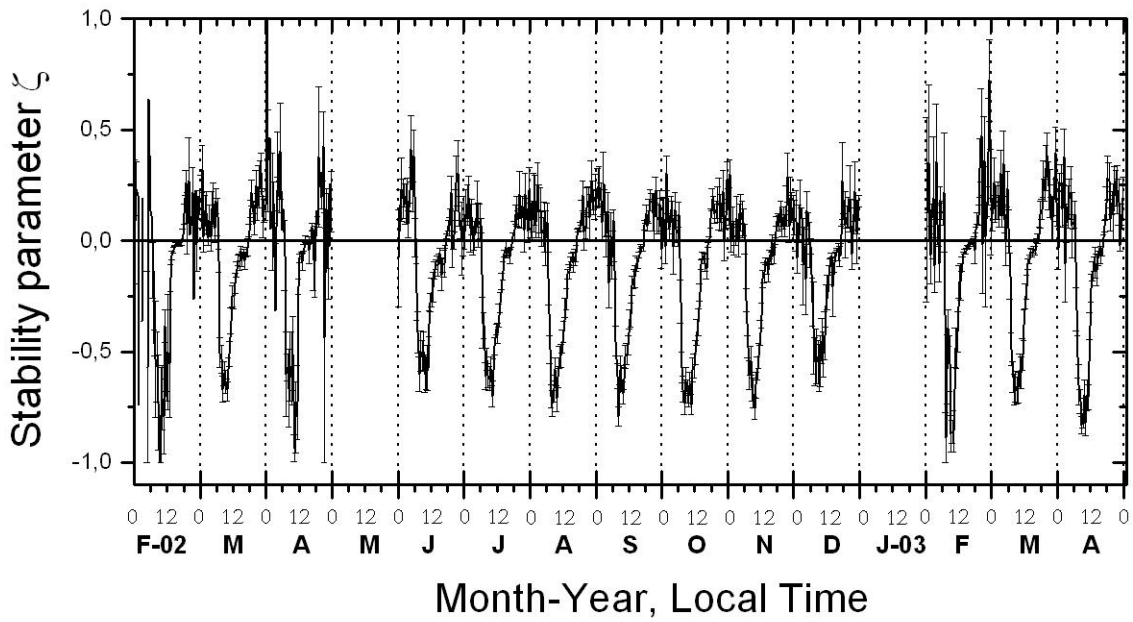
Figure 5.7: Monthly averaged diurnal course of the stability parameter ζ at the Nopu site. The analysis is based on the half-hourly mean values derived from the EC measurements. Measurement period from February 2001 until April 2003. Error bars denote the standard error.
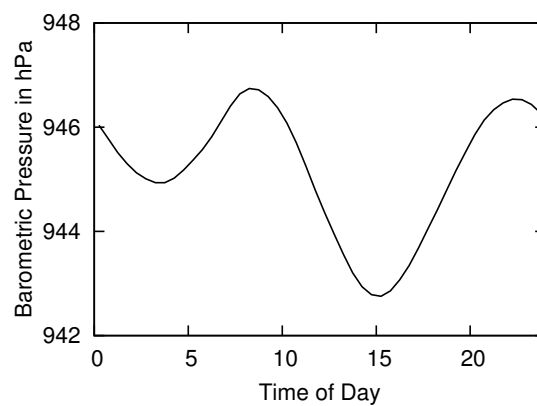
Figure 5.8: Mean diurnal course of stability parameter $\zeta = z/L$ (left) and barometric pressure (right) at the Nopu site. Measurement period from February 2001 until April 2003. Error bars are the standard deviation.
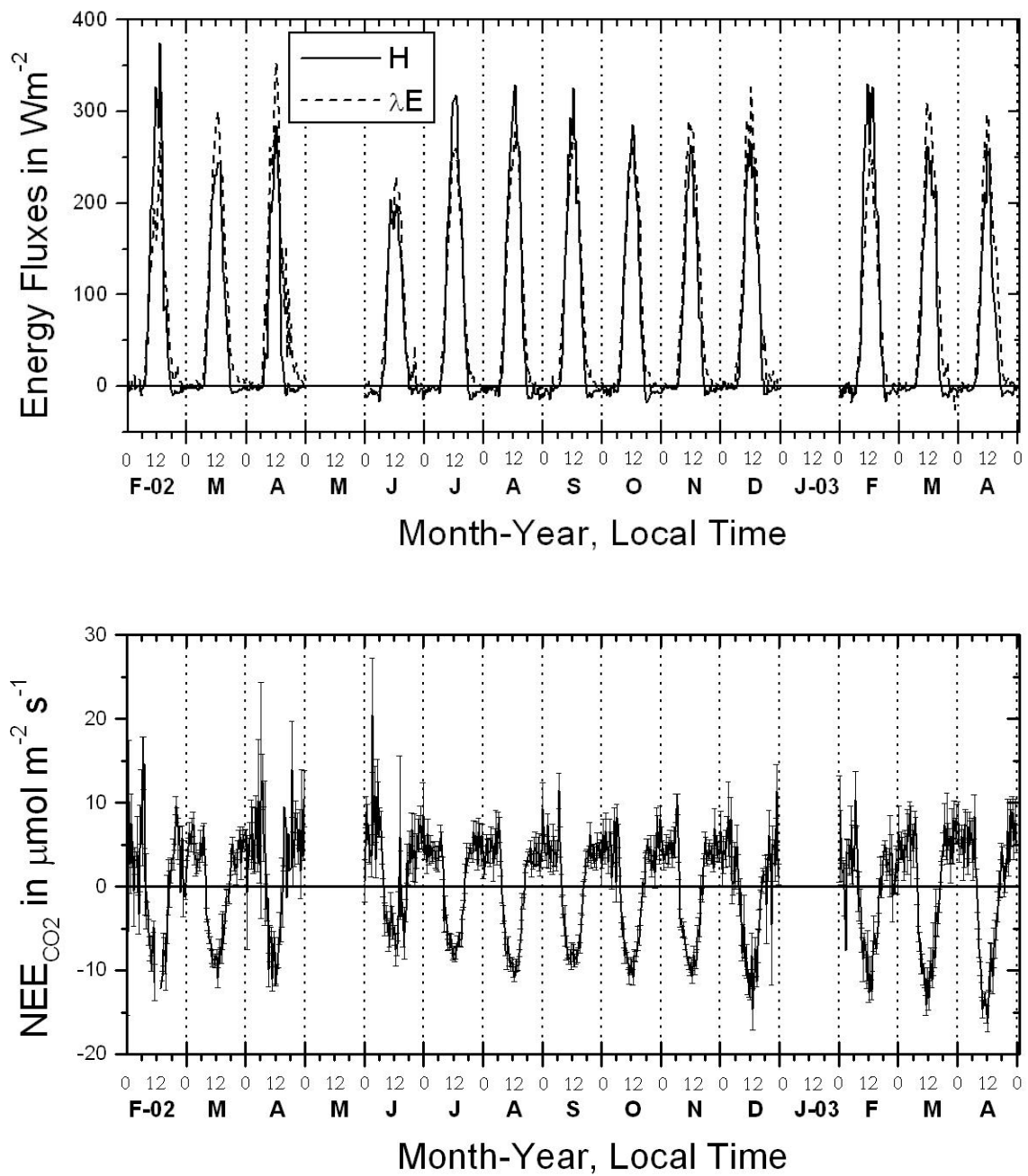
Figure 5.9: Monthly averaged diurnal course of the turbulent fluxes of latent and sensible heat, λE and H (above) and the net ecosystem uptake of CO_2, NEE_{CO_2} (below), at the first Nopu site, Palolo valley in Central Sulawesi, Indonesia. Measurement period from February 2001 until April 2003. Error bars are the standard deviation.

5.2 Footprint analysis of the measured fluxes

The area which exerts a dominating influence on the sampled properties is referred to as the source area and the measurements are called representative of underlying patchy terrain if the scale of the patchiness is small compared to the source area effective for the measurements (Pasquill, 1972). The source area affecting a vertical flux is also called the **footprint**. There exist several approaches for modeling the footprint of scalar fluxes (Leclerc et al. (1997), Leclerc et al. (1997), Schuepp et al. (1990) and Finn et al. (1996)). In this work, the approach by Wilson and Swaters (1991) is used to calculate the maximal source area distance

$$X_{max} = u \frac{z - d}{\kappa u_\star} \phi_M \,.$$

(5.1)

For the calculation of the displacement height, wind profile measurements in the near-surface atmospheric boundary layer are required (see Chapter 2.1.1). These were not measured at the EC site in Nopu, and a displacement height of $d = 6\,m$ estimated. The profile functions for the footprint calculation were calculated using citep

$$-5 \leq \zeta \leq 0: \quad \phi_m\left(\zeta\right) = \left(1 + 16 \cdot |\zeta|\right)^{-0.25} \quad \text{(Dyer and Hicks, 1970)}$$

(5.2)

$$0 < \zeta \leq 1: \quad \phi_m\left(\zeta\right) = 1 + 5 \cdot \zeta \quad \text{(Dyer, 1974)}$$

(5.3)

The air sample is rising from the contact point (Wilson and Swaters, 1991) to the measurement height by turbulent vertical mixing and is transported horizontally by the mean horizontal wind velocity. Figure 5.10 (left) shows the density of the maximal source area distance for the EC measurements in the cocoa plantations in Nopu. 50% of the measured fluxes evolve within an area of $28\,m$ maximal distance and 70% from within $38\,m$ maximal distance to the EC mast. The diurnal distribution of maximal source area distance (see Figure 5.10 (right)) shows higher values of X_{max} during nighttime and 90% of the values of $X_{max} < 50\,m$ during daytime. This is due to the higher friction velocity $u_\star$ (Figure 5.6) and higher vertical mixing in the slightly unstable conditions (Figure 5.7) at daytime. At nighttime, the mean horizontal wind speeds are lower with less vertical mixing ($\zeta > 0$) in the stably stratified boundary layer. The air sample is carried over a greater distance until it reaches the measurement height and can take up the signal from changing underlying surface on its way. To separate out the fluxes that might have not evolved above cacao or that might have been affected by source areas other than cacao trees, e. g. farm houses, the maximal source area distance, X_{max} has to be analyzed with regard to the direction of the incoming flow. The direction of the incoming flow dir_{flow} is controversal to wind direction $wdir$, i.e. $dir_{flow} = 360 - wdir$. Figure 5.11 shows the distribution of X_{max} with regard to direction
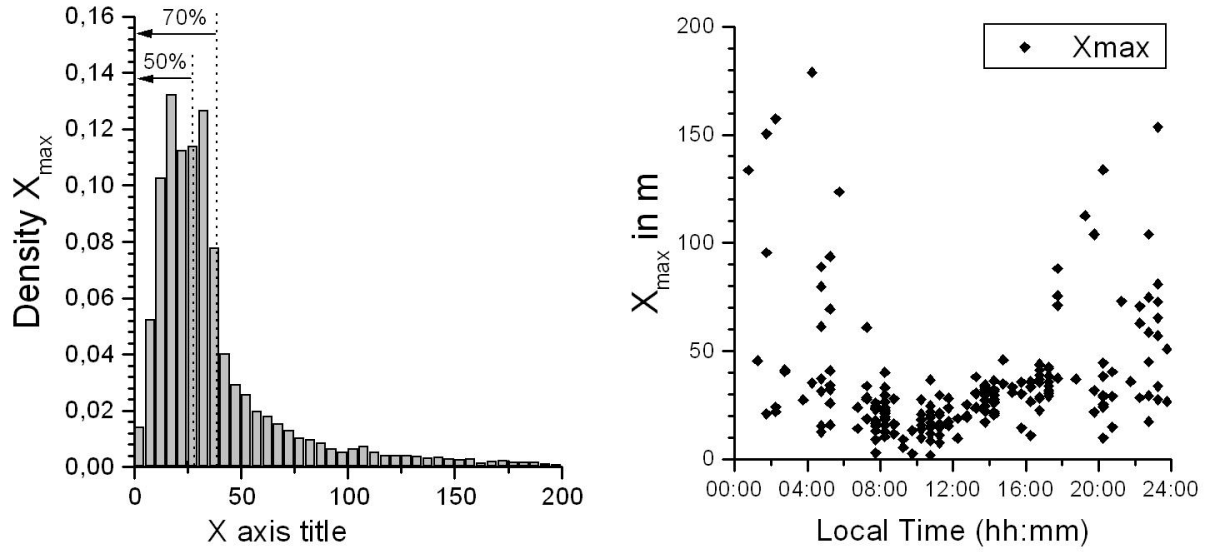
Figure 5.10: Shown is the density of maximal source area distance (ρ_{Xmax}) normalized by number of half-hour observations of the scalar fluxes measured (left), and maximal source area distance (X_{max}) plotted against local time (right) at the EC site in the cocoa plantations, Nopu, Indonesia. Measurement period from February 2002 to April 2003

of incoming flow. Also plotted in this figure is the distribution of households relatively to the EC measurement site with regard to the distance to the EC site. The nearest household is $76\,m$ away from the EC site. For most conditions there is no impact of the different surface conditions and boundary layer structure at farm house sites on the measured fluxes at daytime. During nighttime, there are households lying within the maximal source area distance, X_{max}. These households are situated within $[280° : 296°]$ at a distance in the range of $[144\,m : 190\,m]$ with respect to the EC mast. For these measurements, the fluxes have to be considered as not solely evolved above Cacao trees. This has to be taken into account, when closing the energy balance and looking at the carbon budget of the investigated cocoa plantation. Nighttime flux observations, that originate from areas near households are excluded in the subsequent data analysis in the following chapters. The daytime turbulent fluxes originate from plantation areas at directions below 225° with respect to the EC mast (see Figure 5.6 (above)), and the maximal source area distance is well below the distance to the households. Thus, for the daytime flux observations, the flux observations originate from areas within the investigated cocoa plantation.
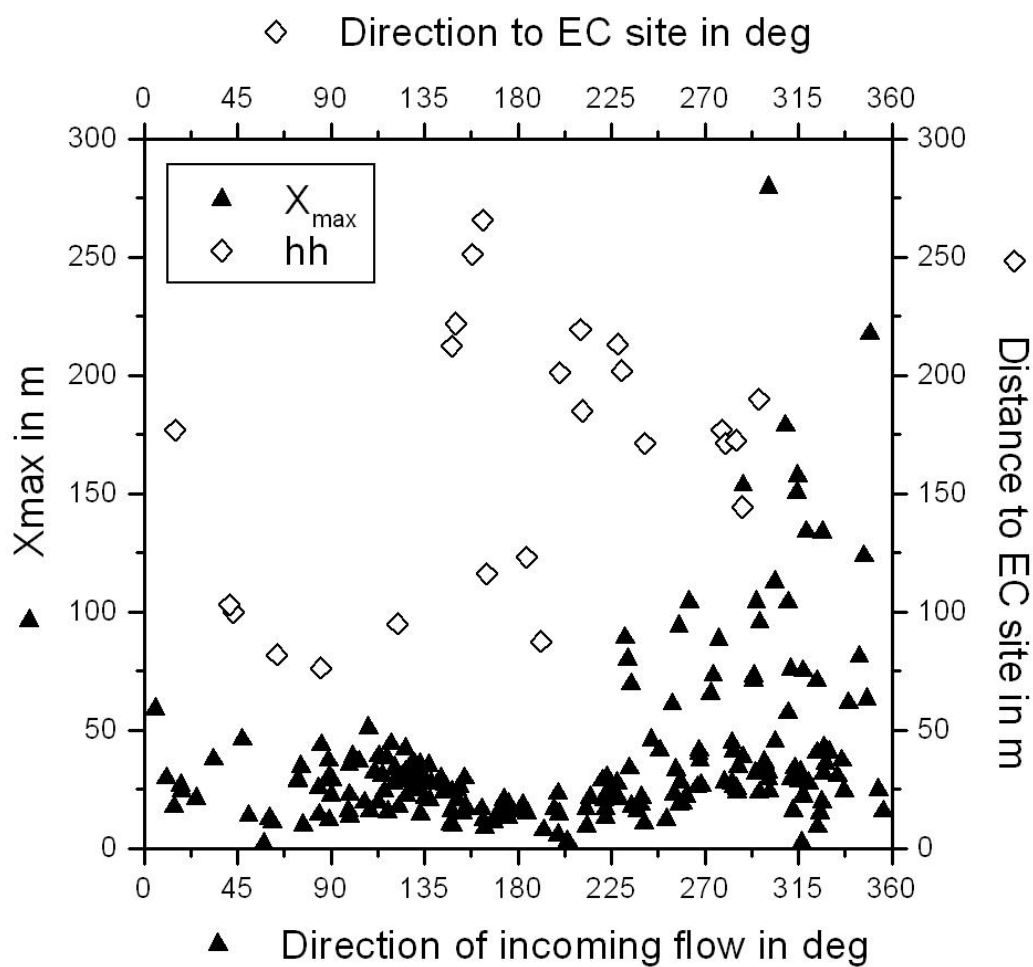
Figure 5.11: Distribution of maximal source area distance to direction of incoming flow with regard to the EC measurement site (triangles) and the distribution of households to their position relatively to the EC measurement site (diamonds)

5.3   Energy balance closure and comparison of the measured tubulent fluxes with a SVAT model

The theoretical boundary restrictions for applying EC technique to measurements in the SBL are not met totally at most experimental sites. The investigated site in Nopu, as described in Chapter 5.1, is not ideal in many aspects, as horizontal homogeneity of surface roughness, carbon sources or vegetation cover. For the correct interpretation of the collected data, the measured fluxes have to be verified. The closure of the energy balance equation (see also Chapter 2.1.3, Equation 2.10)

$$R_n - G_{stor} - H - \lambda E = 0$$

the result of the measured net radiative flux, measured turbulent heat fluxes and the storage heat flux G_{stor}. The storage heat flux, G_{stor}, is computed by a Soil-Vegetation-Atmosphere-Transfer (SVAT) model by Oltchev et al. (2002) (see Chapter 3.2.2 for description). The turbulent fluxes of sensible and latent heat are derived from the EC measurements at the second site in Nopu. The energy balance closure is used in the following as a plausibility test of the turbulent fluxes of latent and sensible heat, measured by the EC sytem in Nopu. The net radiation is calculated by equation (2.11) from measurements of the up- and downward directed components of long- and shortwave radiation. The energy fluxes at the second site in Nopu are displayed in Figure 5.12 for the measurement period from 19 March to 18 April 2003. Figure 5.12 shows the diurnal courses of the energy budget terms over the measurement period in March and April 2003. The net radiation is the energy input by solar radiation to the surface. Deviations from the diurnal course of R_n are due to cloudiness and rain. The term $(R_n - G_{stor})$ is also referred to as the available energy for the distribution on turbulent exchange processes between atmosphere and vegetation. The diurnal course of the storage flux shows slightly negative values during nighttime, compensating for the negative net radiation. At daytime, the storage flux is positive and it changes its direction in the late afternoon, when evaporation is dominating the unstably stratified boundary layer.

The nighttime stably stratified surface boundary layer supresses vertical mixing and turbulence. Thus, the vertical transport of energy by the turbulent fluxes of sensible and latent heat is low. At nighttime, λE is nearly zero, changing the sign during the night and becomes negative in the early morning hours before sunset, meaning λE is directed from the atmosphere to the surface indicating formation of dew or fog below the sensors. The nighttime flux of sensible heat is negative, $H < 0$, and balancing the energy loss of the canopy's longwave radiative emission. In the morning hours H increases at a higher rate than λE, and
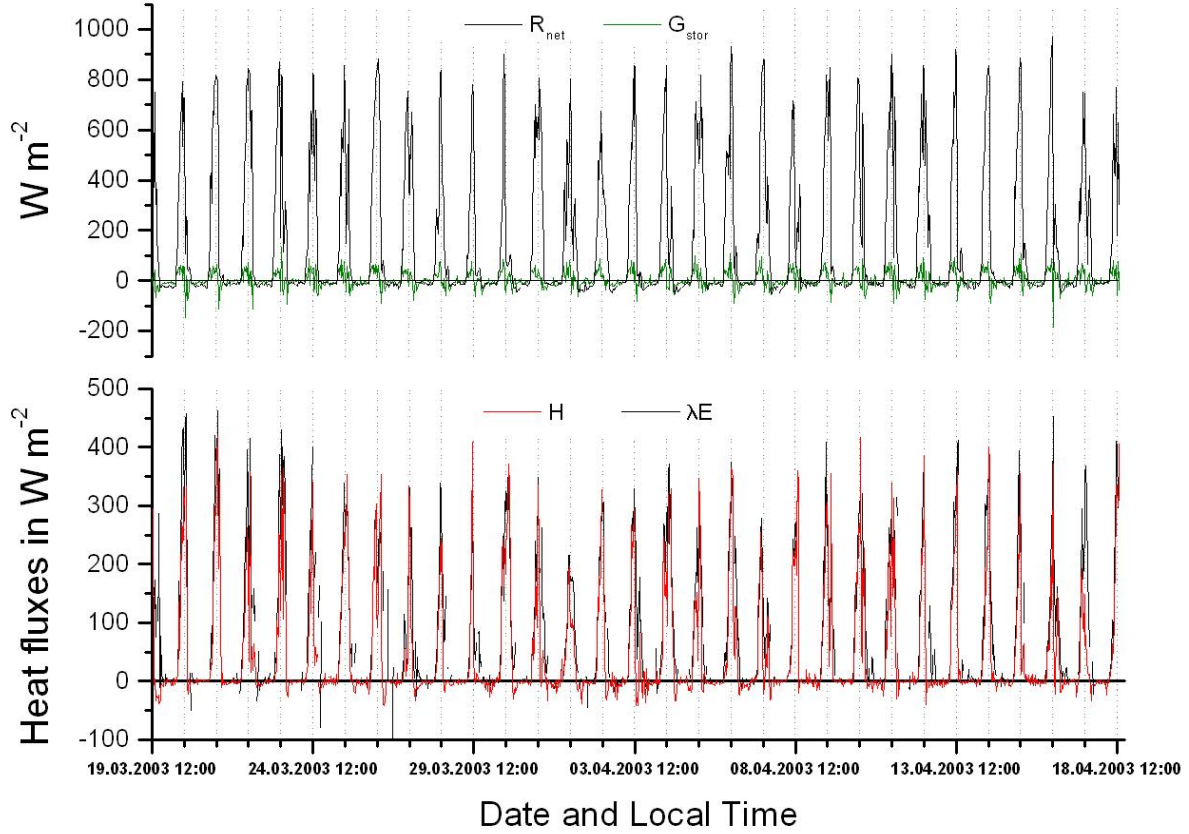
Figure 5.12: Diurnal courses of net radiation and storage flux, R_n and G_{stor}, (above) and turbulent fluxes of latent and sensible heat, λE and H, (below) at the second site in the cocoa plantation for the measurement period from 17-Mar-2003 until 18-Apr-2003, Nopu.

in the late afternoon, the latent heat flux λE is exceeding the sensible heat flux H. In the early evening hours, while λE is still positive, H changes its leading sign, meaning that the sensible heat flux is directed from the atmosphere to the canopy surface and is compensating the surface's energy loss due to the still ongoing evapotranspiration.

The sum of the turbulent energy fluxes $(H + \lambda E)$ is compared to the net radiation minus the storage heat flux, $(R_n - G)$ in Figure 5.13. Theoretically, the linear fit between the two terms should be equal to one. Measurements of the net radiation components were not available for the first site $(=$SO1$)$. The net radiation was modelled within the SVAT model by Oltchev et al. (2002). Since the energy balance closure within the SVAT model is being forced to zero, the better linear fit and higher regressions coefficient $R^2 = 0.89$ are a direct consequence. The energy balance closure assessed for the cocoa plantations in Nopu amounts to 70% at the second site $(=$SO2$)$. The causes for the unbalance of 30% lie within the uncertainties
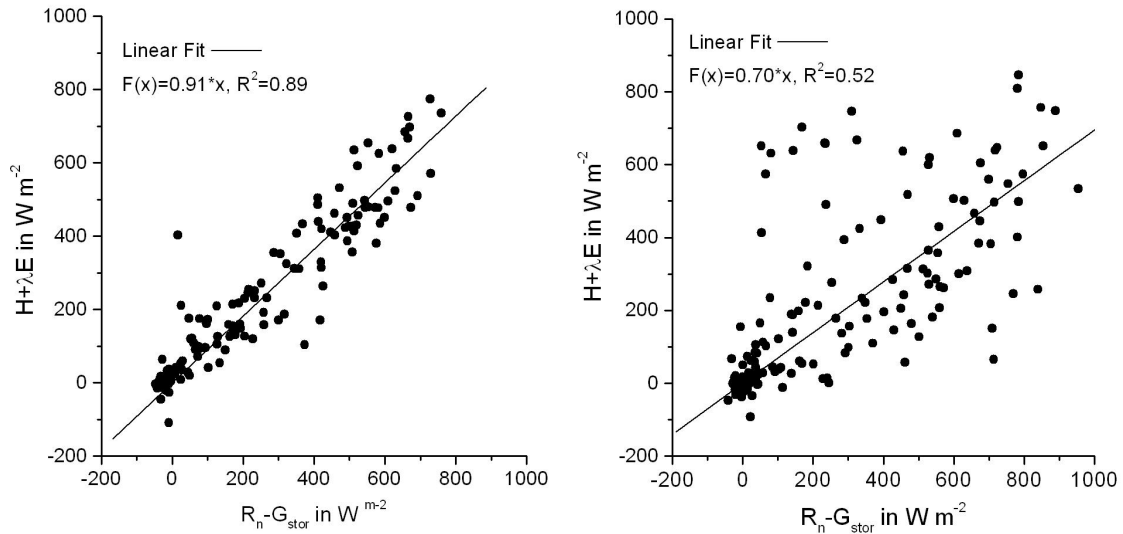
Figure 5.13: The sum of the turbulent energy fluxes, $(H + \lambda E)$, is plotted against the available energy, $(R_n - G_{stor})$ for the measurement period 25-Feb-2002 to 04-Apr-2002 SO1 (left), and for the measurement period from 17-Mar-2003 to 18-Apr-2003 SO2 (right), Nopu.

of the measurements and the computation of the storage flux and will be discussed in the following.

The uncertainty in the measurement of the net radiation is specified by Kipp&Zonen (Instruction Manual) to be $\pm 20 \, W/m^2$. The radiation sensors measure the radiative flux components directly at the EC mast, whereas the turbulent heat fluxes originate from an area further away. The albedos computed using Equation 2.12, amount to $\alpha = 15.0\%$ at SO1, and $\alpha = 15.2\%$ at SO2. The difference in albedos substantiate a difference in canopy surface reflectivity. The comparability of the radiation measurements and the turbulent energy fluxes includes some uncertainties, due to the heterogeneity of the investigated cocoa plantation (see Figure A.1). But since the footprint of the scalar fluxes is relatively small during daytime (see Figure 5.10), the turbulent signal measured at the EC site emerges from an area not very different to the conditions at the radiation measurement site. The heterogenity of the investigated cocoa plantation with regard to health and shape of the Cacao trees and the interspersion with fruit trees and vegetable crops, has a greater impact on the other energy budget terms. The storage heat flux is computed by a SVAT model, that needs as input parameters physiological and meteorological input parameters. The physiological input parameters were retrieved by Merklein (2003) from model areas other than the investigated site, i.e. from areas not within the footprint area of the EC site. As for the parameterization

of the input parameter of the SVAT model by Oltchev et al. (1997), all uncertainties of the measurements contribute to the uncertainty of the model. The higher scattering of the turbulent energy versus the available energy at SO2 compared to SO1 (Figure 5.13) results from the differences in measured and modeled net radiation R_n. In Figure 5.14, the turbu-
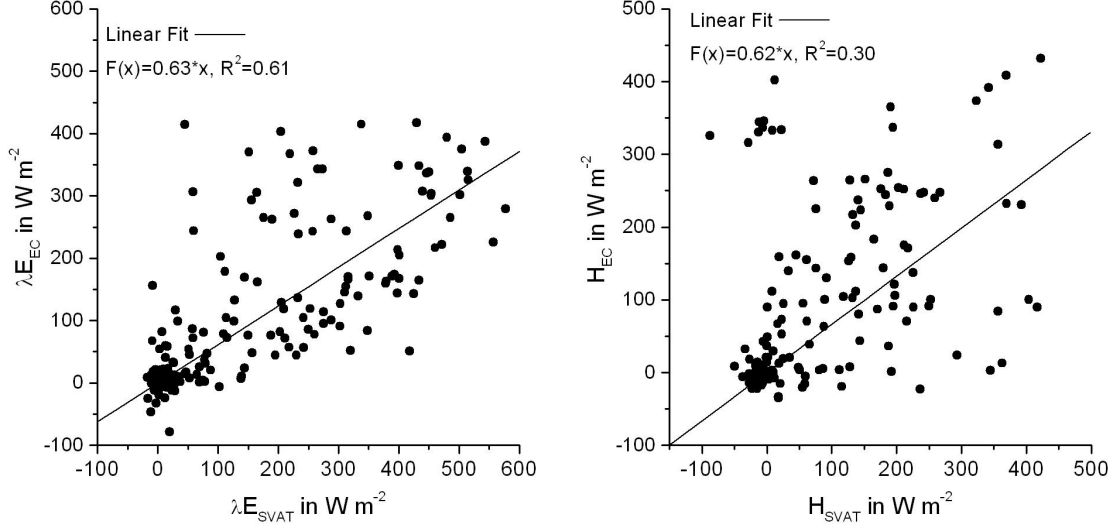
Figure 5.14: The latent heat flux derived from EC measurements, λE_{EC} is plotted versus the computed latent heat flux by a SVAT model, λE_{SVAT}, and fitted by linear regression (left). The sensible heat flux derived from EC measurements, H_{EC} is plotted versus the computed sensible heat flux by a SVAT model, H_{SVAT}, and fitted by linear regression (left). Measurement period from 17-Mar-2003 to 18-Apr-2003, Nopu.

lent heat fluxes derived from the EC measurements is fitted by linear regression against the tubulent heat flux computed by the SVAT model. The graphs show very high scattering and low regression coefficients of the linear fit. Taking only days without rainfall into account, leads to quite different results with better linear fit parameters and lower scattering, i.e. higher values for R^2:

$$\lambda E_{EC} = 1.05 \cdot \lambda E_{SVAT}, \ R^2 = 0.96 \tag{5.4}$$

$$H_{EC} = 1.07 \cdot H_{SVAT}, \ R^2 = 0.98 \, .$$

The high scattering seems to be caused by measurement errors at days with rainfall and the unsufficient model description at times when the canopies are wet. λE_{SVAT}, in the early morning hours as computed by the SVAT model indicates no formation of fog or dew. This contradicts the observations made in the field. When summing up the measured turbulent

energy fluxes and available surface energy fluxes over the measurement period at SO2, the differences are partly compensated and the energy balance closure equals

$$R_n - G_{stor} - H - \lambda E = 82.4\% \,.$$

For the comparison of sums of the turbulent heat fluxes, measured and simulated, the same reasoning applies, and result in linear fits of:

$$\lambda E_{EC} = 0.73 \cdot \lambda E_{SVAT} \tag{5.5}$$

$$H_{EC} = 1.12 \cdot H_{SVAT} \,.$$

The uncertainties in the EC measurements are caused by the reasons already discussed in the previous chapters. The vertical sensor separation of the open-path IRGA to the anemometer can explain up to 10% of the energy budget's unbalance, but is more likely to amount to about 3-5% (see Chapter 4.3.3). Malhi et al. (2002) points out, that taking into account the turbulent transport on timescales of 1 to 4 hours, leads to a significantly better energy balance closure. This means application of longer averaging time to the EC measurements and could not be investigated here, due to the response of the LI-7500 IRGA to solar incidental radiation (see Chapter 4.3.1).
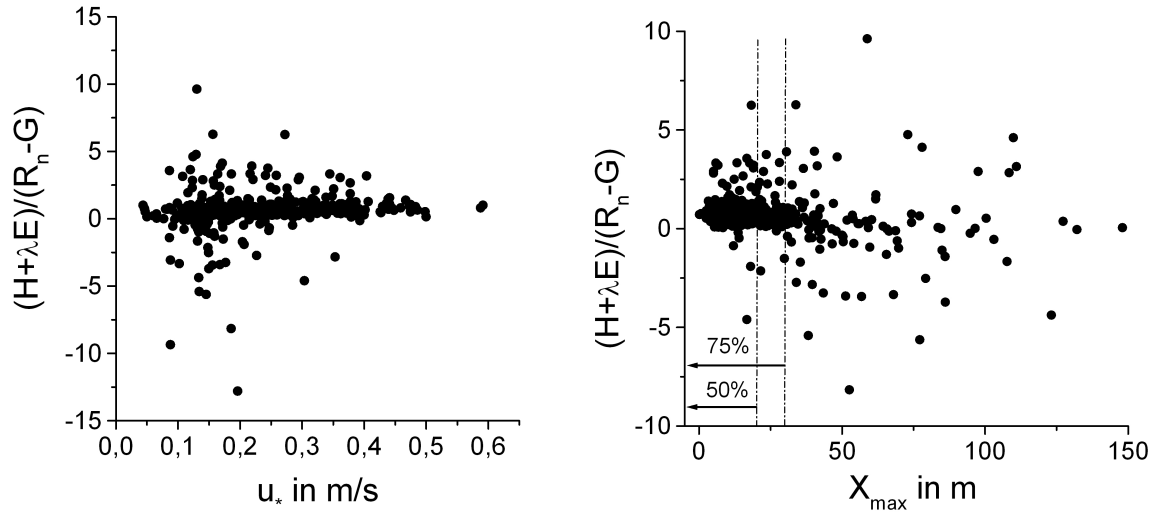
Figure 5.15: The relative energy balance closure, $(H + \lambda E)/(R_n - G)$, is plotted versus the friction velocity, $u_\star$ (left), and versus maximal source area distance (right). Measurement period from 17-Mar-2003 to 18-Apr-2003, Nopu.

Figure 5.15 shows the dependancy of the relative energy balance closure, $(H + \lambda E)/(R_n - G)$, on the friction velocity $u_\star$. The relative energy balance closure is higher for lower values of

$u_\star$ in the nighttime stably stratified boundary layer and lower for higher values of $u_\star$ in the well-mixed daytime boundary layer.

In the inertial subrange, turbulence is carrying the bulk of mass and energy in the frequency range of 1 to 10 Hz (Kaimal and Finnigan, 1994). The Li-7500 IRGA's response of $8 - 9\,Hz$ is slower than the USA-1, which is measuring at $10\,Hz$. The cospectrum of vertical wind, w, and potential temperature, θ is considered ideal, since both variables are measured by the USA-1 (Goulden et al. (1996) and Hollinger et al. (1999)). Loescher et al. (2003) describe an approach using similarity theory (Baldocchi and Meyers, 1988). The information of spectral density from the potential temperature spectrum is used to build a frequency dependant coefficient to correct the high frequency part of the cross spectrum of vertical wind with scalar C, where C is CO_2- or H_2O-density respectively, with the information from the cross spectrum of vertical wind and potential temperature θ. The spectral correction factor SC_f is given by

$$SC_f = \frac{\int_{n=0.1}^{1} n \cdot S_{w'C'} \cdot \overline{w'C'}^{-1} / \int_{n=0.001}^{10} n \cdot S_{w'C'} \cdot \overline{w'C'}^{-1}}{\int_{n=0.1}^{1} n \cdot S_{w'\theta'} \cdot \overline{w'\theta'}^{-1} / \int_{n=0.001}^{10} n \cdot S_{w'\theta'} \cdot \overline{w'\theta'}^{-1}}$$

where $S_{w'C'}$ and $S_{w'\theta'}$ are the spectral densities of vertical wind fluctuation w' and scalar C' or potential temperature θ' respectively. The loss of covariance due to the slower response of the LI-7500, as discussed by Loescher et al. (2003) amounts to an underestimation of the nighttime turbulent fluxes of up to 14% with $u_\star < 0.15\,m/s$, and of up to 6% at daytime with $u_\star > 0.4\,m/s$. This effect is not accounted for in the assessment of the latent heat flux measured at the Nopu site and explains part of the unbalance especially during nighttime.

The higher values of $(H + \lambda E)/(R_n - G)$ for small values of $u_\star$ are also associated with greater maximal source area distances X_{max}. Figure 5.15 (right) shows lower values of the relative energy balance and lower scattering of the data points for maximal source area distances $X_{max} < 20\,m$. These are associated mostly with daytime fluxes, and indicate a smaller residuum of the energy balance equation. The higher variability of the relative energy balance closure for greater values of X_{max} indicates that the EC measurements "see" other vegetation types than Cacao trees. During nighttime, the maximal source area distance X_{max} can be greater than $150\,m$. The air sample measured by the EC system is then influenced by vegetation and surface types other than Cacao trees. The self-drawn map of land-use type in the appendix, Figure A.1, is showing changes in the vegetation cover for source area distances greater than $100\,m$.

Figure 5.16 shows the mean diurnal course for the terms of the energy balance equation averaged over the measurement period in March and April 2003 at the second site in the cocoa plantations in Nopu, Indonesia. Data gaps were filled using the mean diurnal course.
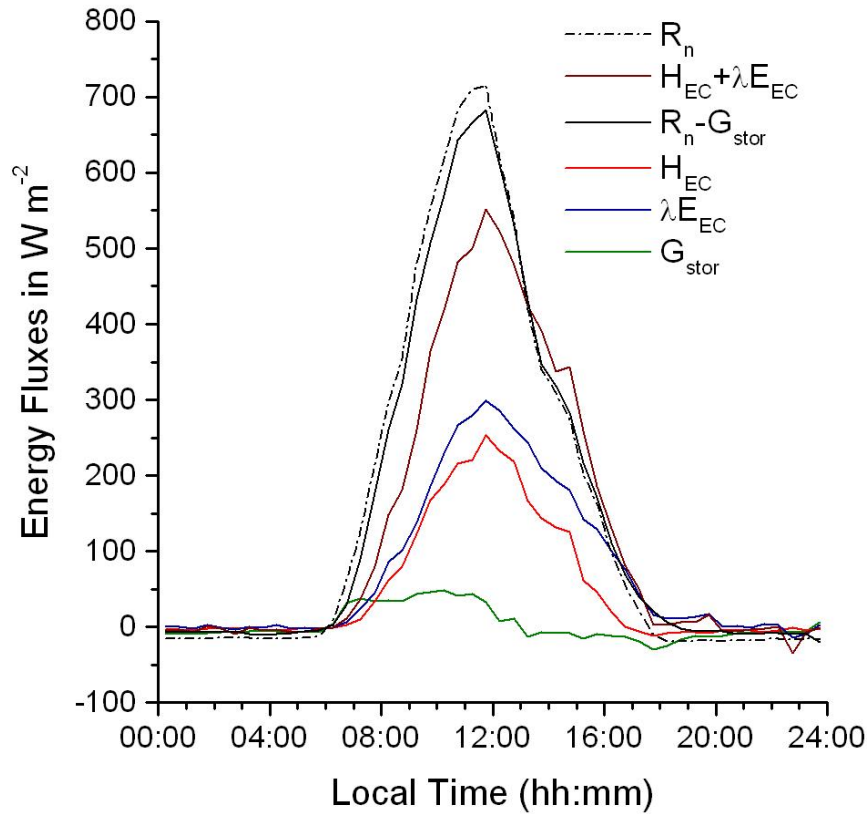
Figure 5.16: Mean diurnal courses for the terms in the energy balance, averaged over the measurement period from 17-Mar-2003 to 18-Apr-2003 at the second site in the cocoa plantation, Nopu.

The course of the net radiation R_n shows the lower values in the afternoon due to higher cloudiness and rainfall events, that happened on a regular basis between 14:00 and 15:00 LT. The energy $(R_n - G_{stor})$ available for distribution on the turbulent heat fluxes, amounts to $683\,W/m^2$ in the mean daily maximum. The turbulent energy of sensible and latent heat $(H + \lambda E)$ as measured by the EC system reaches $552.3\,W/m^2$ in the mean daily maximum, that is 81% of the available energy, This results in a maximal residuum of the energy balance equation of

$$Res_{mean,max} = R_n - G - H - \lambda E = 130.7\,W/m^2\,.$$

Interestingly, there seems to be a "hysteresis" effect in the diurnal course of turbulent heat fluxes $(H + \lambda E)$. In the morning hours the available energy $(R_n - G_{stor})$ at the surface exceeds the turbulent energy fluxes. The daily maximum is reached simultaneously by available and turbulent energy at 11:45 LT and equal each other at 13:15 LT. After noon the available

energy decreases at a higher rate, and after 13:15 LT is lower than the turbulent energy. This effect does also explain the high scatter in the linear regression of tubulent versus available energy (Figure 5.13) and the higher energy balance closure of 84% when summing up the energy fluxes over the month of measurements, than in the actual observations (energy balance closure: 70%).

The closure of the energy balance equation is still a major topic in literature (Wilson et al. (2002), Grace et al. (1995), Shuttleworth et al. (1984) and Ibrom (2000)) and not fully achieved so far. Moreover, the assessment of EC measurements above complex or heterogeneous terrain, as found in the investigated cocoa plantations is still poorly understood (Kaimal and Finnigan, 1994).
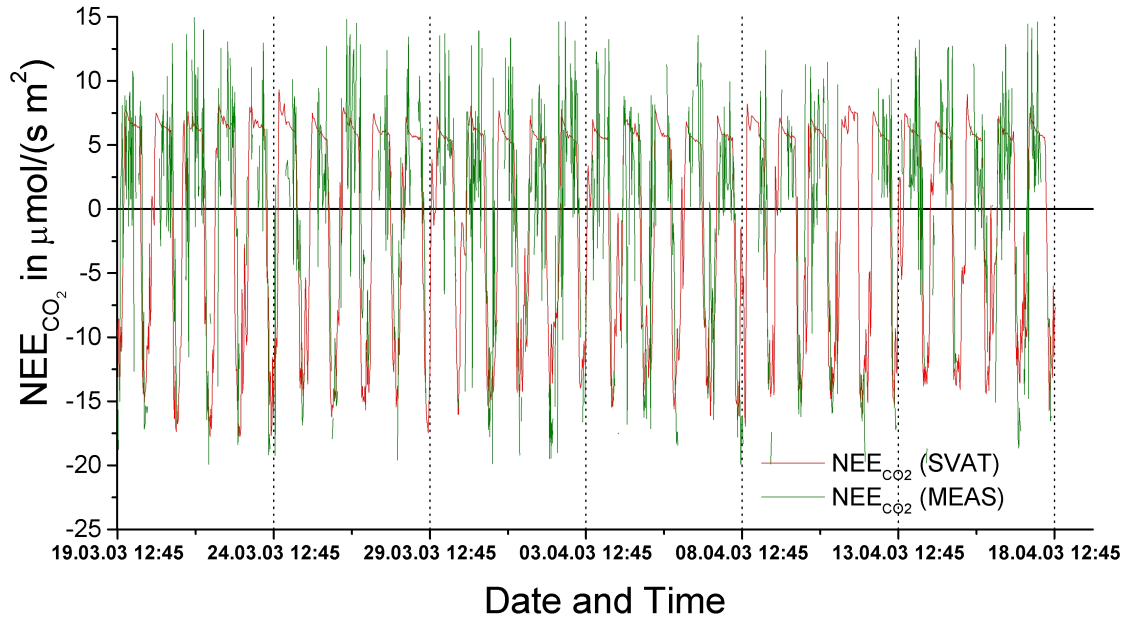
Figure 5.17: Diurnal courses of net ecosystem exchange of CO_2 derived from EC measurements, $NEE_{CO_2}(MEAS) \equiv NEE_{CO2,EC}$, and computed by a SVAT model, $NEE_{CO_2}(SVAT) \equiv NEE_{CO2,SVAT}$. Negative values indicate an uptake of CO_2 by the ecosystem and positive values mean respiration of CO_2 by soil and vegetation. Measurement period from 17-Mar-2003 to 18-Apr-2003, Nopu.

The net ecosystem exchange of CO_2 derived from the EC measurements, $NEE_{CO2,EC}$, is in good accordance with the flux computed by the SVAT model, $NEE_{CO_2,SVAT}$, (Figure 5.17). The maximal daily net ecosystem uptake of carbon dioxide by the cocoa plantation amounts

up to $20\mu mol\,m^{-2}s^{-1}$. The respiration of the cacao trees at night shows good resemblance of measurements and model on the average.
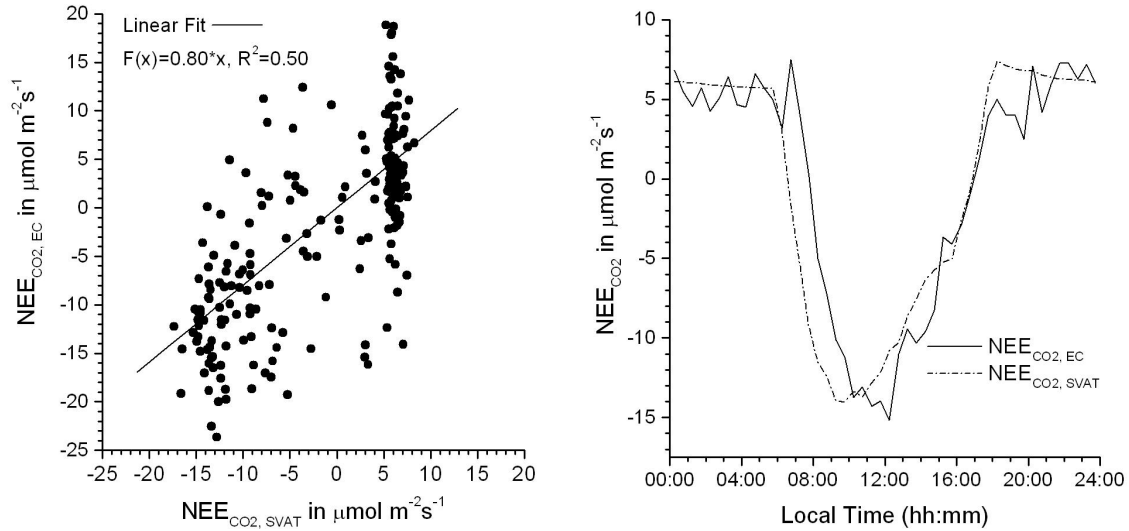
Figure 5.18: The net ecosystem exchange of CO_2 derived from EC measurements, $NEE_{CO2,EC}$, is plotted versus the computed net ecosystem exchange of CO_2 by a SVAT model, $NEE_{CO2,SVAT}$, and fitted by linear regression (left). The mean diurnal courses of $NEE_{CO2,EC}$ and $NEE_{CO2,SVAT}$ are displayed versus local time (right). Measurement period from 17-Mar-2003 to 18-Apr-2003, Nopu.

In Figure 5.18 (left), the net ecosystem exchange of carbon dioxide as measured by the EC system is plotted versus the simulated carbon dioxide exchange by the SVAT model. The linear regression shows good accordance, but also a high scattering, i.e. a low regression coefficient:

$$H_{EC} = 0.80 \cdot H_{SVAT} \ R^2 = 0.5\,.$$

The low regression coefficient or high scatter is partly caused by the uncertainty of measured nighttime respiration of soil and cacao trees. Figure 5.18 (right), the mean diurnal courses of net ecosystem carbon dioxide exchange simulated by the SVAT-model $NEE_{CO2,SVAT}$, and measured by the EC system $NEE_{CO2,EC}$ are displayed. Although the CO_2-net exchange is in good accordance between model and measurements, there seems to be a time shift. The modeled $NEE_{CO2,SVAT}$ reaches its minimum, i.e. maximum uptake by the vegetation, at 9:45 LT, whereas the measured $NEE_{CO2,EC}$ is minimal at 12:15 LT. The monthly sum over all measured $NEE_{CO2,EC}$ amounts to 98% of the simulated $NEE_{CO2,SVAT}$.

The findings in both, energy fluxes as well as net CO_2-exchange, show good accordance

between the SVAT-model and the measurements. But there also exists a time shift between model and measurements, that introduces high scatter into the linear regressions. The clocks of the EC data acquisition system and the radiation system were set with great accuracy, in especially both system clocks were synchronized to one laptop, where the internal clock was set to local time and synchronized to the respective world clock via internet. Since the EC measurements were conducted within the roughness layer, a possible explanation for the time shift in the energy fluxes would be the build-up of an internal boundary layer. Also did the model not simulate formation of dew and fog below the sensors, that were observed regularly in the morning hours. This would potentially lead to a time delay of the measurements versus the model. The uncertainty in the nighttime flux observations measured by the EC system also introduces a high scatter into the linear regressions. Besides that, in summary measurements and model show good accordance.

5.4 Bowen ratio of turbulent heat fluxes above a cocoa plantatation in the Palolo Valley, Sulawesi, Indonesia

The seasonality of precipitation, as discussed in Chapter 5.1.2, has no important influence on the distribution of available energy at the canopy's surface on the turbulent heat fluxes (Figure 5.9, (above)). During months with high precipitation rates the latent heat flux exceeds the sensible heat flux by only 20% on the monthly average (March and April 2002, and December 2003). In days with low precipitation rates, the sensible heat flux exceeds the latent heat flux by 10 to 15% on the monthly average (July and August 2002). This can also be seen in higher daily maxima of the Bowen ratio, as displayed in Figure 5.19. The high standard errors of $\beta = H/\lambda E$ during nighttime are caused by the latent heat flux that is negative and close to zero. There exist days without rainfall in the dry as well as in the rainy season. Analysis of the daytime flux observations for days with no rainfall yield:

$$H = 0.106 * \lambda E, \ R^2 = 0.90$$

In other words, the sensible heat flux equals the latent heat flux at daytime in the mean diurnal course. The mean daytime Bowen ratio observed at the cocoa plantation in Nopu equals $\beta = 1.06$. In the months February 2002 and 2003, monthly averages of daytime Bowen ratio show even higher values of $\beta = 1.3 \ldots 1.6$, indicating an even stronger pronounciation of the sensible heat flux in the atmospheric surface boundary layer.
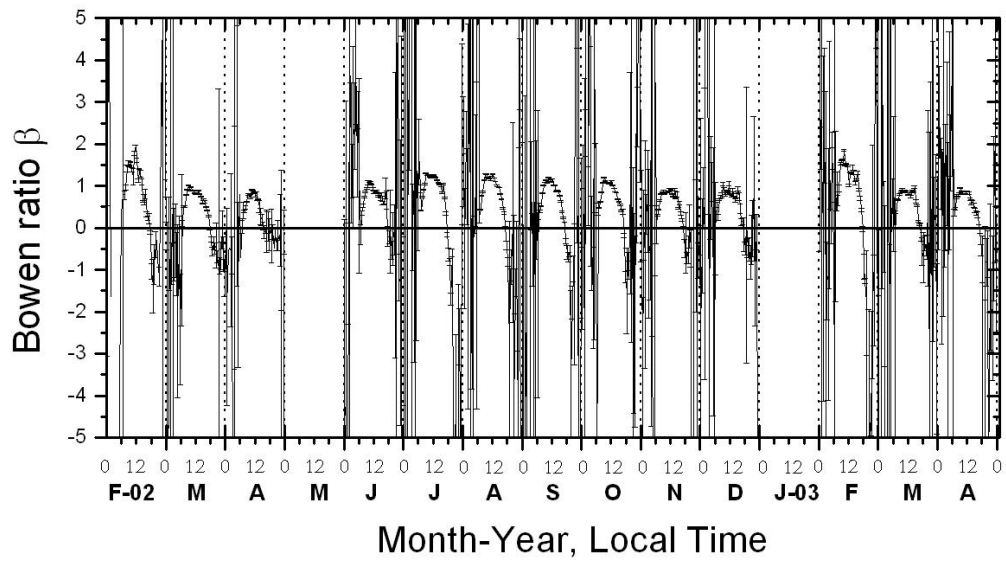
Figure 5.19: Monthly averaged diurnal course of the Bowen ratio $\beta = H/\lambda E$ at the Nopu site, Palolo valley in Central Sulawesi, Indonesia. Measurement period from February 2002 to April 2003. The dashed lines denote the standard error.
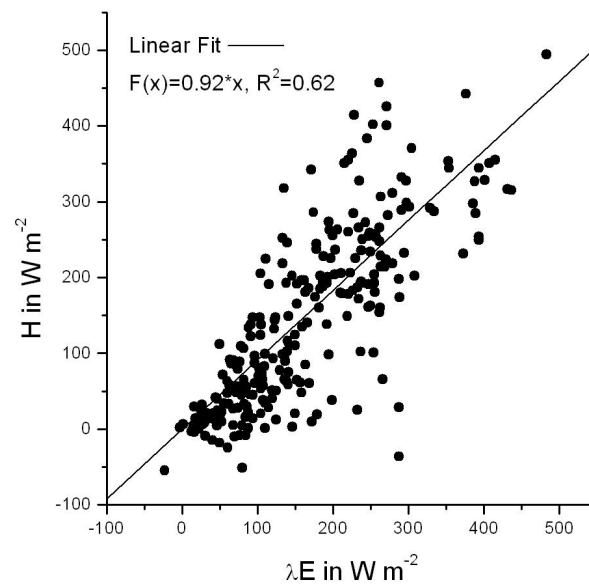
Figure 5.20: Calculation of the Bowen ratio by linear regression of the sensible heat flux H versus the latent heat flux λE at the Nopu site, Palolo valley in Central Sulawesi, Indonesia. Measurement period from February 2002 to April 2003.

Chapter 6

Eddy-Covariance measurements above primary tropical rain forests

6.1 EC measurements at the Micrometeorological Tower above montane primary rain forest in the Besoa valley, TNLL, Indonesia

6.1.1 Setup of the Micrometeorological Tower and site description

The Taman Nasional Lore Lindu (TNLL) is a mountaneous area with several valleys, where settlements have already existed a rather long time. No records exist about the age of the different villages, but every valley (nearly every village) has developed an own language. Throughout the park, ancient belaboured stones called megalith's can be found. These megaliths are dated back to 1000 to 3000 BC (project CARE, Canada), indicating that the area around the National Park has been inhabited for quite a long time. Due to the problem of rising population numbers in Indonesia, there is a growing need for land and growing pressure on the forests. Most of the valleys in the TNLL had already been cleared from former rain forests and transformed to agriculturally used land restricting the undisturbed primary forests to the more mountaneous areas. Micrometeorological and eddy covarinace measurements require a sufficient extensive, flat and homogenuous terrain, especially when measuring at a tower above forest. Also easy and year-round access to the research site has to be granted for good and regular maintenance of long-term measurements. During the preparations for the research project "Stability of Rain Forest Margins" (STORMA), the

site for the micrometeorological tower planned within the research proposal was decided to be situated on a mountain ridge between the Palolo valley and Napu valley about 110 km, a two hours drive, from Palu, the capital city of Central Sulawesi. Since no precise maps existed of that area, a mapping had to be carried out from april to june 2001, using a $50\,m$-rope, compass and barometer. Socialisation of the research project to the village claiming that area of forest to be under their administration by traditional rules, was achieved. A final area for the tower was constituted and negotiations about the involvement of villagers into the project carried out. Biological expertise about the representativeness of the vegetation at the site was contributed by Pak Hary, Herbarium Bogoriensis, Bogor. Finally, a suitable place and a suitable access path to the proposed site, about $900\,m$ away from the road were found. An issue was still the allowance by the governor of Central Sulawesi and Forestry Department. The approval of the National Park administration was already achieved.

Transmigration programs in the 1970's under the Sueharto regime included the resettlement of people from more populated areas, i. e. from Java, to the outer islands, and also to the area around the TNLL on Sulawesi. Unkept promises of land for farming by the government to the transmigrants and the political vacuum that has been created since the resignation of the Sueharto government, created a rather tense situation. The demand for tropical wood by the industrial nations and the paper industry, but also the ongoing political agitation in Indonesia, i.e. the shifting of power from Jakarta to the regencies lead to a massive logging incident and claim of land around the proposed tower site in july 2001. In about 3 days forests of the National Park area in the vicinity of the research site was logged about $18\,km$ along the road and $300\,m$ to the left and right into the forest. The ongoing logging and the tension between local people, non-governmental organizations (NGO) and the government were imperative to abandon the tower site.

In order to find a new site for the micrometeorological tower an investigation of several promising sites was carried out in October 2001, and finally succeeded in finding a suitable forest area in the Besoa valley. The Besoa valley is about $180\,km$, a 2.5 to 5-6 hours drive, away from Palu, depending on the condition of the only road leading into the valley. During rainy season, november to march, road conditions can get extremely difficult and also the many bridges over water creeks and rivers tend to break down every now and then. Two possible sites situated about $7\,km$ away from the next village were investigated and mapped by a team of students from the University of Tadulako (UNTAD), Palu in November and December 2001, to provide information about the surrounding terrain of the proposed new sites. The final decision about the site was felled in December 2001 on the results of this survey, in favor of the site at coordinates $1°39'28.4''\,S$ and $120°10'24.4''\,E$.

In order to provide an easy and year-round access to the site for transport of the tower material, and later-on for maintenance of running measurements, a driveable pathway was planned and constructed from the next village to the tower site. Road construction was under the supervision of the Indonesian B1-counterpart Ir. Abdul Rauf (UNTAD).

Figure 6.1: Picture of the installed micrometeorological tower in the Besoa valley, TNLL, Sulawesi, Indonesia

An extensive socialization was carried out with the help of the STORMA coordinators in Palu, to achieve the support of the surrounding villages and their willing to respect the area around the micrometeorolical area as protected area. Final construction of the tower followed February 2003 under the supervision of Agus Mulyana from Pt. Beton, Jakarta, the

company that delivered the tower. Installation of the EC-system of Nopu and meteorological measurements was accomplished by Heinrich Kreilein (IBK) in July and October 2003. In the following chapter, results of the first measurements of fluxes of CO_2 and H_2O from October 12th to October 15th are discussed with regard to the distribution of available energy to the turbulent heat fluxes.

6.1.2 Turbulent fluxes of heat and CO_2 above montane rain forest

The discussion of the atmospheric surface boundary layer above the montane rain forest at the Besoa site is based on the mean diurnal courses averaged over a measurement period of 3 days, October 12th to October 15th. Although this is not sufficient for a well-founded comparison of the two investigation sites in Central Sulawesi, some significant differences can already be pointed out.

The EC system was installed at $16.3\,m$ above mean canopy height. For the measurement period, the mean daily temperature maximum amounts to $T_{max,mean} = 23.6°C$ and the minimum to $T_{min,mean} = 17.3°C$. The daytime relative humidity averages to $rh = 50\%$. 50% of the observed turbulent fluxes originated from a footprint with a maximum source area of $X_{max} < 44\,m$ and for 75% the maximal source area computes to $X_{max} < 215\,m$ using the approach by Wilson and Swaters (1991).
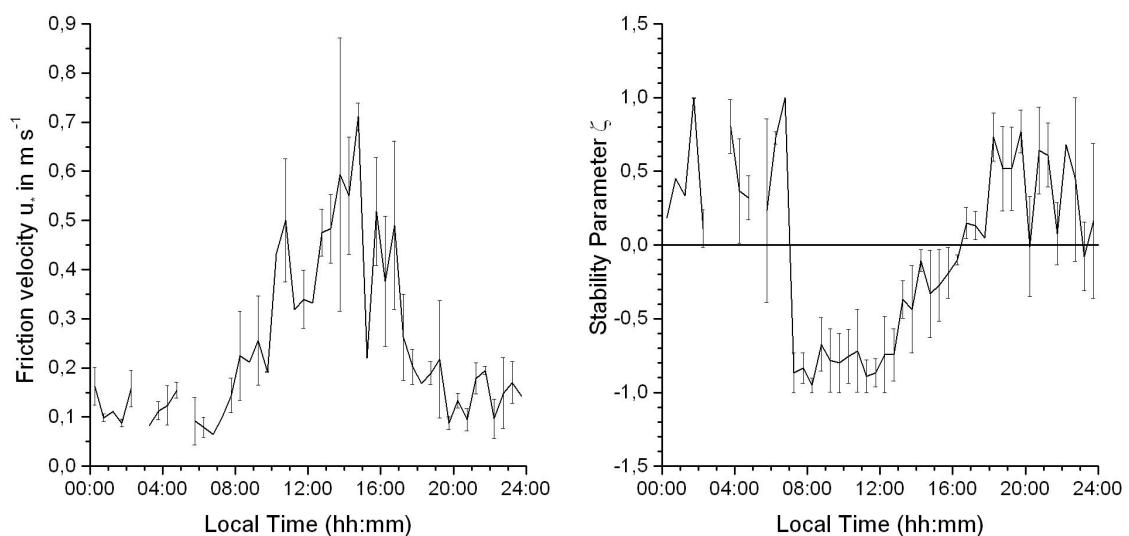
Figure 6.2: Mean diurnal course of friction velocity $u_\star$ (left) and stability parameter ζ (right), averaged over the period from October 12th to October 15th 2003, above montane tropical rain forest in Central Sulawesi, Indonesia. The errorbars denote the standard error.
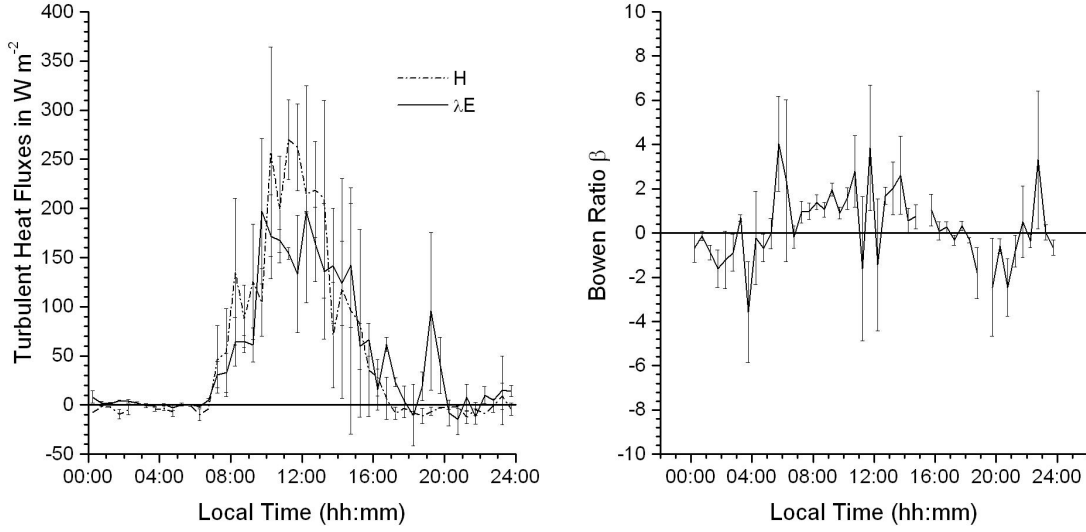
Figure 6.3: Mean diurnal course of the turbulent fluxes of latent (solid line) and sensible heat (dash-dotted line), λE and H (left), and Bowen ratio β (right), averaged over the period from October 12th to October 15th 2003, above montane tropical rain forest in Central Sulawesi, Indonesia. The errorbars denote the standard error.

The diurnal course of the stability parameter $\zeta = z/L$ shows a more distinct stable stratification of the nocturnal boundary layer than observed at the Nopu site (Figure 6.2 (right)). During the day, a slightly unstable convective boundary layer can be observed at mean friction velocities of maximal $u_\star = 0.5\,m$ (Figure 6.2 (left)).

The mean diurnal courses of the turbulent fluxes of latent and sensible heat do not show significant distinctions to the observations above the cocoa plantations in Nopu (Figure 5.9). The sensible heat flux is exceeding the latent heat flux by about $60\,W\,m^{-2}$ in the mean daily maximum. The large error bars indicate the large variance of the mean diurnal courses, that are averaged only over three days. The Bowen ratio computes to

$$\beta = 1.0 \pm 0.6,\ R^2 = 0.54$$

where the high standard error and the low regression coefficient show the uncertainty of the estimated values. The net ecosystem exchange of CO_2 observed at the Besoa site shows a mean maximal uptake of $33.8 \pm 11.1\,\mu mol\,m^{-2}s^{-1}$ by the canopy. Monthly averaged values of NEE_{CO2} observed at the Nopu site did not exceed an uptake of $16.2\,\mu mol\,m^{-2}s^{-1}$. As for the respiration of the ecosystem during nighttime, no significant distinction can be seen. The daily evapotranspiration observed during those first three days of measurements, amounts to $ET = 1.64 \pm 0.76\,mm\,d^{-1}$, and the net ecosystem exchange of carbon to
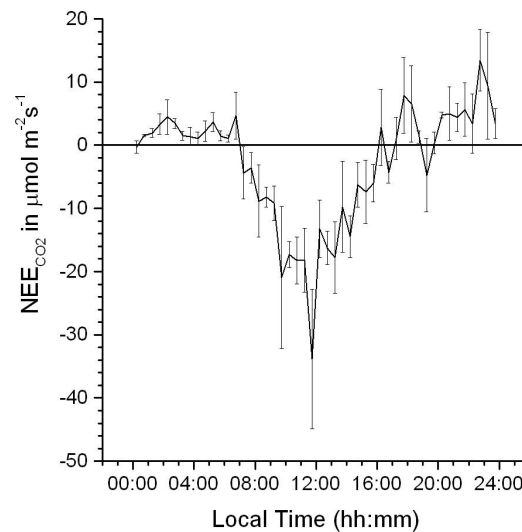
Figure 6.4: Mean diurnal course the net ecosystem exchange of CO_2, averaged over the period from October 12th to October 15th 2003, above montane tropical rain forest in Central Sulawesi, Indonesia. The errorbars denote the standard error.

$NEE_C = -1.53 \pm 0.71$ g-C $m^{-2}d^{-1}$.

Comparing to the EC measurements in October 2002 in Nopu show the same distribution of turbulent heat flux. However it has to be taken into account, that 2002 was a weak El-Ninño year which prolongated the onset of the rainy season. For a thorough investigation, a more comprehensive data basis is inevitable.

6.2 EC measurements above lowland neotropical rain forest at the Surumoni Crane Site, Southern Venezuela

6.2.1 Site description and characterization of surface boundary layer

The research site is situated in the catchment area of the upper Orinoco, Southern Venezuela, in the Estado Amazonas, which covers an area of $175759\,km^2$, nearly 20% of Venezuela. The basic landscape elements in the Estado Amazonas are the Guayana at the eastern border to the Estado Bolivar, and the lowlands in the western part, with the Orinoco as second largest river of Latin America. To the catchment area of the Orinoco belong the Guayana highlands and the Amazonian lowland. The Surumoni Crane Project is subject of an interdisciplinary research focus "Towards an understanding of the structure and function

Table 6.1: Forest types found in the Amazonian lowland rain forest near the research site of the Surumoni Crane project, Anhuf and Winkler (1999)

Forest Type	Exposition to Flooding	height in $m.a.s.l.$
moist evergreen forest	temporarily (seasonally) flooded	98-103
transitional evergreen forest	not regularly flooded	103-104
moist evergreen forest terra firme	non-flooded	>104

of a neotropical rain forest ecasystem with a special reference to its canopy" by the Austrian Academy of Sciences from 1995 to 2000 (Anhuf and Winkler, 1999). The research site is situated at a small black-water tributary of the upper Orinoco, the Surumoni, and also named after it. The Surumoni drains the Cerro Duida, lying about $15\,km$ north of the research site. The Duida-Marahuaca massif is roughly in the center of the state Amazonia and belongs to the sandstone table mountains, the so-called Tepui. The Duida reaches a height of 2358 $m.a.s.l.$ at the south-western face. The seasonal pattern at the Surumoni site is described in detail by Szarzynski (2000), with the dry season lasting from September until March and the rainy season from April until August. The annual rainfall amounts to $2721\,mm$ in La Esmeralda (1970-1995) and to $3245\,mm$ in Tama-Tama (1970-1995), two small villages situated upstream (La Esmeralda) and downstream (Tama-Tama) from the Crane site. The absolute value of water vapour content in the atmosphere varies between 15 to 25 g/kg and the mean annual temperature is 25.5 to 26.5°C (Szarzynski, 2000). The forest is subdivided by Anhuf and Winkler (1999) into three different types, as displayed in Table 6.1.

From January until June 2000, a field campaign was carried out in order to investigate the turbulent surface boundary layer at the Surumoni site with the Eddy-Covariance method. The EC sensors were installed at the top of the crane in a height of $40\,m$, about $15\,m$ above the canopy. The precipitation during June 2000 amounted to 608.6 $mm\,mo^{-1}$ measured on top of the crane, and 601.9 $mm\,mo^{-1}$ in a nearby forest gap.
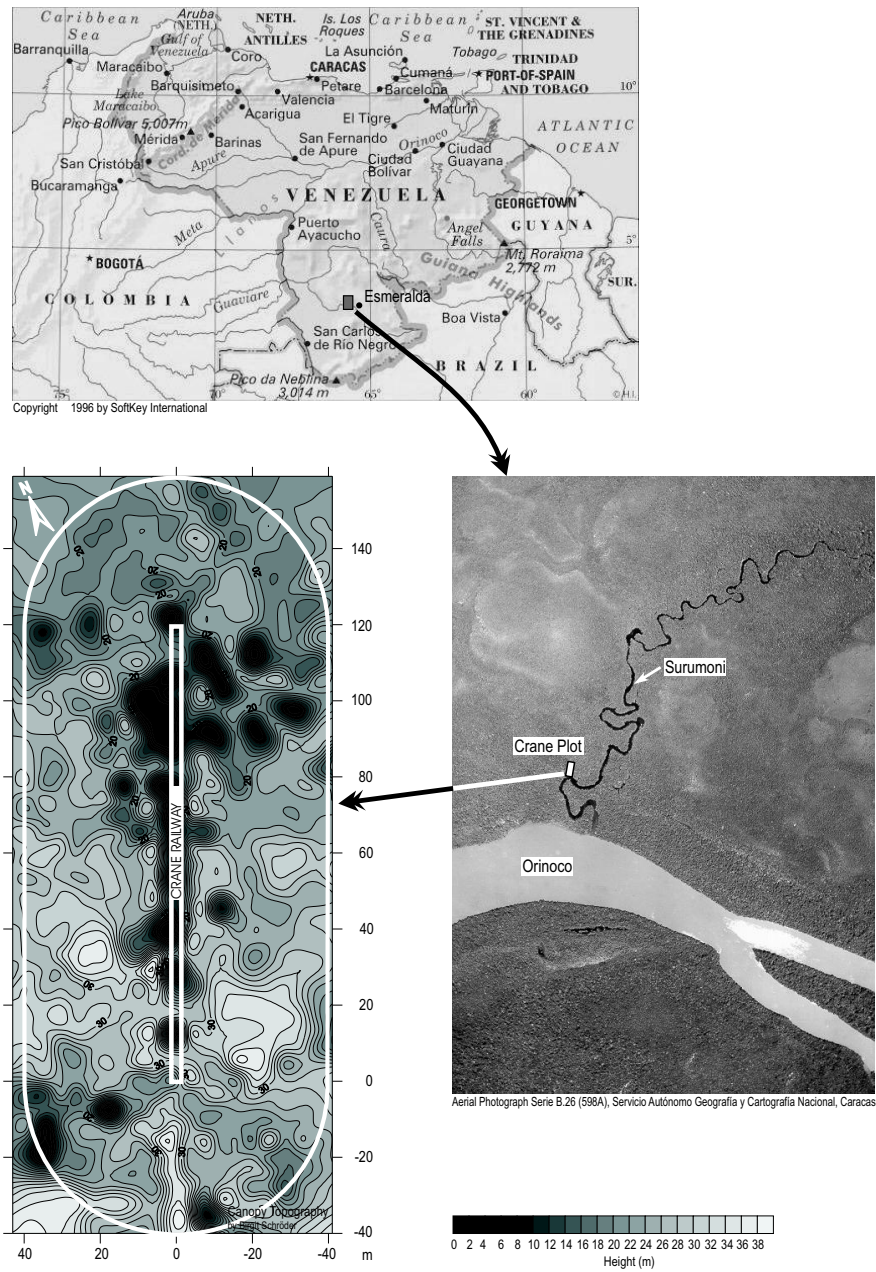
Figure 6.5: Location of the Surumoni Crane Site at the upper Orinoco, Southern Venezuela, from Anhuf et al. (1999)

The EC measurement system used here included a closed-path sensor for CO_2- and H_2O-content of the ambient air (see Chapter 3.1.2). Due to infrastructural problems, especially the insuffient and unstable power supply at the crane site, continuous data of flux measurements exist only for the month June. The measurements then stopped due of a lightning stroke in the direct vicinity of the crane, that caused a break-down of the EC system's central sensor, the ultrasonic anemometer. The stratification of the atmospheric boundary layer during the observation period is changing from slightly stable conditions at nighttime to slightly unstable conditions during daytime, as can be seen in the mean diurnal course of the stability parameter ($\zeta = z/L$) in Figure 6.6.
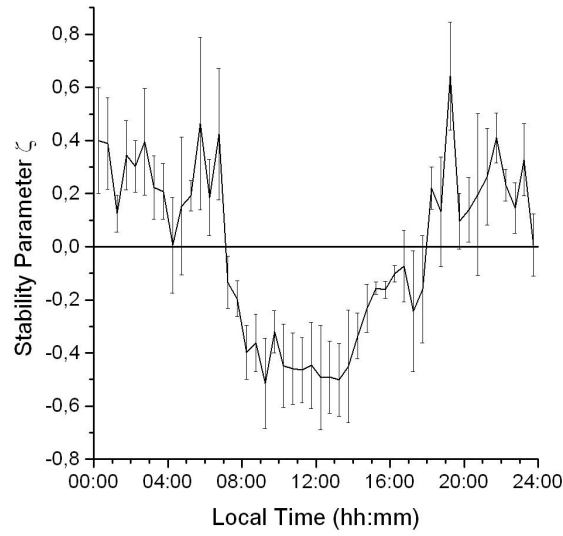
Figure 6.6: Mean diurnal courses of the stability parameter $\zeta = z/L$ at the Surumoni Crane site, averaged over the time period 09. June to 25. June 2000. Error bars denote the standard error

Figure 6.7 shows the mean diurnal courses of the temperature scale $\theta_\star$ and the friction velocity $u_\star$. During nighttime, the turbulence production is low and more dynamically induced (small positive values for $\theta_\star$), whereas during daytime, the generation of turbulence is mainly thermally ($\theta_\star < 0$). Values for $u_\star$ range between 0.1 and $0.2\,m\,s^{-1}$ at night and reach a daily maximum of $0.5\,m\,s^{-1}$. Thus, turbulence in the surface layer is low at nighttime suppressed by the stable stratification of the atmospheric boundary layer.

The footprint analysis of the turbulent signal measured at the EC-site is done by following the approach of Wilson and Swaters (1991). During nighttime, when the vertical mixing of the boundary layer is low due to stable stratification, it takes the air sample longer to rise to the measurement height and thus it can be carried a greater distance by the mean
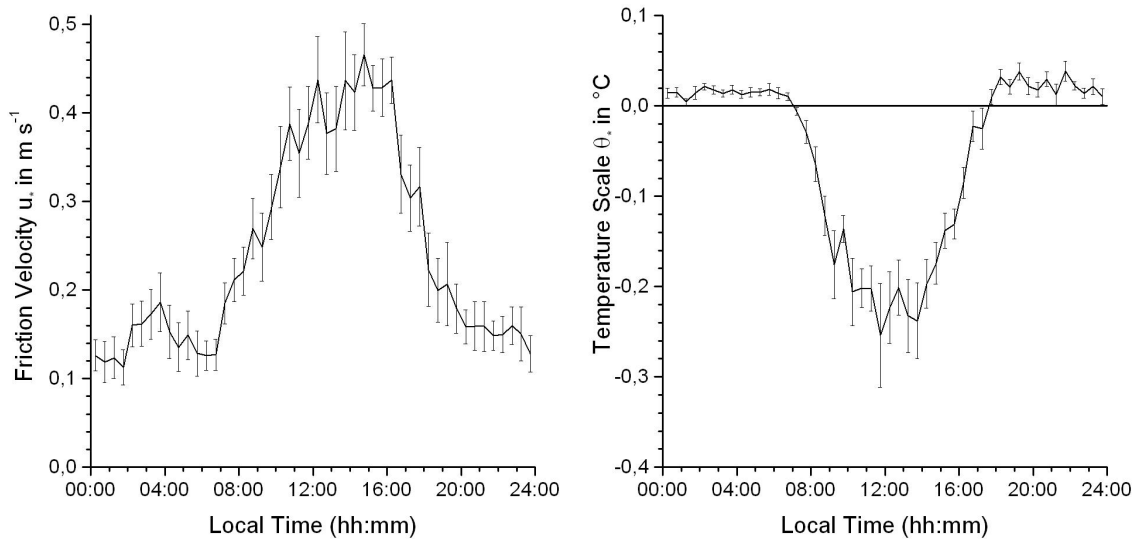
Figure 6.7: Mean diurnal courses of the surface layer temperature scale $\theta_\star$ (left) and the friction veloctiy $u_\star$ (right) at the Surumoni Crane site, averaged over the time period 09. June to 25. June 2000. Dashed lines denote the standard error

horizontal wind until it reaches the EC sensors. The opposite is occuring during daytime, when unstable stratification is enhancing the vertical mixing of the boundary layer. Figure 6.8 diplays the analysis of the footprint for the Surumoni crane site during June 2000. About 50% of the turbulent signal measured by the EC sensors originates from a source area less than $230\,m$ away from the EC site and especially during the daytime convective boundary layer, the source area distance can be much smaller.

6.2.2 Turbulent fluxes of CO_2, latent and sensible heat at the Surumoni crane site

During the observation period in June 2000, the area at the upper Orinoco was flooded on a larger scale. This was observed out of the Çesna used for travel between the research facility at the Surumoni and Puerto Ayacucho, i.e. the reflections of the sun on the water surface in the canopy. Since the Crane plot is situated on more elevated ground (at $104\,m.a.s.l.$) than the surrounding area, the research facility appeared to be situated on an island. Hence, water was available in abundance at the surface and this also explains the high values for the turbulent flux of water vapour shown in Figure 4.4.

The latent heat flux exceeds the sensible heat flux about four times, leading to a Bowen
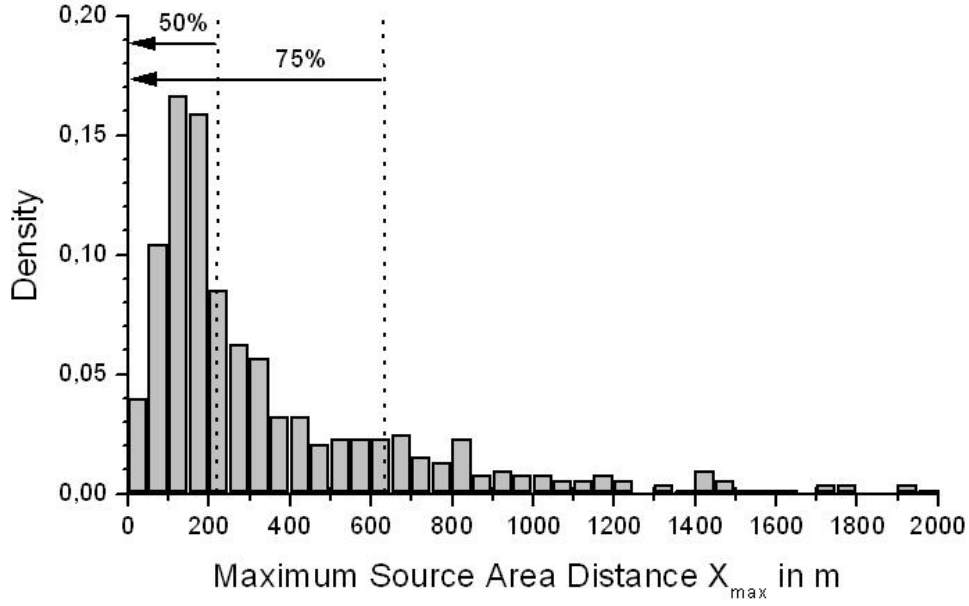
Figure 6.8: Calculation of the maximal source distance X_{max} area after Wilson and Swaters (1991) for the Surumoni Crane site, for the time period 09. June to 25. June 2000. Shown is the density of X_{max}, area normalized to 1.

ratio of $\beta = 0.25$ in the daily maximum. The mean daily sum of evaporation amounts to $4.1\,mm\,d^{-1}$, the mean daily sum of latent heat flux to $117\,W\,m^{-2}d^{-1}$ and of sensible heat flux to $22\,W\,m^{-2}d^{-1}$. The ratio of turbulent sensible heat flux to turbulent latent heat flux (Figure 4.4), the so-called Bowen ratio, is used as a means in meteorology to describe the characteristics of heat exchange between atmosphere and vegetation. The observed daytime Bowen ratio amounts to $\beta = 0.25$ for the Surumoni site (Figure 6.9).

The mean diurnal course of Net Ecosystem Exchange of carbon dioxide, NEE_{CO_2}, is displayed in Figure 6.9. The direction of NEE_{CO_2} is defined positive for a flux of CO_2 from the biosphere to the atmosphere by canopy and soil respiration. Negative values of NEE_{CO_2} represent an uptake of CO_2 by the biosphere through photosynthesis during daytime, where maximal values can exceed an uptake of $15\,\mu mol\text{-}CO_2\,m^{-2}s^{-1}$ by the vegetation (Figure 4.4). Peak values in the early morning or early evening hours can be explained by a flush-out of CO_2 from within the forest into the atmospheric boundary layer during thunderstorms.

The mean carbon uptake of the canopy during the observation period in June 2000 amounts to $1.34\,g\text{-}C\,m^{-2}d^{-1}$, indicating that a neotropical primary rain forest can still be regarded as a carbon sink. For proof though, long-term measurements over several years are inevitable to

account for seasonal and interannual variability as for instance to quantify effects of El-Niño years.

These first measurements showed that the Surumoni Crane site provides excellent site conditions for future long-term investigations of the carbon budget of a diverse lowland rain forest.
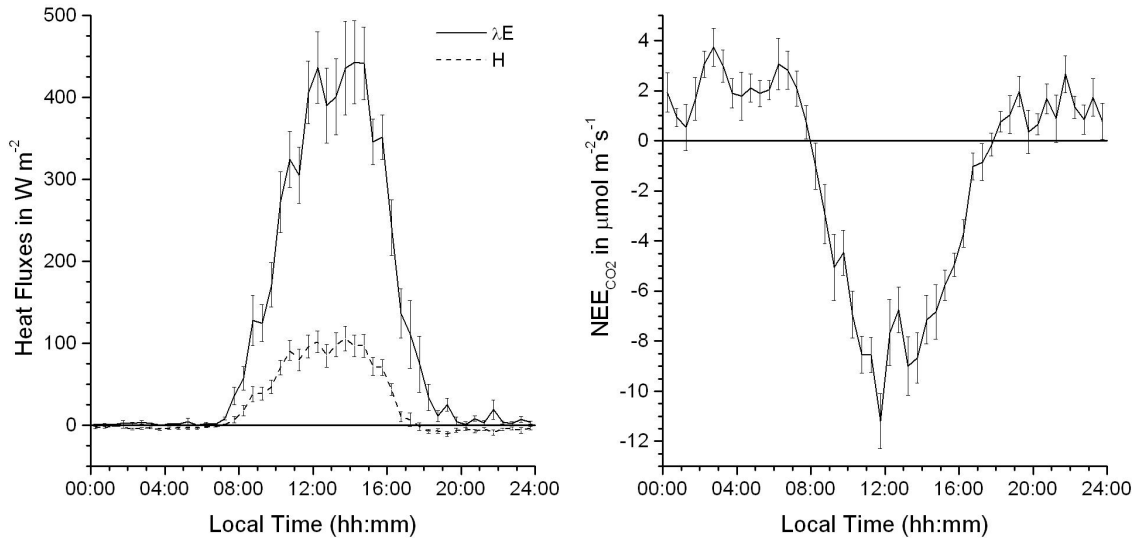
Figure 6.9: Mean diurnal courses of the sensible and latent heat flux, H and λE (left), and the net ecosystem exchange of carbon dioxide NEE_{CO_2} (right) at the Surumoni Crane site, averaged over the time period 09. June to 25. June 2000. Dashed lines denote the standard error.
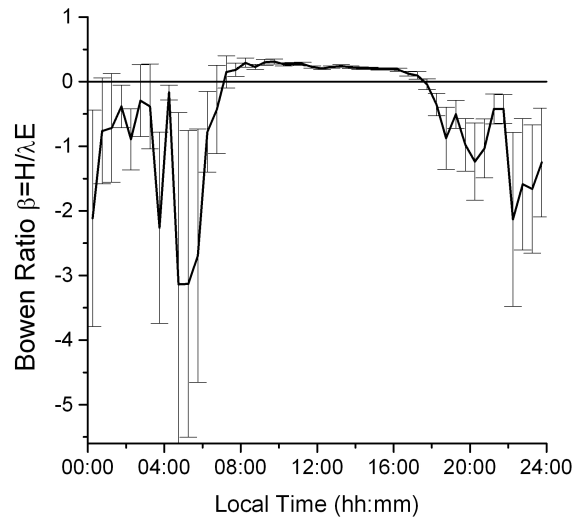
Figure 6.10: Mean diurnal course of the Bowen ratio $\beta = H/\lambda E$ at the Surumoni Crane site, averaged over the time period 09. June to 25. June in 2000. Dashed lines denote the standard error.

Chapter 7

Comparison of net CO_2-exchange and partitioning of turbulent heat observed at the different sites.

A comparison of the measurements at the three different sites can only be selective, since the data sets from the Surumoni site and the Besoa site are on a shorter time basis than the one from the Nopu site, i.e. less than one year. Seasonal variability cannot be investigated for the Surumoni site. The observed fluxes from the 3-days measurement period at the Besoa site show a large variance. Thus, the flux estimations and derived variables can only be taken as preliminary. Other longterm observations above neotropical rain forests found similar results to the results of this work. Loescher (2002) reports an observed Bowen ratio of $\beta = 0.36$ for a wet rain forest in Costa Rica. This is comparable to the Bowen ratio observed during the three-weeks measurement campaign at the Surumoni site.

A significant difference in the Bowen ratio is found comparing the observations at a low-land primary rain forest in the Amazon (Surumoni) to the montane rain forest site (Besoa) and the cocoa plantations in Nopu. The high water availability during the rainy season at the Surumoni results in a mean daytime Bowen ratio of $\beta = 0.25$. The Bowen ratio $\beta = 1.1$ as observed at the cocoa plantation in Nopu, indicates that conversion of tropical rain forest into cocoa plantations, leads to a stronger pronounciation of the sensible heat exchange, and thereby, a heating of the daytime atmospheric surface boundary layer. The results from the micrometeorological tower in the Besoa valley show a high variability in the observed turbulent fluxes. This is due to the sparse data set (three days in October 2003). Longterm measurements will lead to more reliable data on the partitioning of the turbulent heat fluxes.

85

Table 7.1: Daily evapotranspiration ET_d, latent heat flux λE_d, sensible heat flux H_d, daytime Bowen ratio β, and net ecosystem exchange of carbon NEE_{CO2} at the investigated sites in Nopu (Indonesia), Surumoni (Venezuela), and Besoa (Indonesia).

	Nopu	Surumoni	Besoa	Unit
ET_d	2.55	4.1	1.6 ± 0.7	$mm\, d^{-1}$
λE_d	73.6	117	47	$W\, d^{-1} m^{-2}$
H_d	62	22	69	$W\, m^{-2} d^{-1}$
β	1.1	0.25	1.0 ± 0.6	
$NEE_{C,d}$	-0.12	-2.36	-1.5 ± 0.7	$g\text{-C}\, m^{-2} d^{-1}$

Daily evapotranspiration of the different sites are displayed in Table 7.1. For a comparison ot the different sites, the evapotranspiration rates, i.e. the ratio of ET_d to precipitation amount *prec*, are more significant. Loescher (2002) reports $ET_d/prec = 0.54\ldots0.65$ for the Costa Rican site. Calder et al. (1986) gives an estimate of $ET_d/prec = 0.52$ at a natural forest site in Janlappa, Java, Indonesia. The evaporation rate $ET_d = 0.36$ at the cocoa plantation in Nopu is significantly lower compared to the natural rain forest sites, and could be interpreted as a the lower availability of rain water to evapotranspiration due to enhanced rain water run-off.

The net ecosystem uptake of CO_2 by the canopy observed at the Besoa site amounts to $11\,\mu mol\, m^2 s^{-1}$ in the mean daily maximum. Compared to the net ecosystem uptake at the Surumoni of $15\,\mu mol\, m^2 s^{-1}$, shows a slightly higher uptake by the neotropical rain forest site. Comparison of the daily net ecosystem exchange of carbon for the three investigated sites, shows a significantly lower uptake by the cocoa plantation than by the natural rain forest site at the Surumoni. The Besoa site shows an intermediate behaviour, with high standard error of $\pm0.7\,g\text{-C}\, m^{-2} d^{-1}$. As pointed out in Chapter 6.1, the data basis of three days is not sufficient for a meaningful comparison to the other sites.

Chapter 8

Summary and conclusions

The conversion of tropical rain forest to agriculturally used land is a spreading process throughout Indonesia and South-East Asia. Besides the effects on the biological diversity and the hydrological functions of a forest, this also has an impact on the turbulent exchange processes between vegetation and atmosphere, the radiative properties of the surface and therefore on atmospheric boundary layer and local climate. Within the framework of the research project STORMA "Stability of rain forest margins" (SFB 552, University Göttingen, financed by the German Research Foundation), the carbon dioxide, energy and water fluxes between a cocoa plantation and the atmospheric boundary layer were investigated using the Eddy-Covariance (EC) technique. STORMA is a joint project (Sonderforschungsbereich SFB 552) between the universities of Göttingen and Kassel in Germany and the universities in Bogor and Palu in Indonesia (Sonderforschungsbereich 552 (003b) and 552 (003b)). Simultaneous measurements of meteorological variables and the components of the radiation budget were conducted to investigate the dependencies of the turbulent exchange processes on canopy and atmospheric boundary layer conditions. A SVAT model was used to compute the heat exchange between canopy and atmosphere, to conduct a plausibility test to the measured fluxes, and to investigate the component fluxes. Measurements were conducted for 15 months.

The subject of this work presented here are the development of a self-sustaining EC measurement system for measurements in the tropics, the set-up and maintenance, as well as the analysis and interpretation the measurements. EC measurements were carried out in a cocoa plantation in Indonesia and in a tropical lowland rain forest in the Amazon, Venezuela. Part of the work was also to locate a suitable place for the microclimatic tower, as well as part of the establishment and build-up procedures. The measurements in Venezuela were carried out

in 2000 as part of the project "Die atmosphärische und biologische Steuerung des Wasser-haushaltes eines neotropischen Tieflandregenwaldes in Amazonien/Venezuela", also funded by the DFG.

The establishment, i.e. negotiations with land-owners and villagers, and set-up of the EC site in cocoa plantations at the border of the Lore Lindu National Park (TNLL) and the adaptation of the EC measurement system were part of this work. The EC system was designed for self-sustaining long-term measurements at remote sites at high humidities and temperature. This implied low power consumption as the main focus of the EC system design, and careful setup of the technical components in waterproof containers and connector ports. The electrical circuitry was designed to be as simple and efficient as possible to avoid circuits in the signal ground that could lead to a disturb signal and would introduce noise into the data signal. The central sensor of the EC system is an ultrasonic anemometer USA-1 (Metek, Hamburg). One major change to the EC system in Venezuela was the integration of a new open-path sensor, the LI-7500 (LI-COR, Lincoln, Nebraska), into the EC system to sample the CO_2- and H_2O-content of the air.

Unfortunately, the first release of the LI-7500 was sensitive to incidental solar radiation, which introduced additional variance into the measured scalars CO_2 and H_2O. This was corrected by a spectral correction using the similarity of the scalar and the air temperature spectra. In especially, the solar radiation is reflected at the sensor's body and backscattered into the LI-7500's detector, which leads to an offset on the measured signal, since the LI-7500 measures the absorption of CO_2 and H_2O in the near-infrared. The effect of incident radiation on the measurement of ρ_{CO_2} and ρ_{H2O} follows the diurnal cycle of the sun, and is caused by changes in cloudiness. The latter can appear on time scales of greater than 1 hour to less than 1 minute. Since we can assume cospectral similarity between vertical wind velocity and scalar quantities, the cospectral densities of ρ_{CO_2} and ρ_{H2O} with the vertical wind velocity can be removed below a cut-off frequency and replaced by the cospectral density of temperature with vertical wind velocity, weighted by the ratio of the unaltered parts of the spectra.

12540 half-hourly flux observations were collected at the Nopu site in 2002 and 2003 with two major data gaps in April to May 2002, and in December 2002 to February 2003, due to extraneous causes. The data loss in the H_2O-flux amounts to $9 \pm 2\%$ during rain events, and to $34.5 \pm 1.5\%$ of half-hours with precipitation. Higher ratios of data loss are observed in the CO_2-flux with $13 \pm 1\%$ during rain events, and $91 \pm 9\%$ of half-hours with precipitation. The higher sensitivity of the CO_2-flux to precipitation events might be attributed to the cross sensitivity of the CO_2-signal to the H_2O-signal. The high sensitivity of the CO_2-signal to

rain fall can be seen in the high half-hour standard deviation of CO_2-density, $std(CO_2)$, at half-hours of rain fall. The loss of data poses a disadvantage to the closed-path system, but also the ultrasonic anemometer is not functioning properly during rain fall due to scattering of the ultrasonic pulse by rain drops in the pulses pathways. The number of lost half-hourly data is acceptable, since the loss of half-hour data does not exceed the half-hours of rain events, and it can be concluded that the sensor window's surface dries off relatively fast. The ratio of lost measured half-hourly data to the total amount of total measured half-hourly data is approximately 6% for the open-path IRGA (LI-7500). Thus, the open-path IRGA proved to be very suitable for measurements at the conditions met in tropical regions.

The corrections applied to the EC measurements are part of the post-processing, developed in preceeding works at the IBK (Morgenstern (2000) and Ibrom (2000)). Morgenstern (2000) points out that sensorhead correction is the most important correction. As part of the data analysis, the post-processing was augmented with the new sensorhead correction by Andreas Ibrom (IBK) and Krüger (2002). Additionally, the programming code was rewritten partly so that the code was in ANSI-C and, thereby, portable to other operating systems than Unix.

Krüger (2002) carried out an *insitu* sensorhead calibration at the Göttinger forest site (IBK) with Andreas Ibrom (IBK), to derive a sensorhead correction accounting for the whole tilt angle range. Former sensorhead corrections by Bleyl (2001) included a look-up table, derived from wind tunnel measurements for tilt angle ranges of -25° to 25°. The application of both sensorhead corrections to the data of the EC measurements in Nopu shows an average increase in fluxes of approx. 12% for the wind tunnel correction and 24% for the *insitu* correction. (Bleyl, 2001) finds an increase in the horizontal wind velocity w of 15% and in the turbulent sensible heat flux H of 25% compared to the uncorrected values of w and H respectively. Analysis of the data from the Nopu site show an increase in w of 17% and in H of 12% when applying the wind tunnel correction. For the application of the *insitu* correction, an increase in w of 20% and in H of 24% is found. Ibrom (2000) points out, that the vertical fluxes from the canopy to the atmosphere can often be associated with tilt angles of the incoming flow to the ultrasonic anemometer that are not within the tilt range of the windtunnel sensorhead calibration. Thus, the insitu sensorhead correction is better suited for the measurements in the field, since it covers a wider range of tilt angles. Based on the results found by Ibrom (2000), the ultrasonic anemometer was set-up upside down in this work to minimize the distortion of the incoming flow.

Internal lag times of the LI-7500 due to signal processing in the sensor's processor unit is addressed by covariance maximization between vertical wind velocity and ρ_{CO_2} respectively ρ_{H2O}. The vertical sensor separation between the anemometer and the LI-7500 can cause a

loss of covariance of up to 10%.

The stationarity of the scalar fluxes as adressed by Foken and Wichura (1996) poses a major problem for the EC measurements at the Nopu site. About 35% of the covariances of temperature with vertical wind velocity are non-stationary. For the scalars ρ_{CO_2} and ρ_{H2O} about 40% of the respective covariances are non-stationary. The non-stationary fluxes are found to be associated with slightly stable stratified boundary layer conditions and low values of the friction velocity $u_\star$ at nighttime. During daytime, a sufficient stationarity of the turbulent fluxes is observed.

A footprint analysis following the approach by Wilson and Swaters (1991) shows that 50% of the observed fluxes evolve within the maximal source area distance of $28\,m$ and 70% within $38\,m$. For the nighttime fluxes it is shown, that the flux signal carries not only the imprint of the cacao trees but also of other vegetation types or farm houses distributed in the cocoa plantations.

The observed heat fluxes are compared to measurements of net radiation and the storage flux within the canopy computed by a SVAT model (Oltchev et al., 1997). The input parameters to the model are the measured meteorological variables, physiological parameters and parameters derived from the photosynthesis measurements by Merklein (2003).

The energy balance equation can be closed by 70% as a linear regression of the measured turbulent energy fluxes to the available energy. The available energy contains the measurements of net radiation and the storage heat flux modeled by the SVAT model. Measurements of the net radiation were conducted for one month, time period 19 March to 18 April 2003. Summing up the energy fluxes over the period of radiation measurements yields an energy balance closure of 84%. The net ecosystem exchange of CO_2 measured by the EC system is in good accordance with the modeled CO_2-flux.

Comparisons of the measurements in the cocoa plantations in Nopu to measurements above a low-land rain forest in the Amazon show significant differences in the Bowen ratio. There is no significant difference in the Bowen ratio when comparing the measurements in Nopu to a data-set of a few days from EC measurements at the tower site in the Besoa valley, Indonesia. But the large variance of the observed fluxes at the Besoa site suggest, that the Bowen ratio estimated over three-days measurement is likely to change when estimated from longterm measurements. The boundary layer stratification shows higher stability during nighttime for the rain forest sites than for the Nopu site.

For a more thorough analysis, more comprehensive data-sets are needed, especially of the tower site in the Besoa valley. Long-term measurements of turbulent exchange processes

above primary rain forests serve as reference for the investigation of the influence of land-use change on the atmospheric boundary layer and the biophysical interaction processes within the vegetation cover and with the atmosphere.

The sensible heat flux measured above the cocoa plantation in Nopu, Indonesia, showed an unexpected large contribution to the total turbulent heat transport compared to investigations of natural tropical rain forests, and equaled the latent heat flux. This resulted in an averaged daytime Bowen ratio of approximately 1. The seasonal course of Bowen ratio coincided with that of precipitation. The comparison to measurements above undisturbed rain forest indicates a significantly different atmospheric boundary layer above the cocoa plantation. At the Surumoni Crane site, Venezuela (Anhuf and Winkler, 1999), a Bowen ratio of $\beta = 0.25$ was estimated from EC measurements. Daily net ecosystem exchange of carbon show a significantly lower value $NEE_{C,d} = -0.12$ g-C $m^{-2}d^{-1}$ at the Nopu site compared to $NEE_{C,d} = -2.36$ g-C $m^{-2}d^{-1}$ at the Surumoni site. Daily evapotranspiration amounts to $ET_d = 2.55$ mm d^{-1} averaged over the whole measurement period in Nopu, and is significantly lower than $ET_d = 4.1$ mm d^{-1} observed at the Surumoni site.

This work shows that net ecosystem exchange of carbon dioxide and partitioning of energy fluxes between surface layer of the atmosphere and vegetation at the Nopu site differ fundamentally from that of primary rain forests. The conclusion is that conversion of rain forest to land-use types as cocoa plantations leads to enhanced heating of the atmospheric boundary layer during daytime, and to a significant difference in net uptake of carbon by the vegetation.

Appendix A

Map of the cocoa plantation near Nopu in the Palolo valley (TNLL), Indonesia

Table A.1: Positions of farm houses (hh) in the cocoa plantation relative to the EC measurement mast.

Number of hh	Position South	Position East	Distance to EC site in m	Direction from EC-site in degree	Base Area of hh in m^2
1			95,00	122	
2	01-10-20,5	120-05-29,1	76,25	85	120
3	05-10-16,5	120-05-29,5	81,88	64	72
4	05-10-13.9	120-05-29.0	100,00	43	35
5	05-10-13.4	120-05-29.7	103,13	41	72
6	05-10-15.5	120-05-26.7	176,88	15	72
7	05-10-23.9	120-05-26.4	116,25	165	84
8	05-10-31.3	120-05-32.0	251,25	158	80
9	05-10-34.3	120-05-31.4	265,63	163	54
10	05-10-34.4	120-05-31.4	221,88	150	35
11	05-10-30.3	120-05-33.9	212,50	148	96
12	05-10-26.4	120-05-25.1	123,13	184	42
13	05-10-31.0	120-05-23.8	201,25	200	84
14	05-10-31.3	120-05-24.5	219,38	210	60
15	05-10-30.0	120-05-18.0	185,00	211	84
16	05-10-28.2	120-05-20.4	87,50	191	66
17	05-10-24.2	120-05-14.9	171,25	241	50
18	05-10-26.2	120-05-15.1	201,88	230	120
19	05-10-26.1	120-05-14.2	213,13	228	98
20	05-10-17.9	120-05-16.8	144,38	288	84
21	05-10-17.3	120-05-14.5	176,88	278	56
22	05-10-17.0	120-05-15.2	171,25	280	60
23	05-10-16.7	120-05-15.3	172,50	285	28
24	05-10-13.6	120-05-13.1	190,00	296	42
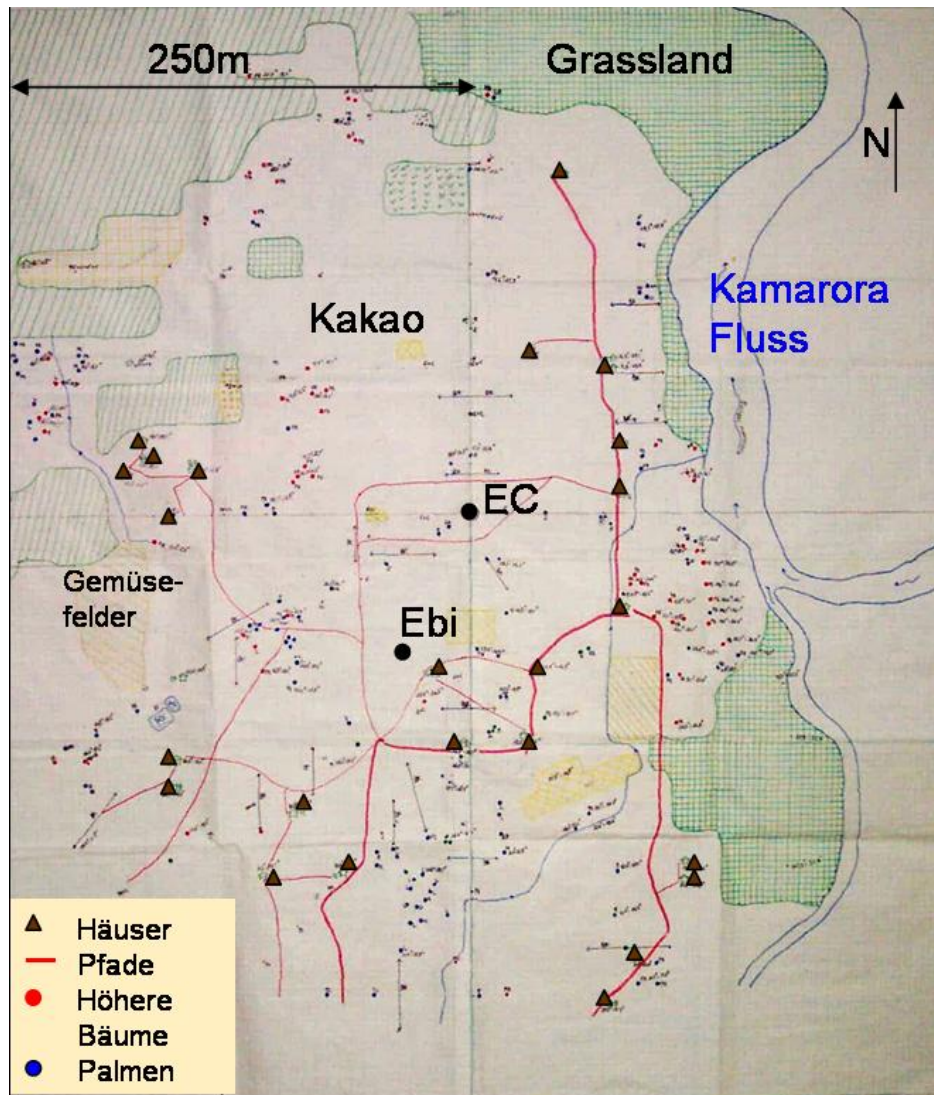
Figure A.1: Self-drawn map of the EC measurement site in the cocoa plantations in the vicinity of Nopu, Indonesia. "EC" denotes the position of the EC mast in time period December 2001 to 07-March 2003. "Ebi" marks the position of the EC mast at the second site from 17-March 2003 to 18-April 2003 with simultaneous measurements of the energy balance components. Non-colored fields are cocoa plantations.

Appendix B

Principal input parameters for the MixFor-SVAT model applied to the measurements in the cocoa plantation, Nopu, Indonesia

Table B.1: The principal input parameters used by the MixFor-SVAT model. Table provided by A. Oltchev

Parameters	Unit	Values
Meteorol. parameters measured above a plant canopy		
Air temperature	$°C$	-
Relative humidity	$\%$	-
Wind speed	m/s	-
CO2 concentration	ppm	-
Precipitation rate	$mm/\Delta t$	-
Global radiation	W/m^2	-
Morphological parameters of the plant canopy		
Plant and leaf area indexes	m^2/m^2	7.8 ; 7.0
Height of the canopy	m	6.0
Root depth	m	0.6
Stem diameter at a breast height	m	0.1
Tree density	Trees/hectare	1140
Physical parameters of the plant canopy		
Reflection coeff. of the leaves for PAR and NIR radiation	-	0.06 ; 0.42
Transmission coeff. of the leaves for PAR and NIR radiation	-	0.05 ; 0.38
Specific hydraulic conductance of tree xylem	m/s	3.125e-5
Specific hydraulic conductance of tree fine roots	m/s	9.600e-5
Leaf storage capacity for intercepted water	m/m^2 foliage	0.0004
Physiological parameters of the plant canopy		
Max. stomatal conductance	$mmol/(m^2 s)$	190.0
Max. Rubisco carboxylation capacity ($T = 25°C$)	$\mu mol/(m^2 s)$	32.1
Max. rate of photosynthetic electron transport (T=25°C)	$\mu mol(\text{el.})/m^2 s$	53.6
Max. mitochondrial respiration (T=25°C)	$\mu mol/(m^2 s)$	0.6
Physical parameters of the soil		
Soil pore space (upper soil layer)	m^3/m^3	0.39
Soil water potential at saturation (upper soil layer)	m	-0.35
Hydraulic conductivity at saturation (upper soil layer)	m/s	1.24e-5

List of Figures

List of Tables

List of Abbreviations

STORMA	Stability Of Rainforest MArgins
EC	Eddy-Covariance
AWS	Automatic Weather Station
TKE	Turbulent Kinetic Energy
SL	Surface Layer
SVAT	Soil Vegetation Atmosphere Transport
TNLL	Lore Lindu National Park (indesian: Taman Nasional Lore Lindu)
UNTAD	Tadulako University (indonesian: Universitas Tadulako)
GPS	General Positioning System
SO1	First Site of EC measurements in Nopu, Indonesia
SO2	Second Site of EC measurements in Nopu, Indonesia
SFB	Sonderforschungbereich
BMG	Meteorological Department of Central Sulawesi

108

Bibliography

552, S., 2003b: *Stabilität von Randzonen tropischer Regenwälder in Indonesien.* Fortsetzungsantrag für die Jahre 2003-2006, Göttingen. 779 S.

Aldrian, E., 2003: *Simulations ofo the Indonesian Rainfall with a Hierarchy of Climate Models.* Fachbereich Geowissenschaften, Universität Hamburg, Hamburg. Dissertation.

Anhuf, D., T. Motzer, R. Rollenbeck, B. Schröder, and J. Szarzynski, 1999: Water budget of the surumoni-crane-site (venezuela). *Selbyana*, **20 (1)**, 179–185.

Anhuf, D. and H. Winkler, 1999: Geographical settings of the surumoni-crane-project (upper orinoco, estado amazonas, venezuela. *Anzeiger Mathematisch Naturwissenschaftliche Klasse, Abt. 1, Biologische Wissenschaften und Erdwissenschaften, Österreichische Akademie der Wissenschaften*, **135**, 3–23.

Aubinet, M., A. Grelle, . Rannik, J. Moncrieff, T. Foken, A. S. Kowalski, P. H. Martin, P. Berbigier, C. Bernhofer, R. Clement, J. Elbers, A. Granier, T. Grünwald, and K. Morgenstern, 1999: Estimates of the annual net carbon and water exchange of european forests: the euroflux methodology. *Adv. Eco. Res.*, **30**, 114–175.

Baldocchi, D. D. and T. P. Meyers, 1988: A spectral and lag correlation analysis of turbulence in a decidous forest canopy. *Bound. Layer Meteor.*, **45**, 31–58.

Betts, A. K., P. Viterbo, and E. F. Wood, 1998: Surface energy and water balances for the arkansas-red river basin from the ecmwf reanalysis. *J. Climate*, **11**, 2881–2897.

B.Fu, C. and G. Wen, 1999: Variation of ecosystems over east asia in association with seasonal, interannual and decadal monsoon climate variability. *Climatic Change*, **43**, 477–494.

Blank, S., 2000: *Eddykorrelationsmessungen turbulenter Wärme- und Wasserdampfflüsse mit open- und closed-path-Sensoren über einem Fichtenbestand im Solling.* Institut für Bioklimatologie, Georg-August-Universität, Göttingen. Diplomarbeit.

Bleyl, M., 2001: *Experimentelle Bestimmung der Depositionsgeschwindigkeit luftgetragener Partikel mit Hilfe der Eddy-Kovarianzmethode über einem Fichtenbestand im Solling.* Institut für Bioklimatologie, Georg-August-Universität, Göttingen. Dissertation.

Businger, J. A., 1982: *Equations and concepts, in Atmospheric Turbulence and Air Pollution Modelling.* eds. F. T. M. Nieuwstadt and H. van Dop, Reidel, Dordrecht. pp. 1-36.

Calder, I. R., I. R. Wright, and D. Murdiyarso, 1986: A study of evaporation from a tropical rain forest-west java. *J. Hydrol.*, **89**, 13–31.

Campbell, G. S. and J. M. Norman, 1998: *An introduction to Environmental Biophysics.* Springer, New York. Sec. Ed., 286 p.

Chapman, S. and R. S. Lindzen, 1996: Atmospheric tides, thermal and gravitational. *Agric. For. Meteor.*, **78**, 83–105.

Culf, A. D., G. Fisch, and M. G. Hodnett, 1995: The albedo of amazonian forest and ranchland. *J. Climate*, **8**, 1544–1554.

Deng, X., R. J. Joly, and D. T. Hahn, 1990: The influence of plant water deficit on photosynthesis and translocation of 14c labelled assimilates in cacao seedlings. *Physiologia Plantarum 78*, **4**, 623–627.

Dyer, A. J., 1974: A review of flux-profile relationships. *Bound. Layer Meteorol.*, **7**, 363–372.

Dyer, A. J. and B. B. Hicks, 1970: Flux-gradient relationships in the constant flux layer. *Quart. J. Roy. Met. Soc.*, **96**, 715–721.

Finn, D., B. Lamb, M. Y. Leclerc, and T. W. Horst, 1996: Experimental evaluation of analytical and lagrangian surface-layer flux footprint models. *Bound. Layer Meteorol.*, **80**, 283–308.

Foken, T. and B. Wichura, 1996: Tools for quality assessment of surface-based flux measurements. *Agric. For. Meteor.*, **78**, 83–105.

Fu, C. B., 1996: *An aridity trend in China in association with global warming. In: Zepp RG (ed) Climate-biosphere Interaction: biogenic emission and environmental effects of climate change.* John Wiley & Sons, Chichester.

Garrat, J. R., 1992: *The atmospheric boundary layer.* Cambridge University Press; Cambridge. 316 pp.

Gash, J. H. C. and C. A. Nobre, 1997: Climatic effects of amazonian deforestation: some results from abracos. *Bulletin of the A. Met. Soc.*, **78(5)**, 823 – 830.

Gibson, J. K., P. Kallberg, S. Uppala, A. Hernandez, A. Nomura, and E. Serrano, 1997: *ERA description*, volume 1. ECMWF Re-Analysis Project Report Series. 72 p.

Goulden, M. L., J. W. Munge, and S.-M. Fan, 1996: Measurements of carbon sequestration by long-term eddy-covariance: methods and critical evaluation of accuracy. *Global Change Biology*, **2**, 169–182.

Grace, J., J. Lloyd, J. McIntyre, A. Miranda, P. Meir, H. Miranda, J. Moncrieff, J. Massheder, I. Wright, and J. Gash, 1995: Fluxes of carbon dioxide and water vapour over an undisturbed tropical forest in south-west amazonia. *Global Change Biol.*, **1**, 1–12.

Gros, D., 1998: *Eddy-Korrelationsmessungen an einem Hang.* Institut für Bioklimatologie, Georg-August-Universität, Göttingen. Diplomarbeit.

Hastenrath, S., 1985: *Climate and Circulation of the Tropics.* D. Reidel Publishing Company, Dordrecht, Holland. 455 pp.

Hollinger, D. Y., S. M. Goltz, and E. A. Davidson, 1999: Seasonal patterns and environmental control of carbon dioxide and water vapour exchange in an ecotonal boreal forest. *Global Change Biology*, **5**, 891–902.

Hunt, E. R., S. W. Running, and C. A. Federer, 1991: Extrapolating plant water flow resistances and capacitances to regional scale. *Agric. For. Meteorol.*, **54**, 169–195.

Ibrom, A., 2000: CO_2-*Bilanz eines Fichtenbestandes.* Institut für Bioklimatologie, Georg-August-Universität, Göttingen. Habilitation.

Kaimal, J. C. and J. A. Businger, 1963: A continous wave sonic anemometer-thermometer. *J. Appl. Meteorol.*, **2**, 156–164.

Kaimal, J. C. and J. J. Finnigan, 1994: *Atmospheric boundary layer flows.* Oxford University Press; Oxford. 289 S.

Kaimal, J. C. and J. E. Gaynor, 1991: Another look at sonic thermometry. *Bound. Layer Meteorol.*, **56**, 401–410.

Kanae, S., T. Oki, and K. Musiake, 2001: Impact of deforestation on regional precipitation over the indochina peninsula. *J. Hydrometeorol.*, **2**, 51–70.

Kleinhans, A., 2004: *Einfluss der Waldkonversion auf den Wasserhaushalt eines tropischen Regenwaldeinzugsgebietes in Zentral Sulawesi (Indonesien). Experimentelle Analyse und Modellierung unter Berücksichtigung von Landnutzungsszenarien.* Geographisches Institut, Georg-August-Universität, Göttingen. Dissertation.

Kolmogorov, A. N., 1941: The local structure of turbulence in incompressible visous flow for very large reynold's numbers. *Doklady ANSSSR*, **30**, 301–304.

Krüger, T., 2002: *In situ Messung der Auswirkungen von Sondenkopfeffekten am Beispiel des Ultraschallanemometer USA-1, METEK.* Institut für Bioklimatologie, Georg-August-Universität, Göttingen. Bachelor Arbeit.

Kristensen, L., J. Mann, S. P. Oncley, and J. C. Wyngaard, 1997: How close is close enough when measuring with a displaced sensor? *J. Atmos. Ocean. Tech.*, **14**, 814–821.

Leclerc, M. Y., S. Shen, and B. Lamb, 1997: Observations and large eddy simulation modeling of footprints in the lower convective boundary layer. *J. Geophys. Res.*, **102**, 9323–9334.

Lee, X. and T. A. Black, 1994: Relating eddy correlation sensible heat flux to a horizontal sensor separation in the unstable atmospheric surface layer. *J. Geophys. Res.*, **99**, 18545–18553.

LI-COR, 1991a: *LI-610 Portable Dew Point Generator instruction manual.* LI-COR, inc., Lincoln, Nebrasca.

LI-COR, 1991b: *LI-6262 CO_2/H_2O analyser instruction manual.* LI-COR, inc., Lincoln, Nebrasca.

Loescher, H. W., 2002: *Ecosystem responses of Carbon and Energy from a tropical wet forest in Costa Rica.* University of Florida, USA. Dissertation.

Loescher, H. W., S. F. Oberbauer, H. L. Gholz, and D. B. Clark, 2003: Environmental controls on net ecosystem-level carbon exchange and productivity in a central american tropical wet forest. *Global Change Biology*, **9**, 396–412.

Malhi, Y., P. Meir, and S. Brown, 2002: Forests, carbon and global climate. *Phil. Trans. R. Soc. Lond.*, **360**, 1567–1591.

Merklein, J., 2003: *Simulation des CO_2- und H_2O-Gaswechsels einer Kakaoplantage in Sulawesi.* Institut für Bioklimatologie, Georg-August-Universität, Göttingen. Master thesis.

Miyaji, K.-I., W. D. Silva, P. Alvim, and T. D. Alvim, 1997: Productivity of leaves of a tropical tree, theobroma cacao, grown under shading, in relation to leaf age and light conditions within the canopy. *New Phytologist*, **137**, 3: 463–472.

Monin, A. S. and A. M. Obukhov, 1954: Basic laws of turbulent mixing in the ground layer of the atmosphere. *Trans. Geophys. Inst. Akad. Nauk. USSR*, **151**, 163–187.

Monteith, J. L., 1965: *Evaporation and Environment. In: The state and movement of water in living organisms. Sumposia of the Society for Experimental Biology.* Cambridge University Press, Cambridge. 205-234.

Monteith, J. L. and M. H. Unsworth, 1990: *Principles of enviromental physics.* Butterworth-Heinemann, Oxford.

Moore, C. J. and G. Fisch, 1986: Estimating heat storage in amazonian tropical forest. *Agric. For. Meteorol.*, **38**, 147–169.

Morgenstern, K., 2000: *Turbulent CO_2-, H_2O- and Energy Fluxes above a Mediterranean Oak and a Mountainous Spruce Forest Investigated by Eddy-Covariance Measurements.* Institut für Bioklimatologie, Georg-August-Universität, Göttingen. Dissertation.

Oltchev, A., J. Cermak, N. Nadezhdina, F. Tatarinov, A. Tishenko, A. Ibrom, and G.Gravenhorst, 2002: Transpiration of a mixed forest stand: field measurements and simulation using svat models. *J. Bor. Env. Res.*, **7 (4)**, 389–398.

Oltchev, A., J. Constantin, G. Gravenhorst, and A. Ibrom, 1997: A six-layer svat model for a simulation of water vapour and sensible heat fluxes in a spruce forest. *J. Hydrol. Hydromech*, **1-2**, 5–37.

Oltchev, A., J. Constantin, G. Gravenhorst, A. Ibrom, J. Heimann, J. Schmidt, M. F. K. Morgenstern, I. Richter, and N. Vygodskaya, 1996: Application of a six-layer svat model for simulation of evapotranspiration and water uptake in a spruce forest. *J. Phys. Chem. Earth*, **21**, 195–199.

Panofsky, H. A. and J. A. Dutton, 1984: *Atmospheric turbulence. Models and methods for engineering applications.* John Wiley and Sons; New York. 397 S.

Pasquill, F., 1972: Some aspects of boundary layer description. *Q. J. Royal Meteorol. Soc.*, **98**, 469–494.

Prandtl, L., 1904: Über flüssigkeitsbewegungen bei sehr kleiner reibung. *Verhandlg. III Intern. Kongr.*, **0**, 484–491. Heidelberg.

Prentice *et al.*, I. C., 2001: *The carbon cycle and atmospheric carbon dioxide.* Cambridge University Press, 183-237. Climate change 2001: the scientific basis (ed. IPCC).

Press, W. H., S. A. Teukolsky, W. T. Vetterling, and B. P. Flannery, 1992: *Numerical Recipes in C. The Art of Scientific Computing.* Cambridge University Press, New York, USA. Sec. Edition.

Running, S. W., D. D. Baldocchi, D. P. Turner, S. T. Gower, P. S. Bakwin, and K. A. Hibbard, 1999: A global terrestrial monitoring network integrating tower fluxes, flask sampling, ecosystem modeling and eos satellite data. *Remote Sensing of Environment*, **70**, 108–127.

Schimel, D. S., 1998: The carbon equation. *Nature*, **393**, 208–209.

Schimel, D. S., D. Alves, I. Enting, M. Heimann, F. Joos, D. Raynaud, T. Wigley, M. Prather, R. Derwent, and D.Ehhalt, 1996: *Radiative forcing of climate change.* Climate change 1995. The science of climate change. Cambridge University Press, UK, 65-131.

Schmidt, W., 1925: *Der Massenaustausch in freier Luft und verwandte Erscheinungen.* Henri Grand Verlag; Hamburg. 118 S.

Schütz, C., 1996: *Eddy-Korrelationsmessungen von CO_2-Flüssen im Solling - Aufbau und Test eines Messsystems.* Institut für Bioklimatologie, Georg-August-Universität, Göttingen. Diplomarbeit.

Schuepp, P. H., M. Y. Leclerc, J. J. MacPherson, and R. L. Desjardins, 1990: Footprint prediction of scalar fluxes from analytical solutions of the diffusion equation. *Bound. Layer Meteorol.*, **50**, 355–373.

Shuttleworth, W. J., 1988: Evaporation from amazonian rain forest. *Proc. Roy. Soc.(Lond.) B*, **233**, 321–346.

Shuttleworth, W. J., J. H. C. Gash, C. R. Lloyd, C. J. Moore, J. Roberts, A. de O. Marques, G. Fisch, V. de P. Silva, M. N. G. Ribeiro, L. C. B. Molion, L. D. de Abreu, J. C. Nobre, O. M. R. Cabral, S. R. Patel, and J. C. de Moraes, 1984: Eddy correlation measurements of energy partition for amazonian forest. *Quart. J. R. Meteorol. Soc.*, **110**, 1143–1162.

Sonderforschungsbereich 552, 2003b: *Stabilität von Randzonen tropischer Regenwälder in Indonesien.* Finanzierungsantrag für die Jahre 2000/2-2003/1, Göttingen. 779 S.

Stull, R. B., 1988: *An introduction to boundary layer meteorology.* Kluwer Academic Publishers; Dordrecht. 666 S.

Suzuki, M., H. Takizawa, N. Tanaka, N. Yoshifuji, and N. Tangtham, 7-9 March (2001): *Energy and water budget in Hill Evergreen Forest, northern Thailand.* Proceedings of the International Workshop on GAME-AAN/Radiation.

Szarzynski, J., 2000: *Bestandsklima und Energiehaushalt eines amazonischen Tieflandregenwaldes.* Mannheimer Geographische Arbeiten. Geographisches Institut, Universität Mannheim, Mannheim. Dissertation.

Taylor, G. I., 1938: The spectrum of turbulence. *Proc. R. Soc.*, **A164**, 476–490.

Toda, M., K. Nishida, N. Ohte, M. Tani, and K. Musiake, 2002: Observation of energy fluxes and evapotranspiration over terrestrial complex land covers in the tropical monsoon environment. *J. Meteorol. Soc. Jpn*, **80(3)**, 465–484.

Van der Hoven, I., 1957: Power spectrum of horizontal wind speed in the frequency range from 0.0007 to 900 cycles per hour. *J. Meteor.*, **41**, 160.

Viterbo, P. and A. Beljaars, 2002: *Impact of land surface on weather.* Vegetation, water, humans and the climate: A new perspective on an interactive system. M. Claussen, P. Dirmeyer, J.H.C. Gash, P. Kabat, M. Meybeck, R. Pielke, C. Vorosmarty, Eds. Springer-Verlag. in press.

Webb, E. K., G. I. Pearman, and R. Leuning, 1980: Correction of flux measurements for density effects due to heat and water vapour transfer. *Quart. J. Roy. Meteor. Soc.*, **106**, 85–100.

Wilson, J. D. and G. E. Swaters, 1991: The source area influencing a measurement in the planetary boundary layer: the "footprint" and the "distribution of contact distance". *Bound. Layer Meteorol.*, **55**, 25–46.

Wilson, K. B., A. H. Goldstein, E. Falge, M. Aubinet, D. Baldocchi, P. Berbigier, C. Bernhofer, R. Ceulemans, H. Dolman, C. Field, A. Grelle, B. Law, T. Meyers, J. Moncrieff, R. Monson, W. Oechel, J. Tenhunen, R. Valentini, and S. Verma, 2002: Energy balance closure at fluxnet sites. *Agric. For. Meteorol.*, **113**, 223–243.

Witte, H., 1993: *Temperaturen der Nadeloberflächen in einem Fichtenbestand im Solling. Feldmessungen und Interpretation.* Institut für Bioklimatologie, Georg-August-Universität, Göttingen. Diplomarbeit.

Wright, I. R., A. O. Manzi, and H. R. D. Rocha, 1995: Canopy surface conductance of amazonian pasture: model application and calibration for canopy climate. *Agric. For. Meteorol.*, **75**, 51–70.

Wyngaard, J. C. and O. R. Coté, 1972: Cospectral similarity in the atmospheric surface layer. *Quart. J. Roy. Meteor. Soc.*, **98**, 590–603.

Danksagung

Lebenslauf

Am 15. Februar 1972 wurde ich, Ulrike Falk, als Tochter von Dr. Martin Falk und Christine Falk, geb. Bünck, in Meerbusch geboren. Meine Staatsbürgerschaft ist deutsch.

Aufgewachsen bin ich in Hillscheid im Westerwald, wo ich bis 1982 die Melchiades-Best-Grundschule besuchte. Im August 1982 wechselte ich zum Kannenbäckerland-Gymnasium, an welchem ich im Mai 1991 das Abitur ablegte.

Mit Beginn des Wintersemesters 1991/1992 immatrikulierte ich mich an der Friedrich-Wilhelm-Universität in Bonn im Studienfach Physik und legte dort meine Diplom-Vorprüfung im April 1994 ab.

Meine Diplomarbeit fertigte ich unter Anleitung von Priv. Doz. Günther Heinemann und Prof. Klaus Heinloth an mit dem Thema: "Bestimmung von Energieflüssen über Grönland mittels Variationsanalyse und ihre Kopplung mit dem katabatischen Windsystem".

Im April 1999 legte ich die Diplomprüfung an der Friedrich-Wilhelm-Universität zu Bonn im Fach Physik ab.

Im November 1999 begann ich als wissenschaftliche Mitarbeiterin am Institut für Bioklimatologie mit meiner Arbeit an der vorliegenden Dissertation.

Göttingen, den 29.01.2004

Ulrike Falk